Universidade de Lisboa

Faculdade de Ciências

Departamento de Biologia Vegetal

Localization and Regulation by GABA of Anion Transporters present in Pollen Grain Protoplasts and Tube of *Arabidopsis thaliana*

Doutoramento em Biologia

Especialidade em Biologia do Desenvolvimento

Patrícia Domingos Gonçalves

Tese orientada pelo Prof. Doutor José A. Feijó e Prof. Doutor Jorge Marques da Silva

2015

Documento especialmente elaborado para a obtenção do grau de doutor

Abstract

Upon hydration in the female gametophyte, pollen grains germinate and develop a cytoplasmic extension designated as the pollen tube. This cell is dramatically polarized, grows exclusively at its apex (apical growth) and responds to specific female cues by changing growth axis in order to direct it towards the entrance of the ovule. When germinated *in vitro*, pollen tubes display oscillations in growth, which is underlied by ion dynamics, namely ion fluxes across the membrane and cytosolic ionic gradients. By means of imaging techniques and by Ion-Specific Vibrating Probes, Zonia et al., (2002) identified and characterized chloride (Cl^-) fluxes in growing pollen tubes from *Lilium longiflorum* and *Nicotiana tabacum*, showing an massive oscillatory efflux of Cl^- at the tip and influxes all over the shank of the tube, starting approximately at 15 µm from the tip. The authors suggested that the Cl^- fluxes are essential to pollen tube growth due to its role on the maintenance of the cellular volume, presumably by water flux control. The molecular nature and mechanisms of the pollen tube anion transporters are still mostly unknown.

This thesis aims at characterizing the anionic currents present in the pollen grain protoplasts of two species, *Lilium longiflorum* (Lily) and *Arabidopsis thaliana*, and to characterize the putative transporters underlying these currents in Arabidopis. Lily pollen was chosen because (1) it's one of the most studied species because of the favourable features of its pollen for Cell Biology studies and (2) it allows for a comparison between the same type of currents in two very different species. During the course of this project single channel events were detected by patch-clamp, and the existence of anionic currents across channels in the plasma membrane of un-germinated grains was demonstrated. In addition, by germinating Lily pollen we were able to find anionic currents similar to those measured in hydrated Lily protoplasts. We speculate that many of the channels present in the plasma membrane of the grain protoplasts may suffer a spatial redistribution to specific regions of the membrane during pollen tube germination and growth or that they undergo recycling.

Arabidopsis was chosen due to its genetic tractability, namely the established resources for reverse-genetics approaches that facilitate the identification of candidate channels and transporters responsible for Cl^- transport determined by patch-clamp. A full search into the available transcriptomic datasets for pollen grain (PG) and tube (PT) resulted in the selection of four candidate proteins that, due to their known electrophysiological profiles, could account for the observed currents and fluxes previously measured, respectively. Four transporter candidates were chosen: AtCCC (The Cation Chloride Cotransporter), SLAH3

(SLow Anion channel Homolog 3), ALMT12 (Aluminum-activated Malate Transporter 12) and At1g73020 (here designated by AtTMEM16, *Arabidopsis thaliana* TransMEMbrane 16). Mutant lines were generated and a electrophysiological characterization study and localization assays were performed.

By patch clamp we could measure current alterations on hydrated pollen grain protoplasts of mutant for these genes. Pollen protoplasts (sporoplats) of the single gene mutants *slah3*$^{-/-}$, *almt12*$^{-/-}$ and *atmem16*$^{-/-}$, and the double mutant *slah3*$^{-/-}$;*almt12*$^{-/-}$ present significant specific differences in currents than those measured in the wild-type (*wt*) group, namely: (1) a higher initial current ($I_{Initial}$) in *slah3*$^{-/-}$ and *attmem16*$^{-/-}$ protoplasts; (2) *almt12*$^{-/-}$ had reduced $I_{Initial}$ and final currents (I_{Final}) for the negative membrane potentials (V_m) tested; (3) increased rundown currents (I_{LostRD}) for the negative V_m in all three single mutants, (4) higher loss of I_{LostRd} in *slah3*$^{-/-}$ and *attmem16*$^{-/-}$ protoplasts for positive V_m; (5) different sensitivities to 5-Nitro-2-(3-phenylpropylamino)benzoic acid (NPPB) were measured for all three single mutants and (6) different sensitivities and conductive states to V_m variations in the three single mutants. In addition, the currents measured from the double mutant line *almt12*$^{-/-}$*; slah3*$^{-/-}$, presented key differences when compared to *wt*, and to the respective single mutants, namely: a significant decrease in $I_{Initial}$, I_{Final} and I_{LostRd}, a higher rundown for the negative V_m, and a higher inhibition of I_{LostRd} in relation to the *slah3*$^{-/-}$ single mutant.

In the mutant context, the observed differences in the current amplitudes throughout the experimental protocol strongly suggest that the regulation of Cl^- transport is very complex and involves several regulatory loops and different types of compensation, either by modulation/activation of the remaining channels or by transcriptional activation of other transporters.

By overexpressing Green Fluorescent Protein (GFP) fusion chimeras of SLAH3, ALMT12 and AtTMEM16 channels and AtCCC under the control of the LAT52 pollen specific promoter we observe that AtCCC localizes to the plasma membrane (PM) in the shank of the PT, but not in the tip; AtTMEM16 localizes to the plasma membrane of the shank, and to enlogated membranous structures, presumably endoplasmatic reticulum, vesicle accumulation, or stretched young vacuoles; SLAH3 and ALMT12 are present in small circular organelles. We were able to successfully establish the localization of AtCCC at the shank of the PT and allocate SLAH3 to the tip. These results are suggestive that SLAH3 and AtCCC transporters could account for the fluxes measured by Zonia et al., (2002) in the growing PT. Vibrating Probe analysis in the 4 selected transporter mutants, further sustains

the previous statement: the anionic fluxes collected from the tip of germinating PTs of *slah3*$^{-/-}$ and *atccc*$^{-/-}$ was significantly lower than those measured from the *wt* and *almt12*$^{-/-}$ *and atmem16*$^{-/-}$ mutants.

We further expressed the candidate genes on mammalian cell lines, in order to characterize them electrophysiologically and to establish their molecular identity. ALMT12 expressed in COS-7 was technically challenging, but we were able to measure statistically relevant inward currents, resembling the electrophysiological profile of that described in Meyer et al., (2010).

Finally, we show a direct regulation of the elicited currents in hydrated PGs by gamma-Aminobutyric acid (GABA). A motif that contains a binding site to GABA is shared between $GABA_A$ receptors and the ALMT family (Ramesh et al., 2015). When added to *wt,* 80-500 µM GABA inhibit significantly the overall currents, but this effect is completely abrogated in *almt12*$^{-/-}$.sporoplasts. In addition, when GABA was added to two *ALMT12* transfected COS-7 mammalian cell it induced single channel flickering events. These results, strongly suggest that GABA directly binds to ALMT12 channels, and establishes ALMT channels as prominent candidates for GABA binding and consequent biological implications in plants.

The physiological implications of the present findings are discussed, in the context of pollen tube growth regulation.

Keywords: *Arabidopsis thaliana,* Pollen Tube, Patch Clamp, Anionic Transporters, GABA

Resumo

Ao germinar nos tecidos femininos, o grão de pólen forma uma extensão citoplasmática designada por tubo polínico. O seu crescimento é polarizado e estritamente apical, e é direcionado para o óvulo através de moléculas libertadas pelos tecidos femininos. Quando germinados *in vitro*, o crescimento dos tubos polínicos distingue-se por ser oscilatório e por estar intimamente associado por uma dinâmica iónica, nomeadamente fluxos iónicos através da membrana plasmática e gradientes citoplasmáticos que os fluxos originam.

Através de técnicas de Imagiologia e de Sondas Vibráteis Auto Referenciáveis, Zonia e colaboradores (2002) identificaram e caracterizaram os fluxos de cloreto (Cl^-) em tubos polínicos de duas espécies, *Lilium longiflorum* e *Nicotiana tabacum*, mostrando que este ião sai do tubo polínico através de um efluxo oscilante no ápice e entra através de um influxo não oscilante nos lados do tubo, e que tem inicio a aproximadamente 15 µm da ponta. Com este artigo, Zonia e colaboradores (2002) mostraram que os fluxos de Cl^- são essenciais ao crescimento do tubo devido ao seu papel na manutenção do volume celular, presumivelmente através do controlo do fluxo de água. A natureza molecular e os mecanismos de regulação dos transportadores de aniões no tubo polínico são ainda praticamente desconhecidas.

Esta tese tem como objetivo caracterizar as correntes aniónicos presentes nos protoplastos de grãos de pólen de duas espécies, *Lilium longiflorum* (Lírio) e *Arabidopsis thaliana*, e caracterizar os transportadores putativos subjacentes a estas correntes em *Arabidopsis*. O pólen de Lírio foi escolhido porque (1) é uma das espécies mais estudadas devido às suas características favoráveis para estudos da biologia celular e, (2) permitir uma comparação entre o mesmo tipo de correntes em duas espécies tão distintas. Durante o decurso deste projeto nós detetamos eventos de correntes unitárias (*single channel*) e demonstrámos a existência de canais iónicos que poderão ser os responsáveis pela geração da corrente global através da membrana plasmática de grãos hidratados. Além disso, ao germinarmos pólen de Lírio e procedermos à medição de correntes aniónicas, observámos correntes similares às medidas em protoplastos de pólen de Lírio hidratado. Especulamos que, muitos dos canais já presentes na membrana plasmática de protoplastos hidratados possam sofrer uma redistribuição espacial para regiões específicas da membrana durante o crescimento do tubo polínico ou, possam ser reciclados.

Arabidopsis foi escolhida devido à sua rastreabilidade genética, nomeadamente, aos recursos estabelecidos para abordagens de genética reversa que facilitam a identificação

de canais e transportadores candidatos responsáveis pelas correntes de Cl^- medidos por *patch-clamp*. Uma pesquisa completa sobre os conjuntos de dados transcriptómicos disponíveis para grão de pólen (GP) e tubo (TP) resultou na selecção de quatro proteínas transportadoras de aniões que, devido aos seus perfis electrofisiológicos conhecidos, podem ser os responsáveis ou contribuir para as correntes e fluxos observados em GPs hidratados e durante o crescimento do TP, respectivamente. Os quatro candidatos escolhidos foram: um AtCCC (Cation Chloride Cotransporter), e três canais, SLAH3 (SLow Anion channel Homolog 3), ALMT12 (Aluminum-activated Malate Transporter 12) e At1g73020 (aqui designada por *Arabidopsis thaliana* AtTMEM16). Linhas mutantes foram geradas, e procedeu-se a um estudo eletrofisiológico caracterizar as correntes medidas para cada mutante. Adicionalmente, também foram efectuados estudos de localização.

A técnica de retalho controlado *(patch clamp*) permitiu analisar a disrupção dos três canais eletrogénicos em protoplastos hidratados. Correntes elicitadas pelos mutantes singulares *slah3*$^{-/-}$, *almt12*$^{-/-}$ e *atmem16*$^{-/-}$, e do duplo mutante *slah3*$^{-/-}$;*almt12*$^{-/-}$ foram medidas e apresentam diferenças específicas e significativas quando comparados com o grupo tipo selvagem (*wt*), nomedamente: (1) uma maior corrente elicitada logo após a entrada na configuração de célula inteira (*whole cell*) ($I_{Initial}$), pelos mutantes *slah3*$^{-/-}$ *e attmem16*$^{-/-}$*;* (2) *a* $I_{initial}$ e as correntes após estabilização da corrente (I_{Final}) elicitadas por protoplastos *almt12*$^{-/-}$ apresentaram uma redução significativa para os potenciais negativos; (3) aumento da corrente perdida por rundown (I_{LostRD}) nos três mutantes para os potenciais negativos; (4) há um aumento da I_{LostRD} nos mutantes *slah3*$^{-/-}$ *e attmem16*$^{-/-}$ para os potenciais positivos testados; (5) diferentes sensibilidades ao inibidor 5-Nitro-2-(3-phenylpropylamino)benzoic acid (NPPB) foram medidas os 3 mutantes singulares; e (6) diferentes sensibilidades e estados de condutância, em resposta aos potenciais de membrana testados, foram observados nos 3 mutantes singulares. Adicionalmente, as correntes eliciadas pelo duplo mutante *almt12*$^{-/-}$*; slah3*$^{-/-}$, também apresentam uma redução significativa das correntes iniciais, depois do Rundown e perdida por Rundown $I_{Initial}$, I_{Final} e I_{LostRd}. Foi também observado um aumento da % de Inibiçao por NPPB, para os potenciais negativos testados, quando comparado com o mutante singular *slah3*$^{-/-}$.

No contexto mutante, as diferenças observadas nas amplitudes de corrente, durante o decorrer do protocolo experimental, sugerem fortemente que a regulação do transporte de Cl^- é muito complexo e envolve vários ciclos de regulação. Nomeadamente, poderá sugerir

diferentes tipos de compensação, quer por modulação/ativação dos canais remanescentes ou por indução da transcrição de outros transportadores aniónicos.

Através de ensaios de sobre expressação de quimeras de fusão com a proteína verde fluorescente (GFP) com os canais candidatos, SLAH3, ALMT12, AtTMEM16 e AtCCC, sob o controlo do promotor específico de pólen LAT52 observamos que: AtCCC localiza-se na membrana plasmática (MP) e ao longo do TP, mas não foi observado sinal na ponta; AtTMEM16 localiza-se na membrana plasmática da haste, e para estruturas alongadas membranosas, presumivelmente retículo endoplasmático, acumulação em vesículas, ou vacúolos jovens estirados; SLAH3 e ALMT12 estão presentes em pequenos organelos circulares. Com estes resultados conseguimos estabelecer com sucesso a localização do AtCCC ao longo da haste do TP e alocar SLAH3 para a ponta. Estes resultados implicam que os transportadores aniónicos, SLAH3 e AtCCC, podem ser os responsáveis pelos fluxos medidos por Zonia e colaboradores (2002) no TP. A aplicação das sondas vibráteis nos 4 mutantes selecionados, sustenta ainda mais a afirmação anterior: os fluxos aniónicos medidos na ponta de tubos germinados de *slah3*$^{-/-}$ e *atccc*$^{-/-}$ foram significativamente inferiores aos medidos a partir de *wt*, e dos mutantes singulares *almt12*$^{-/-}$ e *atmem16*$^{-/-}$.

Efectámos a expressão heteróloga dos genes candidatos usando para isso linhas de células de mamíferos, por forma a estabelecer o perfil eletrofisiológico e estabelecer a identidade molecular de cada um. A transfeção de canais de ALMT12 em COS-7 foi tecnicamente desafiante, mas foi possível medir correntes de entrada estatisticamente relevantes. A corrente observada enquadra-se ao perfil de eletrofisiológico já descrito para estes canais (Meyer et al., 2010).

Finalmente, mostramos também uma regulação direta das correntes por ácido gama-Aminobutírico (GABA), em grãos de pólen hidratados. Foi descrito que, os recetores $GABA_A$ e a família ALMT partilham um motivo proteico que contém um local de ligação ao GABA (Ramesh et al., 2015). A adição de 80, 200 e 500 µM de GABA a protoplastos de *wt* inibe significativamente as correntes globais, mas este efeito foi completamente abolido em protoplastos de *almt12*$^{-/-}$. Adicionalmente, quando o GABA foi adicionado a duas células COS-7 transfetadas com *ALMT12* foi possível visualizar um aumento de correntes unitárias (*single channel*). Estes resultados, sugerem fortemente que o GABA liga-se diretamente aos canais ALMT12, e estabelece os canais ALMT como candidatos de destaque para a ligação do GABA e consequentes implicações biológicas em plantas.

São discutidas as implicações fisiológicas dos resultados durante o crescimento do tubo polínico.

Palavras Chave*:* *Arabidopsis thaliana,* Tubo Polínico, *Patch Clamp*, Transportadores de Aniões, GABA

Table of Contents

1. Introduction 14

1.1. Flowering Plant Reproduction 14

1.2. The Pollen Tube 15

1.3. Ion Dynamics during Pollen Tube Growth 16

1.3.1. Calcium (Ca^{2+}) Fluxes 17

1.3.2. Protons (H+) Fluxes 18

1.3.3. Potassium (K^{+}) Fluxes 19

1.3.4. Chloride (Cl^{-}) Fluxes 19

1.4. Pollen Transporters 21

1.4.1. Calcium (Ca^{2+}) Transporters 22

1.4.2. Proton (H^{+}) Transporters 23

1.4.2. Potassium (K^{+}) Transporters 23

1.5. The Chloride Transport Conundrum 24

1.5.1. Pollen Anion Channel/Transporter Candidates 26

1.5.1.1. R-type and S-type channels are key players in stomatal movement 26

1.5.1.1.1. Aluminum-activated Malate Transporter 12 – ALMT12 28

1.5.1.1.2. SLow Anion channel Homolog 3 – SLAH3 28

1.5.1.2. The Cation:Chloride Cotransporter – *At*CCC 29

1.5.1.3. The Calcium activated Chloride Channels (CaCC) – AtTMEM16 29

1.5.1.4. The ChLoride Channel family – CLC 31

1.6. Pollen Tube Regulation by gamma-amino butyric acid (GABA) 32

1.7. The Patch Clamp Technique 33

1.7.1. Membrane Potential 33

1.7.2. Electrical equivalent circuit of cell membrane 34

1.7.3. Voltage Clamp 35

1.7.4. The four patch clamp configurations 36

2. Project Goal and Objectives 39

3. Materials and Methods 40

3.1. Plant Material and Growth Conditions 40

3.1.1. Pollen germination assays 41

3.2. Molecular Biology 42

3.2.1. Analysis of the candidate mutant lines 42
3.2.1.1. DNA extraction 42
3.2.1.2. Isolation of homozygous T-DNA insertion mutants 42
3.2.1.2.1. mRNA isolation 44
3.2.1.2.2. cDNA synthesis 44
3.2.2. Generation of transgenic *Arabidopsis* lines overexpressing the candidate genes 46
3.2.3. Cell Line Cultivation and Transient Transfection 48
3.2.3.1. Trasient Transfection 49
3.2.3.2. Constructs for heterologous expression 49
3.3. Live-Cell and Confocal Imaging 50
3.4. Electrophysiology 50
3.4.1. Protoplast isolation 50
3.4.2. Patch Clamp Set up 52
3.4.3. Patch Clamp Protocol 52
3.4.4. Recording solutions 53
3.4.4.1. Pollen protoplasts 53
3.4.4.2. Mammalian Cells 53
3.4.5. Voltage Protocols 54
3.4.6. Data analysis 55
3.4.7. Anion-selective self-referencing probe 56

4. Results 58
4.1. Molecular Characterization of the Anionic Protein Transporters 58
4.1.1. Pollen expresses 4 anionic transporter proteins 58
4.1.2. Expression validation of anionic channels and Mutant Genotyping 59
4.1.3. Morphological Phenotype 60
4.2. Electrophysiological Characterization of the Anionic Transporters 62
4.2.1. Patch Clamp Analysis of the Anionic Currents in Pollen Grain Protoplasts from Lilium longiflorum and *Arabidopsis* thaliana 62
4.2.1.1. Anionic single-channel currents across the plasma membrane of *Lililum longiflorum* pollen protoplasts 63
4.2.1.2. Lily PT presents similar current activities to those measured in hydrated pollen protoplasts 66
4.2.1.3. The absence of AtTMEM16 and SLAH3 channels, but not ALMT12, generates higher $I_{initial}$ 69

4.2.1.4. Disruption of AtTMEM16 and SLAH3 channels generates higher current loss by Rundown for depolarizing V_m 71
4.2.1.5. AtTMEM16, SLAH3 and ALMT12 channels are sensitive to NPPB 75
4.2.1.6. The absence of ALMT12 channel causes a significantly decrease in the backward conductance 79
4.2.1.7. The double mutant almt12$^{-/-}$;slah3$^{-/-}$ causes a significantly decrease in all currents analyzed, Iinitial, I_{Final}, I_{LostRD} and $I_{LostNPPB}$ 81
4.2.1.8. Disruption of different anionic channels results in different biophysical properties in the overall current 83
4.3. Regulation of Anionic Currents by GABA 85
4.3.1. Muscimol reduces tube elongation in vitro, and bicuculline antagonizes muscimol regulation 85
4.3.2. 500 µM GABA reduces anionic currents in the wild type, but not in the mutant line almt12$^{-/-}$ 86
4.3.3. Anionic currents showed higher inhibition between 200 µM to 500 µM GABA 91
4.5. Heterologous expression of *Arabidopsis* ALMT12 transporter protein in COS-7 mammalian cell line 92
4.5.1. ALMT12 transporter shows inward and outward currents in COS-7 cells 93
4.5.2. GABA regulates ALMT proteins activity in COS-7 cells 95
4.6.. Vibrating Probe Analyses of the 4 anion transporter mutants 95
4.7. Anionic Transporter Localization 98

5. Discussion 106
5.1. Electrophysiological characterization of atccc$^{-/-}$, almt12$^{-/-}$, slah3$^{-/-}$, and attmem16$^{-/-}$ single mutants and almt12$^{-/-}$; slah3$^{-/-}$ double mutant 106
5.2. Currents of Lily germinated pollen 112
5.3. Localization of the 4 anionic transporters in the tube 112
5.4. The GABA effect in the anionic currents from WT hydrated protoplasts 114
5.5. An integrated view of Anion tramsport and regulation in pollen tubes 119

6. Annex 1 122

7. Bibliography 127

ACKNOWLEDGMENTS

Dedicated to my dearest friend (and boss) Ana Bicho, hope you don't mind but I am taking care of your parents, whom I took as my own family.

To my family, my husband António and my lovely baby daughter Cecília whom I love so much, my parents and parents in law.

To my patch clamp buddies, couldn't make this trip without you. You will have a special place in my heart forever.

To all my precious friends and group colleagues.

To Faculdade de Ciências Médicas da Universidade de Lisboa, and to Gulbenkian Institute of Science for having me as a PhD Student.

And to the FCT for the fellowship, and FCUL for the PhD extension scholarship.

And last but not least, to my courageous supervisors, Prof. José Feijó and Prof. Jorge Marques da Silva, I thank you for your patience and guidance.

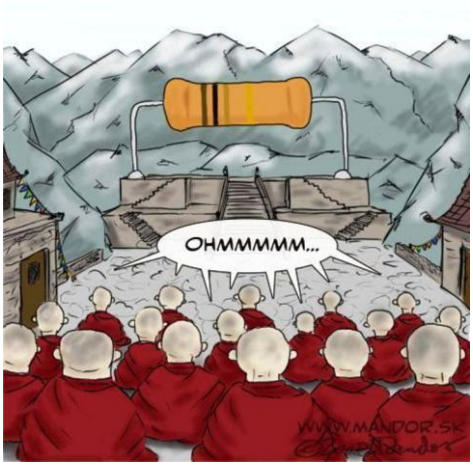

"Join the Resistance"

1. Introduction

Plants are one of the most important groups of living organisms on Earth. They serve as the conduit of energy into the biosphere, provide food, and shape our environment (Ehrhardt & Frommer, 2012). They are sessile, and because of this, they have developed ways to adapt to their surroundings, obtaining nutrients from the soil and air and surviving in extreme adverse environmental conditions. Plants have also acquired robust defense mechanisms against pathogens and herbivores. Their study is essential to comprehend how different wirings can create such fundamental differences in form, biochemistry, and function (Ehrhardt & Frommer, 2012).

1.1. Flowering Plant Reproduction – they do it too

Flowering plants changed land conditions during the Cretaceous period approximately 100 million years ago to suit their own needs, and, their rapid dissemination led to improved edibility of the leaves and fruits which ultimately, opened the way to the rapid evolution of mammals (Berendse & Scheffer, 2009). Angiosperms, or flowering plants, cover almost every terrestrial ecosystem, making them the most successful group of land plants. This evolutionary success is due, in part, to their sophisticated reproductive biology centered on the eponymous flower. In this structure the female gametophyte is hidden and protected by the sporophyte carpel/pistil (Hiscock, 2011). Flowers have a wide array of colors, shapes, and smells, all of which are for the purpose of attracting pollinators. Thus fertilization no longer requires water since it depends on the male gametophyte, the pollen grain, a highly specialized organ that uses animals and wind as vectors, and later germinates to produce the pollen tube, one of the fastest growing cells in nature, that carries the sperm into the ovules.

In higher animals, meiosis produces eggs and sperm directly. The sexual life cycle of vascular plants is more complex (Holsinger, 2000). Fertilization, besides its obvious role in genetic recombination, essentially denotes the fusion of the egg and sperm to form a zygote, in a coordinated manner to initiate seed development. Unambiguous proof of the actual fusion of the male and female gametes embodied in fertilization in flowering plants came in the late 19th century by two independent discoveries by Sergius Nawashin and Léon Guignard (Raghavan, 2006). Both authors showed that, in ovules of several Liliaceae plants, both male gametes from the pollen tube penetrated the embryo sac. One fuses with

the egg cell producing the embryo, and the other fertilizes the central cell to develop the endosperm, which protects the embryo and regulates trophic interactions between the embryo and the mother (Raghavan, 2006; Berger et al., 2008).

1.2. The Pollen Tube

In flowering plants the embryo sac (female gametophyte) resides within each ovule, and is typically composed of seven cells: an egg cell, a central cell, two synergid cells, and three antipodal cells. In contrast, the male gametophyte – the pollen grain – is either bi- or tricellular at maturity, depending on the species, with the generative cell or the two sperm cells being enclosed entirely within the cytoplasm of the vegetative cell (McCormick, 2007). After landing on the stigma, pollen grains germinate and develop a tube, a cytoplasmic extension that grows through the pistil into the ovule through an opening called the micropyle. The tube then, penetrates the ovule and bursts, releasing the two sperm cells. They will randomly fuse, one with the egg cell to form a zygote, the other will fuse with the central cell to form the primary endosperm cell (McCormick, 2007; Hamamura et al., 2011).

Therefore, the pollen grain function is to germinate, and produce a tube that elongates and redirect itself, deriving nutrients and directional cues from the female tissues, to target the female gametophyte. Elongation is achieved by apical growth, a form of growth specific of pollen tubes and roots hairs in plants, most fungal hyphae and some developing neurites (Cheung & Wu, 2008). Growth is rapid and polarized, restricted to the narrow apical zone, and is supported by an elaborate and dynamic actin cytoskeleton and a highly active membrane trafficking system that together provide the driving force and secretory activities needed for tip growth. Polarization is accompanied by an asymmetric distribution of cellular organelles that move through cytoplasmic-streaming in a reverse-fountain pattern i.e. they move towards the tip along the edge of the tube, there reverse direction and flow towards the grain through the centre of the tube. At the apex it is possible to visualize, through light microscopy, a smoother cytoplasmic region usually refers as the clear zone. This zone is almost exclusively occupied by transport vesicles (Cheung & Wu, 2007).

As the tube elongates, periodic callose deposition occurs distal to the migrating cell front, restricting the pollen protoplast to the apical region of the elongating tube (Cheung & Wu, 2008). Degradation of starch granules and lipid bodies provides the initial energy and cell wall material during germination and growth of pollen tubes (Nakamura & Miki-Hirosige, 1982). These metabolic processes may be necessary to maintain continuing turgor

pressure. Benkert et al., (1997) demonstrated that there is no linear correlation between turgor pressure and cell enlargement, but a minimum intracellular turgor is needed for pollen growth.

Remarkably, the distribution of specific molecules and proteins, organelles and physiological processes allows spatial cytoplasmic differentiation along the length of the pollen tube. This architecture is thought to be related to an intricate ion dynamics, namely tip-focused Ca^{2+} and H^{+} concentration gradients (Feijó et al., 1995; Michard et al., 2009). When germinating *in vitro*, all of the above physiological parameters may oscillate along with growth rate. Therefore, pollen tubes provide a cell growth model system that impacts our overall knowledge on tip growth, cell expansion, proliferation, and differentiation (Cheung & Wu, 2008; Kroeger & Geitmann, 2012).

1.3. Ion Dynamics during Pollen Tube Growth

The pollen tube cell is one of the fastest growing plant cell types known in nature. *In vitro*-grown pollen tubes of Lily and *N. tabacum* grow at an average speed of 200–300 nm/sec, and ~25–30 to ~80–100 nm/sec, respectively (Cheung & Wu, 2008). In *Arabidopsis* extension lengths *in vitro* go up to 800 µm within the first 6 hours of growth (Cheung & Wu, 2008). Thus, pollen tube elongation and navigation has a very high energy demand, which includes the balancing of the ATP/NAD(P)H ratio, by malate valves and NAD^{+} biosynthesis, and the regulation of several other different ions, notably calcium and protons (Holdaway-Clarke & Hepler, 2003; Selinski & Scheibe, 2014). Moreover, the passage of ions across membranes is a fundamental process of cellular energetics. Ions mediate the interconversion of chemical, osmotic, and electrical forms of biological energy, and they support a range of physiological functions, including active transport and motility (Sze et al., 1999). They also participate in the self-incompatibility response of some species (Holdaway-Clarke & Hepler, 2003). In order to do so, pollen tubes must have by default an efficient ion transport system at the plasma membrane. Extension of the tube increases its volume through water and solute influx into the cell and accumulation into its expanding vacuole, which implies the corresponding entry of specific ions to compensate the charge balance of the newly acquired or synthesized molecules (Michard et al., 2009).

The use of non-invasive methods, namely the extracelluar vibrating ion-probes, has demonstrated a close link between the intracellular ion fluctuations and ionic fluxes across the plasma membrane, and the cellular phenomena undergoing during formation and

elongation of the pollen tube (Mascarenhas, 1993; Feijó et al., 1995, 2001; Cheung, 1996; Hepler et al., 2001; Feijó et al., 2004). Further improvements to this method, specifically the use of selective ionophores and advances in imaging techniques and in the development of fluorescent molecules, allowed a deeper understanding of the ionic fluxes and the discovery of the respective intervening intracellular ionic gradients. Both phenomena are essential for pollen tube growth as they were found to oscillate with a similar period as that of growth, though with distinct phase delays (Holdaway-Clarke et al., 1997; Messerli et al., 1999; Feijó et al., 2001; Zonia et al., 2002; Holdaway-Clarke & Hepler, 2003; Certal et al., 2008; Michard et al., 2008; Gutermuth et al., 2013).

The pollen tube was shown to behave as an electrical dipole, with outward (positive charges) currents arising from the grain, and inward currents leaking into the apical parts of the tube (Michard et al., 2009). Non-oscillatory ionic fluxes from typical permeable ions in cells, such as H^+, Ca^{2+}, K^+ and Cl^-, were observed from the grain and along the tube shank, while the tip zone, in most species, displays distinctive oscillatory fluxes for the same ions. Likewise, oscillatory H^+ and Ca^{2+} and Cl^- gradients have been shown to exist and to be intimately associated with polarized pollen tube growth and orientation, including the existence of a constitutive alkaline band in the clear zone and a growth dependent acidic tip (Holdaway-Clarke et al., 1997; Feijó et al., 1999; Gutermuth et al., 2013).

1.3.1. Calcium (Ca^{2+}) Fluxes

Measurements of the extracellular flux of Ca^{2+} using an ion-selective vibrating electrode revealed a tip-directed Ca^{2+} influx in growing pollen tubes of up to 20 pmol cm^2 s^{-1} (Kühtreiber & Jaffe, 1990; Holdaway-Clarke et al., 1997; Messerli et al., 1999). Disruption of the cytoplasmic Ca^{2+} concentration ($[Ca^{2+}]_{in}$) gradient invariably resulted in cessation of *L. longiflorum* pollen tube extension, while inhibition of elongation by various means resulted in a concomitant dissipation of the gradient (Pierson et al., 1994). These studies demonstrated that there is a close coupling between the intracellular tip-focused gradient, the extracellular tip-directed influx, and the elongation of the pollen tube. Several groups have detected the presence of Ca^{2+} tip focused gradients (Obermeyer and Weisenseel, 1991; Rathore et al., 1991; Miller et al., 1992; Malhó et al., 1994; Pierson et al., 1994; Messerli & Robinson, 1997; Holdaway-Clarke et al., 1997; Messerli et al., 1999, 2000; Michard et al., 2009, 2011). The tip focused intracellular Ca^{2+} gradient was firstly examined with fura-2-dextran in *L. longiflorum* growing pollen tubes, with values estimated to range from 3 μM (at the tip) to 200 nM (basal $[Ca^{2+}]$ in level reached 20 μm from the tip) (Rathore et al., 1991; Miller et al.,

1992; Pierson et al., 1994, 1996; Holdaway-Clarke et al., 1997).Later, aequorin, a bioluminescent $[Ca^{2+}]_{in}$ indicator with a better range, was used In *L. longiflorum* and the magnitude of the $[Ca^{2+}]_{in}$ at the tip oscillated in the 3 - 10 μM range, and that its peak was 4 sec delayed in relation to the growth oscillation peak (Messerli et al., 2000).

The influx of Ca^{2+} at the tip, observed in *L. longiflorum* pollen tubes, were shown to oscillate from 1.4 to 14 pmol cm^{-2} s^{-1} (Miller et al., 1992; Pierson et al., 1994), and presented an 11 sec delay in relation to the tube growth (Holdaway-Clarke et al., 1997; Michard et al., 2009; Pierson et al., 1996). Michard et al. (2008) studied the Ca^{2+} apical gradient in *N. tabacum* pollen tubes, by means of the fluorescent genetic probe YC3.1 yellow CaMeleon, coupled to confocal microscopy. A V-shaped gradient extending from the tip to 40 μm into the tube was visualized. The $[Ca^{2+}]_{in}$ at the tip varied from 0.2 to 1 μM with a period of 1 to 4 min. A strong Ca^{2+} influx at the tip, which oscillated between 2 and 50 pmol cm^{-2} s^{-1}, and a small nonoscillatory efflux, approximately 100 μm down the shank of the tube, were also observed.

1.3.2. Proton (H^+) Fluxes

H^+, like Ca^{2+}, enters through the tip (Feijó et al., 1999; Messerli et al., 1999; Robinson & Messerli, 2002; Certal et al., 2008; Michard et al., 2008). H^+-selective vibrating electrode and ratiometric widefield fluorescence microscopy allowed observation for the first time of H^+ fluxes and intracellular distribution of pH in pollen tubes from *L. longiflorum*, respectively. The pollen tubes presented a constitutive alkaline band at the base of the clear zone and an acidic area at the tip. The distribution of the H^+ fluxes agreed with the intracellular H^+ gradient, with an oscillating H^+ influx at the tip, that varied between 0 and 4 pmol cm^{-2} s^{-1}, and a non-oscillating efflux in the region that corresponds to the alkaline band (Feijo et al., 1999). Furthermore, the intracellular gradients of $[H^+]$ were shown to be intimately associatiated with growth and with the spatial organization of the organelles in the cytoplasm, namely in the correlation of the alkaline band with the apical clear zone (Feijo et al., 1999).

Michard et al. (2008) studied the H^+ fluxes and the respective intracellular concentration ($[H^+]_{in}$) gradients in pollen tubes from *Nicotiana tabacum*, the latter by means of the fluorescent genetic probe pHluorin. Changes in the pH manifested itself up to 40 μm along the tube, from between 6.6 and 7.2 (at the tip) to between 7.2 and 7.7 (at 35 μm from the tip). This gradient intensity displayed 1–4 min period oscillations and is reduced in the non-

growing phase of an oscillatory cycle. Some of the pollen tubes observed presented a narrow alkaline region appressed to the plasma membrane of the tube's shank, most likely representing a ring-shaped area close to the membrane (Michard et al., 2008).

1.3.3. Potassium (K^+) Fluxes

K^+ fluxes across the plasma membrane of the pollen tubes have been associated with the control of the turgor pressure and the plasma membrane potential (Holdaway-Clarke & Hepler, 2003). A strong oscillating K^+ influx, varying between 0 and 690 pmol cm^{-2} s^-1 at the tip of pollen tubes from *L. longiflorum* were detected with a K^+- selective vibrating electrode (Messerli et al., 1999). The authors suggested that the transport of K^+ could be facilitated by a H^+:K^+ cotransporter, since both cations shared equally high oscillating influxes (H^+ influx of 0 to 490 pmol cm^{-2} s^{-1}) (Messerli et al., 1999). However, no other coupled fluxes able to drive and balance these charge fluxes were mentioned, implying various biophysical incongruences. Our group has intensively worked on K^+ fluxes around pollen tubes, and the reproducibility of these tip influxes remains challenging, because of the relatively poor performance of the K^+-selective electrodes, fluxes of this ion are not always detected (Michard et al., 2009). It is noteworthy that the experiments published were performed using the ion-vibrating probe technique, with very high buffer (MES, 5 mM), but more importantly, high K^+ backgrounds (possibly over 3 mM) (Michard et al., 2009).

1.3.4. Chloride (Cl^-) Fluxes

In particular, the participation of anionic fluxes in the formation and growth of the pollen tube has remained controversial since the first germination studies performed in the 70's. The nature of the anionic fluxes observed with extracellular electrodes during the past decade and the reliability of the measuring method has also been a source of debate–(Messerli et al., 2004; Hepler et al., 2006; Tavares et al., 2011b). Pollen tubes are one of the plant cells better explored in terms of chloride biology (Zonia et al., 2002; Breygina et al., 2009). $Cl^–$ fluxes in growing pollen tubes from *L. longiflorum* and *N. tabacum*, were first described by Zonia et al., (2002) by means of the ion-specific vibrating probe. Strong oscillatory $Cl^–$ efflux occurs specifically at the tube apex (50–8000 pmol cm^{-2} s^{-1} in *Lilium* and 400–1200 pmol $cm^{-2}s^{-1}$ in *N. tabacum*) with a period of 13.2 and 105 s, respectively. The remainder of the tube shank showed a non-oscillatory influx. In *N. tabacum*, this influx started at ~12 µm from the tip and peaked at ~26 µm from the tip (4000 pmol cm^{-2} s^{-1}; Zonia et al., 2002). These $Cl^–$ fluxes were further confirmed by the use of known $Cl^–$ channel blockers Disodium 4,4′-

diisothiocyanatostilbene-2,2′-disulfonate (DIDS), niflumic acid (NA), and 5-Nitro-2-(3-phenylpropylamino)benzoic acid (NPPB). These compounds not only completely inhibited *N. tabacum* pollen tube growth, but also induced an increase in apical volume. Furthermore, DIDS did not affect cytoplasmic streaming, but disrupted the Cl^- efflux. Inositol-3,4,5,6-tetrakisphosphate [Ins(3,4,5,6)P4], a known Ca^{2+}-activated Cl^- conductance blocker (Carew et al., 2000), inhibited pollen tube growth, induced cell volume increase, and interrupted Cl^- efflux. These effects were specific for Ins(3,4,5,6)P4, the close analogues Ins(1,3,4,5)P4 and Ins(1,3,4,5,6)P5 having no significant effect on these parameters. The Cl^- efflux oscillation was coupled to and temporally in phase with the growth oscillations. All these data indicated a role for Cl^- fluxes in osmotic homeostasis and apical growth regulation in pollen tubes (Zonia et al., 2002; Tavares et al., 2011b).

Further evidence supporting the existence of Cl^- fluxes in growing pollen tubes was provided by several reports from different research groups (Matveyeva et al., 2003; Breygina et al., 2009; Breygina et al., 2010; Tavares et al., 2011a). The use of different anion blockers inhibited pollen germination and significantly reduced Cl^- efflux from the grain, which suggested the sensitive anion channels were involved in the activation of pollen grains during germination (Matveyeva et al., 2003). During pollen germination, the plasma membranes of *N. tabacum* and *L. longiflorum* become hyperpolarized and an uneven potential distribution on pollen grain and tubes occurs (Breygina et al., 2009). Interestingly, it was later found, via fluorescence microscopy and flow cytometry, that NPPB completely blocked pollen tube growth in *N. tabacum* but caused no increase in its diameter, while DIDS induced pollen tube swelling and bursting; isolated pollen mitochondria treated with DIDS showed hyperpolarized membranes and a variation in reactive oxygen species content and excretion (Breygina et al., 2010). This study suggested that pollen tube growth is dependent on the activity of different anion channels, namely in localization and function (Breygina et al., 2010). Regardless of the overwhelming evidence supporting the existence of Cl^- fluxes, these have been involved in controversy for a long time. Of note, Messerli et al., (2004) attempted to create a number of experimental conditions to dismiss a role for Cl^- in pollen tube, claiming that the electrodes used in Zonia et al., (2002), were poorly selective for Cl^- over other anions and that the electrode could indirectly detect H^+ gradients. Nevertheless, these authors obtained the same results and were unable to dismiss the pharmacological evidence presented by Zonia et al., (2002) (Moreno et al. 1997; Michard et al., 2009).

1.4. Pollen Transporters

Cell shape and sub-cellular polarization in plants are central issues that often arise from the studies of pollen tubes and root hairs. The study of ion transporter systems address these questions because of the polarization of fluxes, intracellular free ion concentration, and sub-cellular localization. Furthermore, compelling evidence has shown the involvement of ion transporters in cell organization, presumably through the control of polarization via signaling networks, and in organ physiology, namely allowing a fast growth and rapid uptake of ions in plants (Michard et al., 2009; Tavares, et al., 2011). The transcriptome of *Arabidopsis* pollen grain and tube has been described (Becker et al., 2003; Honys & Twell, 2003, 2004; Pina et al., 2005; Wang et al., 2008; Loraine et al., 2013). Its analysis has shown the expression of at least 459 possible transporter genes, some being pollen specific.

Fertilization initiates when mature pollen grains adhere to the papillae cells of the stigma and are recognized through specific and selective biding. After recognition and compatible pollination takes place, the pollen hydrates and germinates. Several transporters have been linked to pollen grain and tube development.

Efficient sugar transport is needed for pollen development and to support the high metabolic activity of pollen tubes as they grow through the pistil; failure of this transport results in male sterility (Cheng et al., 2015). Sucrose and hexose transporters have been shown to play a major role in pollen tube development, e.g. AtSUC1 (*Arabidopsis* proton-coupled sucrose uptake transporter, highly expressed in pollen), and CsHT1 (hexose transporter from cucumber) (Sivitz et al., 2008; Cheng et al., 2015). Furthermore, two reports disclosed functions of two Mg^{2+} transporters in pollen development in *A. thaliana*. The disruption of either Mg^{2+} transporter led to pollen abortion due to lack of fertility, shown through crossing experiments for one of the mutated transporter alleles (Li et al., 2008; Chen et al., 2009). Interestingly, the ATP-binding cassette (ABC) transporters, a highly conserved protein super-family that uses the energy released in ATP hydrolysis to transport substrates, as also linked to pollen maturation (Kuromori et al., 2011; Yadav et al., 2014). 5 of the 130 genes from the ABC transporter family are pollen enriched and 3 are pollen specific (Pina et al., 2005; Becker & Feijó, 2007; Song et al., 2009), but the function and location of these putative transporters in pollen growth is unknown. To date only two genes, *AtMRP1* and *AtMRP2* (*Arabidopsis* ATP binding cassette transporter 1 and 2), were associated with anionic transport in plants, none of which is expressed in pollen (Pina et al., 2005). AtMRP1

was reported to promote accumulation of folates in the vacuole (Raichaudhuri et al., 2009), while AtMRP2 was found to contribute to cell detoxification and to chlorophyll degradation, and to transport organic anions into the vacuole (Frelet-Barrand et al., 2008).

There has been a continued effort in the identification of possible ion transporters underlying the detected macroscopic fluxes in growing pollen tubes. Ion transporters are both involved in signaling, *via* Ca^{2+} and H^{+} or membrane potential and in cell growth, by permitting the accumulation of ions inside the cell, and/ or promoting turgor pressure (Holdaway-Clarke & Hepler, 2003; Michard et al., 2009; Song et al., 2009). As mentioned, the different spatial patterning of Ca^{2+} and H^{+} as second messengers seem to play a role in the pollen tube polarization and spatial organization of the tip domain (Michard et al., 2009).

1.4.1. Calcium (Ca^{2+}) Transporters

The use of Ca^{2+} channel inhibitors disrupts pollen tube growth and dissipate the steep tip focused Ca^{2+} gradient, demonstrating that the Ca^{2+} gradient is apparently triggered by its influx at the tip (Reiss & Herth, 1985; Obermeyer & Weisenseel, 1991; Malhó et al., 1995). Ca^{2+} channels in the plasma membrane from pollen tubes were first postulated in 1985, by use of nifedipine, a well known Ca^{2+} channel blocker, on germinating pollen and on pollen tubes from *Lilium longiflorum* (Reiss & Herth, 1985). The application of Lanthanum (La^{3+}), vanadate and compound 48/80 were suggestive of the existence of calmodulin-dependent Ca^{2+}-ATPases in pollen tube tips (Obermeyer & Weisenseel, 1991). Under hypertonic conditions both the gradient and fluxes of Ca^{2+} were abolished in Lily pollen tubes, suggesting the involvement of stretch activated Ca^{2+}-channels present at the tip (Pierson et al., 1994). A voltage-gated Ca^{2+}-channel was reported that might be involved in pollen tube reorientation in *Agapanthus umbellatus* (Pierson et al., 1994; Malhó et al., 1995). In addition, two stretch-activated Ca^{2+} channels were reported in pollen and pollen tube tip protoplasts from *Lilium longiflorum* (Dutta & Robinson, 2004). Ca^{2+} currents activated by hyperpolarization have also been described in pollen grains of *Lilium davidii* and *Arabidopsis*, and in *Pyrus pyrifolia* tube protoplasts (Shang et al., 2005; Qu et al., 2007; Wu et al., 2007; Michard et al., 2009). All currents showed similar characteristics, including inhibition by trivalent ions. The genetic identity of these hyperpolarization-activated Ca^{2+} permeable and stretch activated channels has yet to be determined or reproduced by other labs.

The *Arabidopsis* genome encodes 14 Ca^{2+} pumps, 10 of which belong to a family of autoinhibited Ca^{2+} ATPases (ACA) that are predicted to be activated by Ca^{2+}/calmodulin. *Arabidopsis* mutants defective in a plasma membrane–associated Ca^{2+}-ATPase (ACA9) are male deficient, and show reduced seed sets and reduced pollen tube growth rates *in vitro* (Schiøtt et al., 2004; Cheung & Wu, 2008). Remarkably, the molecular identity of two of the channel classes responsible for generating the changes in $[Ca^{2+}]_{cyt}$ has been uncovered. Through pharmacological and loss-of-function mutants in *N. tabacum* and *Arabidopsis*, Michard et al., (2011) showed that glutamate receptor-like channels (GLRs) facilitate Ca^{2+} influx across the plasma membrane, and modulate apical $[Ca^{2+}]_{cyt}$ gradient, which consequently affects pollen tube growth and morphogenesis. A putative gene family of non-specific cation channels, CNGC (Cyclic Nucleotide Gated ion Channel) was also found in the *Arabidopsis* genome. CNGC7, 8, 9, 10 and 16 are expressed in pollen, but their cellular localization and function has yet to be established. Interestingly, CNG18, was shown to be specifically expressed in pollen of *Arabidopsis thaliana*, and localized in the plasma membrane of growing pollen tube tips; loss of function of this protein caused male sterility by pollen tube growth disruption (Frietsch et al., 2007).

1.4.2. Proton (H^+) Transporters

Protons are actively pumped out of the tube at the sides (corresponding with the alkaline band found in *Lilium*) and passively permeated everywhere else (Feijo et al., 1999). Using *Nicotiana tabacum* as a model, Certal et al., (2008) cloned a pollen plasma membrane H^+-ATPase (Nt AHA). In growing pollen tubes, Nt AHA were shown to be absent from the apical domain but present in the shank plasma membrane region of the tube which corresponded to the location of an alkaline domain in the cytoplasm (Certal et al., 2008). In addition, localized applications of the cation ionophore gramicidin A had no effect where Nt AHA was present but acidified the cytosol and induced reorientation of the pollen tube where Nt AHA was absent. Remarkably, pollen overexpressioning Nt AHA-GFP developed the formation of abnormal, irregular callose plugs accompanied by abnormal H^+ flux profiles, proving the involvement of the Nt AHA in callose plug formation (Certal et al., 2008). The family of genes encoding plasma membrane H^+-ATPases in *Arabidopsis* has 11 members (Pina et al., 2005). Of these 11 only AHA3 was confirmed to be essential for pollen development (Robertson et al., 2004; Song et al., 2009).

1.4.2. Potassium (K^+) Transporters

Several studies detected K^+ currents with different characteristics by the patch-clamp technique (Weisenseel & Jaffe, 1976; Fan et al., 2001; Mouline et al., 2002). This technique allowed the identification of inward and outward K^+ channels in pollen grain protoplasts and pollen tube protoplasts (Obermeyer & Kolb, 1993; Fan et al., 1999, 2001, 2003; Griessner & Obermeyer, 2003; Qu et al., 2007; Wu et al., 2011). K^+ regulates several basic cellular parameters, such as turgor and membrane potential during pollen tube growth (Holdaway-Clarke & Hepler, 2003). It was shown that the functional expression of the Shaker Pollen Inward K^+ channel (SPIK; also named AKT6) plays a role in K^+ uptake in the growing pollen tube, and thereby in tube development and pollen competitive ability (Mouline et al., 2002). Disruption (T-DNA insertion) of the SPIK coding sequence affected inwardly rectifying K^+-channel activity in the pollen-grain plasma membrane, resulting in impaired pollen tube growth (Mouline et al., 2002). Furthermore, a member of the *Arabidopsis* tandem-pore K^+ channel (TPK/KCO) family, TPK4, has a small contribution in the pollen tube K^+ conductance and function in the control of membrane potential (Becker et al., 2004). K^+ is also implicated in pollen tube bursting in maize, the channel Zea mays 1 (KZM1) is activated by defensin-like protein Embryo Sac 4 secreted from the synergid cells to facilitate K^+ influx and sperm release (Amien et al., 2010). Besides K^+ channels, two predicted cation/proton exchangers (CHX) in *Arabidopsis thaliana*, CHX21 and CHX23 expressed preferentially or specifically in the endoplasmic reticulum of pollen and pollen tubes may also play important roles in H^+ fluxes and K^+ homeostasis (Sze et al., 2004; Bock et al., 2006; Wang et al., 2008; Song et al., 2009; Lu et al., 2011). The *chx21 chx23* double mutant pollen grains germinated and grew tubes down the transmitting tract, but the tubes failed to target the ovule (Lu et al., 2011). As stated previously, H^+ enters the tip passively, and co-transporters and exchangers, namely members of the CHX transporters family may play an important role in H^+ fluxes at the tip (Cellier et al., 2004; Sze et al., 2004; Pina et al., 2005; Bock et al., 2006). Despite the identification of many cationic channels in pollen, the attempt to identify and to localize anionic channels has proved unsuccessful.

1.5. The Chloride Transport Conundrum

Chloride is a vital ion for all living forms and in most cells it appears to be linked to the transport of water. The most important genetic disease in humans, cystic fibrosis (CFTR), is caused by mutations on an ABC anionic transporter member. Higher plants, on the other hand, are absolutely dependent on the hydrodynamics of their cells to survive and adapt to

the sessile conditions they have evolved into. There is much information that suggests an equally important role for chloride as in humans, though shared with other plant ubiquitous anions, like ammonia and nitrate. Several anion channels have been reported in plasma membrane of plant cells. These have been associated with various processes in plants such as stomata closure, hormone signaling, membrane excitability, cellular osmoregulation, growth regulation and anionic nutrition (Barbier-Brygoo et al., 2000; Roberts, 2006; de Angeli et al., 2007; Tavares et al., 2011). Most of the described anion channels are inward rectifiers (channels through which the exit of anions from the cell is greater than its entrance). Some outward rectifiers have been detected in root cells and were suggested to be involved in repolarization of the membrane potential after sodium uptake by roots in saline soils (Roberts, 2006). The anionic selectivity of the channels found in plant membranes to NO^{3-} and Cl^{-}, as well as their pharmacology and regulation, varies according to species and cell type. Anions may thus play a vital role not only in the maintenance of the membrane potential, by preserving the electroneutrality and cell osmotic potential, but also by directly controlling important cellular events (Tavares et al., 2011). The cellular processes stated above have been proposed as the physiological effectors of the Ca^{2+} gradient (Roy et al., 1999; Parton et al., 2003; Becker et al., 2004; Hwang et al., 2005; Helling et al., 2006). Recently, a link between anions and Ca^{2+} homeostasis was observed by transient transformation of *N. tabacum* pollen grains with the $[Ca^{2+}]_{cyt}$ reporter Yellow-Cameleon YC3.6 (Gutermuth et al., 2013). Ca^{2+} concentration transients were shown to be strictly accompanied by growth oscillations if changes in the extracellular Cl^{-} concentration exceeded 10 mM. Furthermore, both the cytosolic anion and Ca^{2+} gradients were eliminated by the application of the anion channel inhibitor NPPB, which resulted in the immediate cessation of tube growth (Gutermuth et al., 2013). The authors suggested that a $[Ca^{2+}]_{cyt}$-dependent anion release at the pollen tube tip would generate a cytosolic anion concentration gradient, a notion that is further supported by the measurement of Ca^{2+}-dependent anion currents with the patch-clamp technique in both pollen grains and tube protoplasts (Tavares et al., 2011a). The signaling cascades downstream of Ca^{2+} are multiple (Malhó et al., 2006), and may imply phosphorylation through Ca^{2+}-dependent protein kinases (Yoon et al., 2006), small GTPases (Gu et al., 2005) or calmodulins (Rato et al., 2004; Berkefeld et al., 2010), and could plausibly regulate anionic currents. (Zonia et al., 2002; Tavares et al., 2011b). A link between Cl^{-} and Ca^{2+} ions was shown to involve an interaction of SLAH3 anion channels with the Ca^{2+}- dependent Protein Kinase 2 and 20 (CPK2/CPK20) (Gutermuth et al., 2013).

Plasma membrane anion channels play fundamental roles in plant tissues. The best known example is their involvement in stomata closure or nutrition, but not much is known of the cellular localization or molecular nature in pollen grain and pollen tubes. In recent years an effort was put forward to identify the putative anionic transporters involved in pollen tube physiology (Tavares et al., 2011a). The patch-clamp data on pollen protoplasts demonstrated, for the first time, the presence of three Cl^- conductivities with distinct regulation by $[Ca^{2+}]_{in}$ and external pH (Tavares et al., 2011a, Dias P., unpublished data). These channels may account for the large anionic effluxes previously reported by means of self-referencing vibrating probes. In the next subchapter a description of the anionic transporters candidates is given, in terms of their physiological involvement in different plant (and animal) tissues and biophysical properties.

1.5.1. Pollen Anion Channel/Transporter Candidates

1.5.1.1. Rapid- and Slow-type channels are key players in stomatal movement

Stomatal aperture is tightly regulated according to environment fluctuations, facilitating gas movement and limiting water loss. As water enters osmotically and increases guard cell volume, the cells swell and move apart, enlarging the stomatal aperture. On the other hand, salt loss upon anion channel activation causes the guard cells to shrink and the stomata to close. Guard cells have highly specialized ion transporters because, unlike in other plant tissues, ion transport occurs in both directions to allow for stomatal opening and closing (Roelfsema & Hedrich, 2005). Several types of plasma membrane anion channels or transporters have been positively implicated in stomatal movement. The best known are the anion channels that mediate anion efflux, which were first discovered in *V. faba* and were classified electrophysiologically as rapid [R-type or Guard Cell Anion Channel 1 (GCAC1), or outwardly rectifying anionic channel (ORAC)], or slow (S-type) anion channels (Roberts, 2006; Pandey et al., 2007). The two voltage dependent anion channels (R- and S-type) have been described in the guard cells of several other species, and were shown to co-exist at the plasma membrane of *V. faba* guard cells (Schroeder & Keller, 1992) and *Arabidopsis* hypocotyl cells (Frachisse et al., 2000). R- and S-type channels exhibit divergent properties not only in terms of voltage dependence, and activation and deactivation kinetics, but also in terms of selectivity, nucleotide regulation, and pharmacological sensitivity. This last one, in particular, is dependent on both species and cell type, which might indicate a variation in the nature of these channels (Keller et al., 1989; Schroeder & Hagiwara, 1989; Hedrich et al.,

1990; Schroeder et al., 1993; Schmidt & Schroeder, 1994; Pei et al., 1996; Tavares, et al., 2011b).

The R-type channel mediates a strongly voltage dependent activated anion current with rapid activation and deactivation kinetics, and the S-type channel mediates a weak voltage-dependent activated anion current, with slow activation and deactivation kinetics. Nevertheless both channel types show a higher permeability to NO^{3-} than to Cl^- and are characterized by a U shaped *I/V* (current–voltage) curve, the current amplitude of which peaks at V_m (membrane potentials) more negative than E^-_A (anion equilibrium potential). S-type channels show a peak that is substantially less pronounced and occurs at more positive V_m than in R-type currents, allowing a wider range of voltages in which this channel is open. Both have small to moderate unitary conductances. R-type channels are closed at hyperpolarizing V_m and open with the depolarization of the membrane. Functionally, S-type channels are responsible for the sustained anion efflux during stomata closure. They are highly regulated by phosphorylation, $[Ca^{2+}]_{in}$, ABA, and CO_2 or by switching off photosynthetic active radiation in *V. faba* (Schroeder & Hagiwara, 1989; Schmidt et al., 1995; Brearley et al., 1997; Roelfsema et al., 2002; Tavares et al., 2011b), *N. tabacum* (Marten et al., 2007, 2008), and *A. thaliana* guard cells (Pei et al., 1997; Allen et al., 1999). Marten et al., (2008) showed that Ca^{2+} signals enhance the degree of S-type anion channel activity during light–dark transition. Additionally, Colcombet et al., (2005), using the patch–clamp technique on *Arabidopsis* hypocotyl cells, reported that R-type and S-type anion channels at the plasma membrane were both regulated by pH via distinct mechanisms. This regulation via pH might occur in several signaling networks including anion fluxes and pH variations, such as those observed in response to pathogens or hormones. Furthermore, it constitutes a powerful argument in favor of the existence of two different channels, contradicting the hypothesis of Dietrich & Hedrich, (1994) which accounts for an interconversion from rapid to slow mode of a single channel (Tavares et al., 2011b).

The R-type anionic channels are involved in membrane excitability and auxin sensing. These channels are activated by nucleotide binding and $[Ca^{2+}]_{in}$ (Hedrich et al., 1990; Colcombet et al., 2001), and regulated by intracellular pH (SchulzLessdorf et al., 1996; Colcombet et al., 2005) and extracellular anions. Similarly, in *Chara corallina*, protons have a direct effect on Cl^- efflux during intracellular acidosis, suggesting that the regulation of anion channels by cytosolic pH plays a specific role in cytosolic pH regulation in plant cells by providing an anionic shunt conductance (Johannes et al., 1998). Particularly in the

presence of extracellular anions, including malate and Cl^-, which would accumulate in the apoplast during stomatal closure, the voltage regulation of guard cell R-type channels shifts to more negative voltages, contributing to membrane depolarization (Roelfsema et al., 2004; Roelfsema & Hedrich, 2005; Pandey et al., 2007).

1.5.1.1.1. Aluminum-activated Malate Transporter 12 – ALMT12. ALMTs were found to promote Al^{3+} tolerance in several cultivars of maize, by excreting into the root system Al^{3+}-chelating organic anions, such as malate and citrate, in response to Al^{3+} exposure. Al^{3+} was shown, by means of electrophysiological assays, to activate these channels in cortical cells in the maize root apex (Kollmeier et al., 2001; Piñeros & Kochian, 2001; Ward et al., 2009). Further evidence for the regulation of these channels by Al^{3+} was provided by the expression of ALMTs in *Xenopus* oocytes. This was enough to mediate Al^{3+} -induced malate currents, suggesting a direct Al^{3+} sensor role for ALMT transporters (Hoekenga et al., 2006). There are 14 predicted members of the ALMT channel family in the genome of *A. thaliana*. Of these only three, AtALMT1, AtALMT9, and ALMT12, have had their physiological role unraveled. AtALMT1 was found to be a plasma membrane Al^{3+}-activated malate transporter expressed in the roots, and was associated with Al^{3+} tolerance in *Arabidopsis* (Hoekenga et al., 2006). AtALMT9 is targeted to the tonoplast and mediates malate uptake into the vacuole (Kovermann et al., 2007; Tavares et al., 2011b).

Sasaki et al., (2010) using electrophysiological and loss-of-function mutation studies, showed that ALMT12 (a homologue of the Al^{3+}-activated malate transporter of wheat, TaALMT, in *Arabidopsis*) is an anion transporter, particularly permeable to Cl^- and NO_3^- , and a key regulator of stomatal closure, localized to both endomembranes and plasma membrane of guard cells of *A. thaliana*. Meyer et al., (2010) showed that ALMT12 represented the guard cell R-type anion channel, and was highly expressed in guard cells and allocated to the plasma membrane. Furthermore, expression of this protein in *Xenopus* oocytes rendered voltage-dependent anion currents, for which the voltage activation threshold is shifted towards more hyperpolarized potentials in the presence of extracellular malate. Plants deficient in this gene are impaired in stomatal closure induced by dark, CO_2 and abscisic acid (ABA), and their guard cell protoplasts display reduced R-type currents (Meyer et al., 2010; Tavares et al., 2011b).

1.5.1.1.2. SLow Anion channel Homolog 3 – SLAH3. Slowly activating anion efflux channels or S-type channels have been described in the guard cells of several species such as *V. faba, A. thaliana, N. tabacum*, and *Xanthium strumarium*, in the epidermal cells of *A.*

thaliana hypocotyls, and in *Coffea arabica* suspension-cultured cells. The molecular identity of the S-type channel activity in the plasma membrane of the guard cells from *A. thaliana* has been recently attributed to a distant homologue of fungal and bacterial organic acid transport proteins. The voltage dependent channel was designated SLAC1 for SLow Anion Channel (along with its homologues, carries out S-type anion channel activity in guard cells) and was found to be preferentially expressed in guard cells, and to be permeable to malate. This protein is fundamental for stomatal closure in response to CO_2, ABA, ozone, light/dark transition, humidity variation, elevation of $[Ca^{2+}]_{cyt}$, H_2O_2, and nitric oxide. Mutation in this protein results in an ozone-sensitive plant, with impaired S-type current activity, but with no change in R-type currents or Ca^{2+} channel activity (Negi et al., 2008; Vahisalu et al., 2008; Geiger et al., 2011; Tavares, et al., 2011b).

As mentioned, SLAH3 and ALMT12 channels are both localized to the plasma membrane in guard cells and are voltage dependent. The rapid anion flux variations associated with the pollen tube tip favor a passive anion channel–driven ion translocation mechanism rather than a carrier-driven transport. Transcripts of both channels were detected in *Arabidopsis* pollen tubes (Gutermuth et al., 2013). Hence, it is possible that the efflux of Cl^- observed at the tip of growing pollen tubes could be due to the activity of SLAH3 and ALMT12 channels.

1.5.1.2. The cation:chloride cotransporter (AtCCC)

The cation:chloride cotransporter (CCC) showed a preferential expression in the root and the shoot vasculature at the xylem–symplast boundary, root tips, trichomes, leaf hydathodes, leaf stipules, anthers, and pollen grains (Colmenero-Flores et al., 2007). Plants mutated for the AtCCC transporter presented shorter organs, inflorescence necrosis, reduced seed production, and defective Cl^- homeostasis under high-salinity conditions. In *Xenopus laevis* oocytes, *At*CCC proved to be a $1K^+$:$1Na^+$:$2Cl^-$ symporter, and its activity was inhibited by bumetanide (Colmenero-Flores et al., 2007). The physiological profile and the high expression in pollen of this transporter makes it a good candidate to explain the influx of Cl^- in the pollen tube (Tavares et al., 2011b).

1.5.1.3. The Calcium activated chloride currents (CaCC's) - AtTMEM16

CaCC's have first been described in salamander photoreceptors (Bader et al., 1982) and *Xenopus* oocytes (Miledi et al., 1982; Barish, 1983), and are implicated in important physiological functions. These include, membrane potential stabilization in photoreceptors of the retina, the secretion of fluids in glands and airway epithelia, the high-gain low-noise

amplification in olfactory transduction, taste adaptation, control of action potential waveform in neurons, and positive feedback regulation of smooth muscle contraction induced by G-protein coupled receptors that is important to control vascular tone or uterus contraction (Schroeder et al., 2008).

The hallmark feature of CaCC's in many native cells including *Xenopus* oocytes is the strong outward rectification at submaximal cytosolic calcium levels in the range of 0.2–5 μM, whereas the current-voltage relationship is linear at high calcium concentrations. This is normally explained by a calcium-binding site located in the electric field of the membrane, thereby facilitating calcium binding to the channel at positive voltages (Hartzell et al., 2005). Whereas CaCCs are likely activated by direct calcium binding in multiple cell types, such as salivary gland acinar cells and pulmonary endothelial cells, some CaCCs may be stimulated by the calcium-calmodulin dependent protein kinase CaMKII or other calcium-dependent mechanisms (Hartzell et al., 2005). Two independent teams successfully unraveled the molecular identity of endogenous CaCCs. Yang et al., (2008) selected Anoctamin-1 (ANO1), also known as Transmembrane member 16A (TMEM16A), by searching public domain databases for putative channels or transporter-like genes with multiple transmembrane domains and multiple isoforms. The expression of mouse ANO1 with endothelin receptor (ETA) in HEK 293T cells resulted in endothelin-induced Cl^- currents. The current presented the appropriate reversal potential for a Cl^- current; when extracellular Cl^- was replaced with gluconate it abolished the current; and it was blocked by low concentrations of classical Cl^- channel blockers (Yang et al., 2008). On the other hand, Schroeder et al., (2008) identified the CaCC subunit as the *Xenopus* TMEM16A (xTMEM16A) using oocytes from the physiologically polyspermic Axolotl as an expression system. The xTMEM16A current resembled the *Xenopus* oocyte CaCC, in its outward rectification, voltage dependence of calcium activation, and sensitivity to several chloride channel blockers. Furthermore, the expression of two mouse homologs, mouse TMEM16A (mTMEM16A) and mouse TMEM16B (mTMEM16B), generated CaCCs currents in axolotl oocytes with different kinetics, suggesting that different ANOs are likely to have different gating characteristics (Schroeder et al., 2008; Hartzell et al., 2009).

By applying patch-clamp whole cell measurements in *A. thaliana* and lily pollen protoplasts, our group demonstrated the presence of three Cl^- conductances with distinct regulation by $[Ca^{2+}]_{cyt}$ (Tavares, et al., 2011a). The strong outward rectification and the activation by intracellular Ca^{2+}, led to a search for a CaCC homologue in the *Arabidopsis* genome. A

sequence with a low similarity level was found and its theoretical protein structure topology analyzed, which made us include the AtTMEM16 channel as a strong candidate that could account, at least partially, for the observed currents.

1.5.1.4. The chloride channel (CLC) family

CLC proteins constitute anionic channels/transporters ubiquitously found in eukaryotes and prokaryotes (Mindell et al., 2001). The first member of this family to be characterized was the CLC-0, a voltage-gated Cl^- channel found in the electric organ of *Torpedo californica* (White & Miller, 1979). Mammalian CLCs are the best-known elements of this family, and they encompass both Cl^- channels, in the plasma membrane, and Cl^-/H^+ antiporters in intracellular compartments (Zifarelli & Pusch, 2007; Jentsch, 2009). In *A. thaliana* seven homologues, AtCLCa–g, have been identified (Hechenberger et al., 1996; Lv et al., 2009). According to Lv et al., (2009) these homologues form two distinct subclasses with a low similarity level (26–29%) between them. The first subclass is constituted by AtCLCa–d and AtCLCg and has greater similarity to other eukaryotic CLC subclasses, while subclass II, composed by AtCLCe and AtCLCf, has low homology to the other plant CLCs and is more closely related to prokaryote CLCs. The expression of the AtCLC family was studied and it was found to be ubiquitous both temporally and spatially, but with distinct expression patterns between the two subclasses. Lv et al., (2009) found that all members of the AtCLC family were predominantly expressed in the vascular tissues, especially those from subclass I, in both roots and shoots, implying a possible role for this family in long-distance ion transport within the plant. Strong expression of all AtCLCs, particularly AtCLCc, was also found in guard cells (Lv *et al.*, 2009) where they are involved in the regulation of stomatal movement and contribute to salt tolerance (Jossier et al., 2010). The specificity of this channel for NO_3^- has recently been found to be associated with a single amino acid residue, proline 160 (Wege et al., 2010). The cellular localization of CLCs placed them all in intracellular membrane systems: AtCLCa–c and g were localized in the tonoplast (De Angeli et al., 2006; Lv et al., 2009; von der Fecht-Bartenbach et al., 2010), while AtCLCd and f were targeted to Golgi vesicles (Marmagne et al., 2007; von der Fecht-Bartenbach et al., 2007; Lv et al., 2009), and AtCLCe was localized in the chloroplasts (Marmagne et al., 2007; Lv et al., 2009).

Two CLC transporters, AtCLC-c and AtCLC-d, have been found in the pollen transcriptome, with the former being pollen enriched. AtCLCc homozygous knockout mutants were found to present significantly lower NO_3^-, Cl^-, malate, and citrate concentrations than their wild-

type counterparts (Lv et al. 2009). This gene was also found to be down-regulated in the presence of NO_3^- (Harada et al., 2004). AtCLCd was co-localized with the VHA-a1 subunit of the V-type ATPase in the trans-Golgi network (TGN), suggesting that AtCLCd mediates the transport of an anion, Cl^- or NO_3^-, into the TGN to counter the pumping of H^+ by the V-ATPase (von der Fecht-Bartenbach et al., 2007). Their localization in the growing pollen tube is unknown.

1.6. Pollen Tube Regulation by gamma-amino butyric acid (GABA)

γ-Aminobutyric acid (GABA) is a four-carbon, nonprotein amino acid, that acts as a neurotransmitter to control the excitation and inhibition of the mammalian central nervous system (Yu et al., 2006). In animals, GABA operates through ionotropic $GABA_A$ and $GABA_C$ receptors, and through G-protein coupled metabotropic $GABA_B$ receptors. The $GABA_A$ receptor selectively conducts Cl^-, whereas the $GABA_B$ receptor mainly regulates K^+ and Ca^{2+} because it is a G protein-coupled receptor that can regulate Ca^{2+} and K^+ channels (Yu et al., 2006).

In plants, GABA levels are rapidly elevated in response to a range of abiotic and biotic stresses, including pathogen infection, wounding, cold and heat shock, drought and hypoxia (Lancien & Roberts, 2006). As a result, a number of roles in plants for GABA and the GABA shunt, the pathway in which it is synthesized, have been proposed (Lancien & Roberts, 2006). In plants, metabolism of GABA takes place in different cellular compartments: synthesis and degradation occurs in the cytosol and in the mitochondrion, respectively. GABA is synthesized from glutamine in a reaction catalyzed by the cytosolic enzyme glutamine decarboxylase (GAD; Bown & Shelp, 1997; Shelp et al., 2006). Subsequently, GABA is converted into succinic semialdehyde, and then to succinate, in reactions catalyzed by two mitochondrial enzymes, GABA transaminase and succinic semialdehyde dehydrogenase, respectively (Shelp et al., 2006). In plants, GABA has been mostly studied as a metabolite and is thought to function in the tricarboxylic acid cycle and C/N balance control (Shelp et al., 2006).

A role for GABA in pollen tube growth and guidance was proposed when Palanivelu et al., (2003) screened a mutant for the *Arabidopsis* POP2 (pollen pistil interaction 2) gene, which encodes a transaminase that degrades GABA and contributes to the formation of an increasing gradient from stigma to the mycropyle. *pop2* pollen tubes failed to grow on the pistil, because they were not able to degrade the excess of GABA, while wild-type pollen

tubes could grow in *pop-2* pistils, demonstrating that disruption of GABA degradation in *Arabidopsis* flowers caused aberrant pollen tube growth and infertility..Moreover, in vitro GABA was shown to stimulate pollen tube growth, although it had an inhibitory effect at high concentrations (Palanivelu et al., 2003). On the other hand, in *in vivo* assays, GABA alone, whether delivered from a filter disc or an agarose plug, was not sufficient to elicit any chemotactic response. This result suggests that other molecules may be involved in this process. Consequently, further analyses of the molecular intervenients in this signaling pathway were warranted (Palanivelu et al., 2003; Boavida et al., 2005).

1.7. The Patch Clamp Technique

In the fifties Alan Hodgkin and Andrew Huxley studied macroscopic ion fluxes in giant squid axon (Hodgkin & Huxley, 1952). The experiments led to the ion channel concept formulation (unit conductivity in biological membranes) and the establishment of their importance in pulse generation and signal propagation in excitable cells (Liem et al., 1995). The first physical evidence of ion channels in living cells came in the seventies, through the application of the patch clamp technique, introduced by Erwin Neher and Bert Sakmann (Neher & Sakmann, 1976). They were able to detect unitary currents in frog muscle fibers by applying the neurotransmitter acetylcholine in the medium, and measure their amplitude and duration. The development of this technique and its results gave its creators the Nobel Prize for Medicine and Physiology in 1991 (Neher & Sakmann, 1992). The principle of this method is to isolate a snip of membrane from the extracellular solution and record the current flowing through this membrane portion. This is achieved by pressing a glass pipette (a micropipette, which functions as an electrode), which is filled with a given saline solution, against the surface of the cell and applying slight suction (Liem et al., 1995). A seal with an electrical resistance higher than a gigaohm (GΩ) is then formed between the two surfaces. The high resistance seal enables the acquisition of low electrical noise records (Ashley, 1996) and the measurement of currents in the order of picoamperes (10^{-12} A) (Ogden & Stanfield, 1988). The reduction of noise is due to the gigaseal condition that lowers the level of current that passes between the pipette and the extracellular solution (Ashley, 1996). Nowadays, patch clamp studies are well diversified, allowing the classification of different types of ion channels in different cell types and characterization of their biophysical properties in terms of conductance, voltage dependence, selectivity, open probability and pharmacological profile (Ashley, 1996).

1.7.1. Membrane Potential

The electrical properties of a cell are mainly derived from its membrane, more specifically its lipids and proteins. Thus, the patch clamp recordings are based on electrical and physical principles. The predominant equation which pervades the study of electric circuits is Ohm's law (I = V/R), a powerful predictor of the relationship in a conductor between, electric potential difference (V, volts), current I (A, ampere), and the resistance of the conductor (R, Ohm). In electrophysiology, is often preferable to use the conductance G (S, siemens), which is the inverse of resistance (G = 1/R). On the other hand, the circulation of ions across the membranes provides a fundamental source of energy to the cell, through their key role during respiration and photosynthesis (Sze et al., 1999).

All cells have a charge separation across the plasma membrane, which acts as capacitor and a barrier to ion diffusion. The transmembrane potential, or voltage, is usually referred to as membrane potential (V_m), and it refers to the difference in electric potential between the interior and the exterior of a biological cell, with an excess of positive charges on the extracellular side and an excess of negative charges on the intracellular side. In plant and fungal cells, the negative membrane potential inside is generated by transport of H^+ ions out of the cell by an ATP-powered proton pump. The proton motive force generates a proton electrochemical gradient (-120 to -160 mV relative to the outside, resting potential) which provides stored energy for the uptake and release of solutes via symporters, antiporters and channels (Sze et al., 1999).

The polarization across a membrane is altered whenever the charge separation is disturbed, either by activation of an active transport or by imposition of a potential to the membrane through an external electrical circuit to the cell. When the membrane potential becomes more positive than the resting potential, there is a depolarization of the membrane, whereas the opposite is called hyperpolarization. By convention, the direction of current is set with the direction of flow of positive charges. Thus, the exit of positive charges or entrance of negative charges from a cell is referred to as positive current (outward current). In contrast, negative currents (inward currents) correspond to positive charges entering the cell (or the exit of negative charges) (Koester, 1991).

1.7.2. Electrical equivalent circuit of cell membrane

The electrical properties of ion channels, the equilibrium potentials of permeable ions and the accumulating charge capacity of the membrane, can be represented as components of

an electrical equivalent circuit (Figure 1). The bilipidic membrane is represented by a capacitor, since it is an excellent insulator due to its phospholipid composition. The capacitance (C) is measured in Faraday, and quantifies the membrane's ability to store charge (Q) when a potential is applied to the cell. The ion channels are responsible for most of the electrical conductance of a cell and are represented by a resistance (R) in parallel with the capacitor. Both are in series with a battery (which is the electromotive force for each ion).

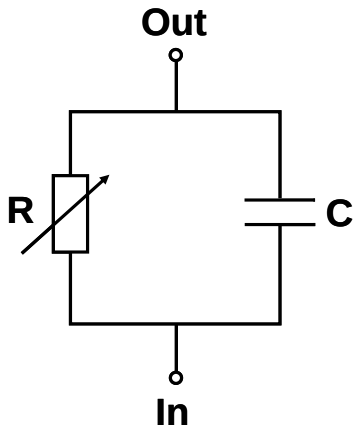

Figure 1. Equivalent circuit of a cell membrane. Image removed from Halliwell et al., (1987).

1.7.3. Voltage Clamp

The voltage clamp method is the most widely used within the patch clamp technique and consists in monitoring the potential value of the membrane of a single cell (through an external circuit to the cell) in order to register evoked ionic currents. The potential is fixed through a feedback amplifier circuit that allows the membrane potential to be kept in a steady-state value or altered in successive steps (Figure 2). Potential injection and current measurement is performed through one electrode that is in electrical continuity with the cell interior.

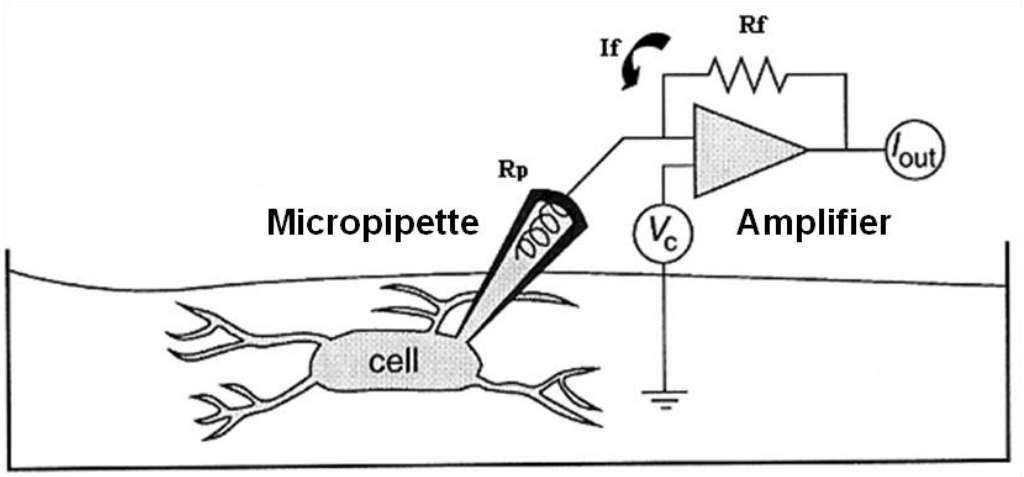

Figure 2. Electric circuit that controls membrane potential in whole cell configuration. R_f- feedback resistance; I_f- feedback current; V_c- command potential; R_s- series resistance; R_p- pipette resistance; I_{out} measured current. Adapted from Jackson, (1997).

V_c is the command potential of the amplifier that is applied to the cell membrane through the pipette. The generated ion current will dissipate a portion of the applied potential. The amplifier compares the membrane potential with the potential command values and corrects the difference by applying an equivalent current (I_f) through the feedback resistance (R_f). Through this potential feedback mechanism it is possible to maintain a fixed membrane potential at a value determined by the operator. The connection of the amplifier to the reference electrode lying in the bath (and earthed) closes the circuit.

Thus, the voltage clamp method is commonly used to study the functional characteristics of voltage-dependent channels. In addition to the electrical gradient manipulation, this method is also used to induce conversion between different conductive states or conformations of a protein, which are monitored as changes in current, and to selectively activate different channel populations (Liem et al., 1995; Jackson, 1997).

1.7.4. The four patch clamp configurations

The giga-seal resistance is mechanically stable which allows to electrically isolate the membrane snip at the tip of the pipette from the solution bathing the cell, and to derive different settings. There are four basic configurations for current acquisition, which are represented in figure 2. The cell-attached, inside-out and outside- out configurations are used to acquire individual currents. A pipette with a high resistance allows measuring currents flowing through isolated channels in small membrane areas (few pA). The whole cell configuration records the current through the entire cell membrane (Ashley, 1996).

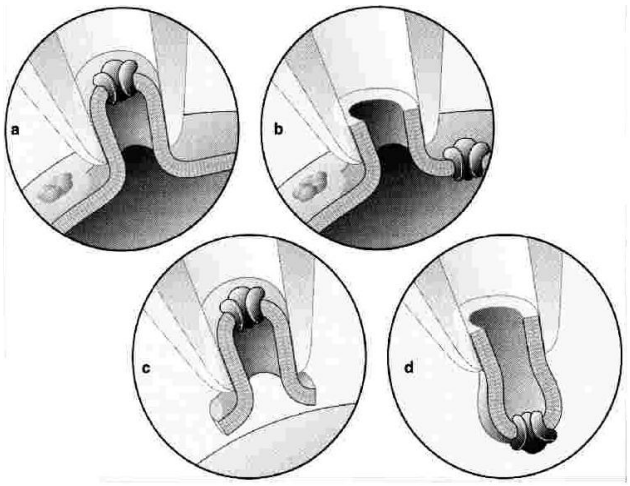

Figure 3. Illustration of the four patch clamp technique configurations: a. cell-attached, b. whole cell, c. inside-out and d. outside-out. Image taken from Numberger & Draguhn, (1996)**.**

The cell-attached configuration results directly from the giga-seal establishment and allows the measurement of current through membrane channels in the pipette tip (Figure 3a). This configuration preserves the intracellular environment; the composition of the pipette solution will mimic the extracellular side of the cell. It is usually used to study the regulation by external effectors. The main disadvantage of this configuration is the inability to effectively manage and change the ionic composition of the intracellular medium (Penner, 1995). To obtain the inside-out configuration, negative pressure is applied to the pipette to remove the membrane patch; the pipette is then gently pulled upward making the intracellular side exposed to the bath solution (Figure 3c). It is commonly used to observe changes in the measured current properties and behavior after excision can reveal the existence of intracellular regulators. The easy exchange of the intracellular solution (bath) allows the analysis of channel regulation by secondary messengers and other cytosolic signaling molecules (Ogden & Stanfield, 1988).

In the present study the whole cell configuration was used. This is achieved by breaking the patch of isolated membrane in the pipette tip (Figures 3b and 4). In this situation the interior of the cell comes into contact with the pipette solution. The latter will substitute the intracellular content, since it has a volume of several orders of magnitude higher (as can be seen by a color change in Figure 4). With this method it is possible to study ion channel populations and measure macroscopic currents (nA) by manipulating the bath solution, and the interior of the cell compositions. As with the inside-out and outside-out configurations, the main disadvantage is the loss of cytosolic content (Liem et al., 1995). Furthermore, pulling the pipette from the whole cell condition, the edges of the membrane will adhere and

a vesicle membrane at the tip of the pipette will be formed – outside out configuration (Figure 2d). This configuration is similar to the whole cell situation, with the intracellular medium of the cell facing the pipette solution, and the extracellular medium facing the bath solution. Furthermore, both configurations are widely used to study ion channels and receptors operated by different effectors (Penner, 1995).

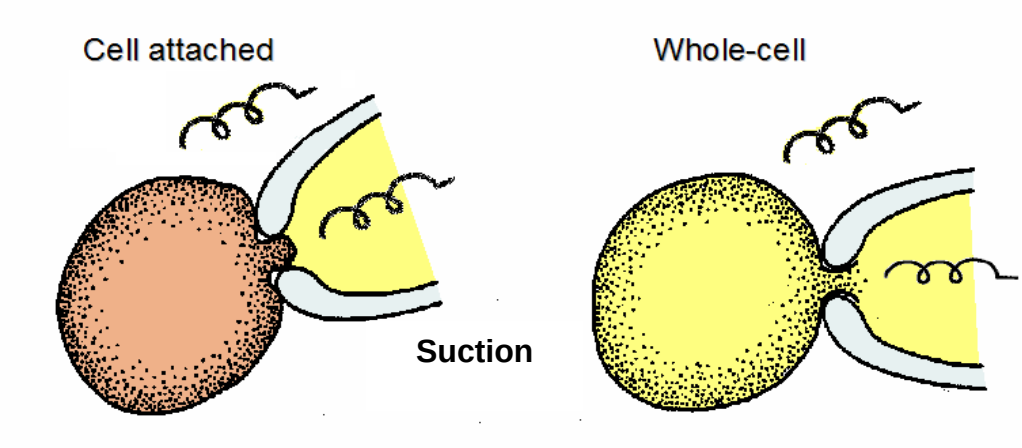

Figure 4. The whole cell configuration. The spirals indicate electrodes Ag / AgCl of the pipette (measurement) and the bath (reference). Adapted from Schindl and Derler, 2005.

2. Project Goal and Objectives

The general objective of the project was to investigate the anion transport role in protoplasts of pollen grains and germinated pollen tubes, with particular focus on a set of anionic channels and transporters shown to have expression in pollen. Two hypotheses were tested: that i) these transporters directly account for the anion currents (via ion fluxes across the plasma membrane) observed in hydrated pollen protoplasts and ii) GABA may play a role in their regulation. The results obtained will contribute to a broader understanding of the participation of anions during plant fertilization.

To solve these questions, electrophysiologic and localization assays were performed. The specific objectives were:

1. To identify the gene candidates coding for the channels or transporters responsible for the observed currents/fluxes and to obtain the respective electrophysiologic characterization;
2. To investigate the regulation of these currents by GABA;
3. To assign the different candidates to different domains of the pollen tube membrane;
4. To build a physiological model that highlights, for the first time, the functional role of chloride/anions transport during pollen tube growth.

3. Materials and Methods

3.1. Plant Material and Growth Conditions

Arabidopsis thaliana ecotype Colombia (Col-0) seeds were obtained from the Nottingham *Arabidopsis* Stock Centre (NASC). *Lilium longiflorum* plants was purchased from local suppliers.

A. thaliana ecotype Col-0 was used as wild type (WT). Col-0 *atcacc* and *slah3* mutant lines were obtained from NASC, Gabi-Kat_238B02 and Gabi-Kat_371G03, respectively. a*ttmem16*$^{-/-}$, *At1g73020* gene, has a T-DNA insertion in an intron between the tenth and eleventh exons, while *slah3*$^{-/-}$*, At5g24030* gene, has a T-DNA insertion in the third exon. The *atalmt12*$^{-/-}$ (*At4g17970* gene) and the double mutant *atalmt12xslah3* were kindly provided by Kai Konrad (*atalmt12*-1 single obtained from Meyer et al., (2010), JIC collection). Similarly, a*tccc*$^{-/-}$ (*At1g30450 gene*) mutant lines were kindly provided by Colmenero-Flores et al., (2007) (*ccc-1*, SALK_048175). *atccc*$^{-/-}$ has a T-DNA insertion in the first exon of the *At1g30450* gene. Figure 5 shows the T-DNA insertion maps in each gene.

The mutant line seeds were transferred to 10 cm Ø Petri dishes containing 50 mL Murashige and Skoog Medium supplemented with 1x Gamborg's B5 vitamins and 8% (w/v) Agarose, and complemented with kanamycin (50 μg.mL^{-1}) or sulfadiazine (Gabi-kat, 7.5 mg.mL^{-1}). They were left to germinate in a growth chamber for 2 weeks and then were transferred to pre-prepared pots. Plants were grown in pots (Desch Plantpak), which were filled with a 3:1 mixture of soil and vermiculite. The soil mixture was soaked with water and left to drain. They were then cultivated in growth chambers for 4 to 6 weeks under short-day conditions (8 h light/16 h darkness, 22/18°C) and after that in a greenhouse in long-day conditions (12 h light/12 h darkness, 22/18°C) to promote flowering, with illumination provided by 60 and 80 μmol.m^{-2} s^{-1} (μE.m^{-2}.s^{-1}) fluorescent tubes. The humidity levels ranged between 60 and 65%.

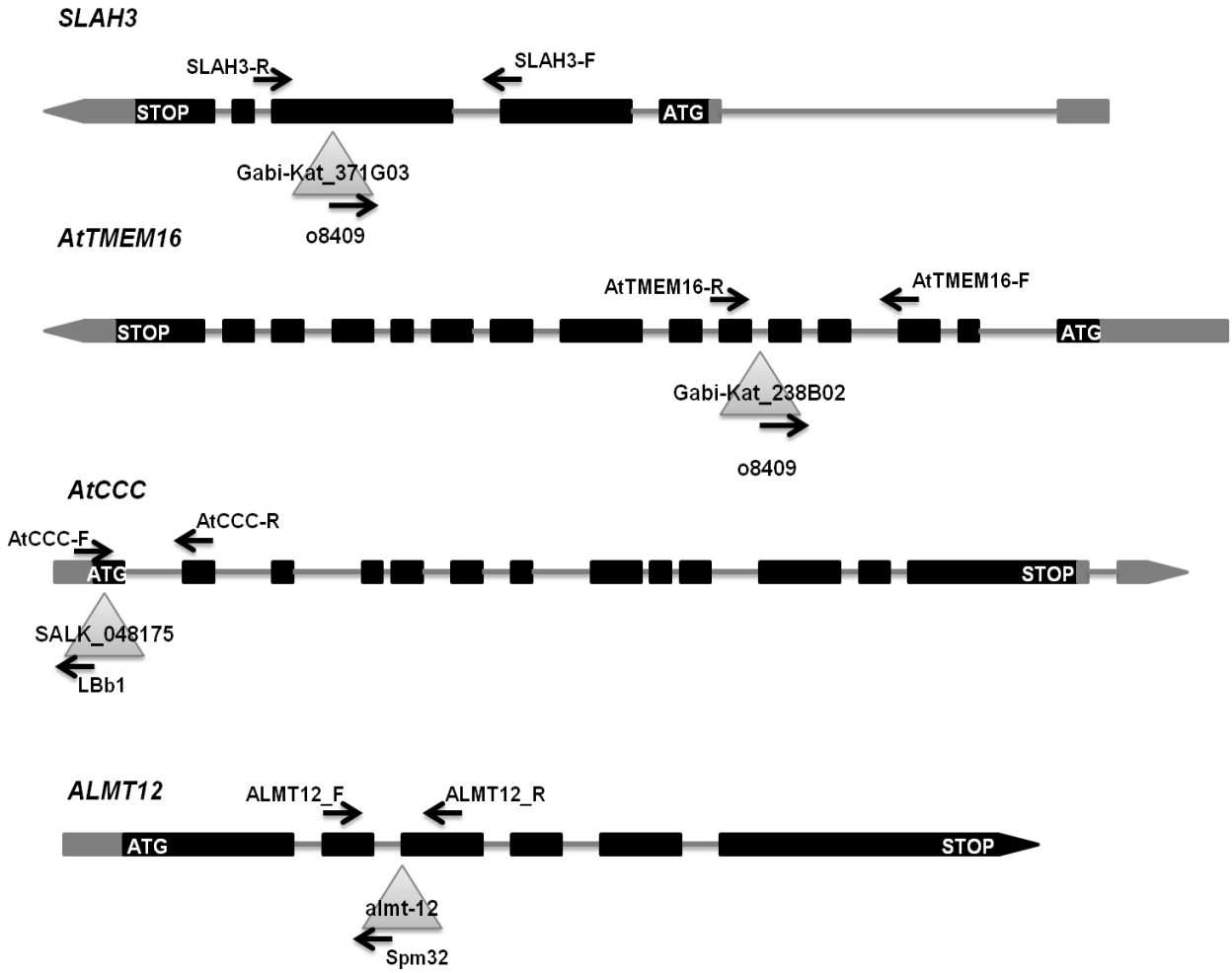

Figure 5. Maps of the T-DNA insertion lines for *SLAH3*, *AtTMEM16*, *AtCCC* and *ALMT12* mutant lines. The primers depicted for each mutant line are shown in Table 1. Black boxes depict exons, straight gray lines depict introns, and gray boxes the UTR regions.

3.1.1. Pollen germination assays.

Arabidopsis pollen grains from open flowers were suspended on pollen germination medium based on that of Boavida & McCormick, (2007), and containing the basic components (0.01% boric acid, 5 mM $CaCl_2$, 5mM KCl, 1 mM $MgSO_4$, 250 µM HEPES, 10% sucrose and pH 7.5-7.8), and incubated at 22ºC. Pollen germination medium (final volume 20 mL) was always prepared fresh from 100x stock solutions of the main components (KCl, H_3BO_3, $CaCl_2$, $MgSO_4$) using autoclaved MilliQ water (Millipore, http://www.millipore.com) (Boavida & McCormick, 2007). The data was collected from the same sample after 1 and 3 hours of germination, and are in accordance with previous studies (Palanivelu et al., 2003; Boavida & McCormick, 2007). The germination percentage and pollen tube length were analyzed in the presence of different gamma-aminobutyric acid (GABA) concentrations, and Muscimol

(500 µM, 1 mM and 10mM, and 20 µM, respectively) a universal agonist for all GABA type A receptors ($GABA_A$). Moreover, the known competitive antagonist of $GABA_A$ in animals, Bicuculline, was used to inhibit the Muscimol phenotype (200 µM). Images were acquired on a Leica DMIRE2 inverted microscope, equipped with a Hamamatsu C9100 EM-CCD camera, using the 10x 0.30NA objective, controlled with the MicroManager v1.14 software. Pollen germination counts and tube lengths were performed manually with the IMAGEJ software, NeuronJ tool (http://rsb.info.nih.gov/nih-image/index.html). The different compounds tested were prepared with water. The procedures for Live-Cell Imaging are described in M.M. section 3.2.3..

3.2. Molecular Biology

3.2.1. Analysis of the candidate mutant lines

3.2.1.1. DNA extraction. The experimental protocol used was modified from Cenis, (1992) and Edwards et al., (1991). All chemicals and the molecular biology material were purchased from Sigma Aldrich and New England Biolabs®Inc., respectively, unless stated otherwise.

The plant material was collected from leaves (~50 mg). A sample of the WT plants was also collected for control purposes. These were stored in a 1.5 mL centrifuge tube and frozen in liquid nitrogen. To each sample 300 µL of DNA Extraction Buffer (200 mM Tris-Cl, 250 mM NaCl, 25 mM EDTA, 0.5% (w/v) SDS, pH 8) was added. The tissue was crushed, and 150 µL of Sodium Acetate (3 M; pH 5.2) was added. The mixture was then vortexed and left to incubate at -20 ºC for 10 min, it was then centrifuged for 5 min at 14250 g and the supernatant was transferred to a new 1.5 mL centrifuge tube, where 400 µL of isopropanol was added. The mixture was then vortexed and left to incubate for 5 min at room temperature. After incubation the mixture was centrifuged for 5 min at 14250 g and the pellet was washed with 200 µL of 70% ethanol. This centrifugation step was repeated. Finally, the pellet was left to dry at room temperature, and was resuspended in 50 µL of H_2O MilliQ. The concentration of the DNA in solution was determined in a NanoDrop 1000 Spectrophotometer (Thermo Fisher Scientific, USA). The DNA sock solutions were stored at -20 ºC until use.

3.2.1.2. Isolation of homozygous T-DNA insertion mutants. The DNA stock solution was used to determine the genotype of plants by Polymerase Chain Reaction (PCR). Two pairs of primers were used, two gene-specific primers flanking the insertion point of the wild-type

allele and a second, the gene-specific primer and a T-DNA left border-specific primer for SALK lines 5'-GCGTGGACCGCTTGCTGCAACT-3' (LBb1) (http://signal.salk.edu), for GABI lines 5'-atattgaccatcatactcattgc-3' (GABI_o8409), or for JIC line (Smp32, Meyers *et al*., 2010) 5'- TACGAATAAGAGCGTCCATTTTAGAGT-3'.The primers used for each mutant line are shown in Table 1.

Table 1. Primers used to genotype each mutant line, and the respective combinations.

Mutant Line	Primer name	Direction	Sequence 5´ to 3'	Primer Combination	T-DNA
GABI_238B02	AtTMEM16-F	Forward	aatcattccaaactgcaaagc	AtTMEM16-F + LP	absent
	AtTMEM16-R	Reverse	aatctcggaaatgagagagcc	AtTMEM16-R + LBb1	present
SALK_048175C	AtCCC-F	Forward	taagaaagcttcgagcattagttctg	AtCCC-F + LP	absent
	AtCCC-R	Reverse	caacgagcatcccatttctactg	AtCCC-R + LBb1	present
GABI_371G03	SLAH3-RP	Forward	tcatagtaacggtccacaggc	SLAH3_RP + LP	absent
	SLAH3-LP	Reverse	aaagcggtaatggtgatgatg	SLAH3_RP + LBb1	present
almt12-1	ALMT12-F	Forward	gttgtgcaaagggcttaatagag	ALMT12_F + R	absent
	ALMT12-R	Reverse	caagaaggctcatgaaaagacag	ALMT12_R + Smp32	present

The PCR was conducted in a Programmable Thermal Controller PTC-100 (MJ Research, Inc., USA) according to the following protocol,

PCR protocol (total volume 25 µL)

Step	Temperature (ºC)	Time
1	**95**	**2 min**
2	**95**	**30 sec**
3	**54**	**30 sec**
4	**72**	**1 min**
5	**Repeat steps 2-4 34 times**	
6	**72**	**7 min**
7	**11**	

The reaction mix per sample used was, Buffer DreamTaq™ DNA polymerase Thermo Scientific™) (10x) 2,5 µL, 1 µL dNTPs, forward and reverse primers 0.628 µL each, 0.25 µL DreamTaq™ DNA polymerase (Thermo Scientific™), 1 µL genomic DNA and 19 µL H_2O MilliQ. Agarose gel electrophoresis was used to separate and analyze the PCR products; two wells with the two pair of primers were loaded. The agarose gel was constituted by a TAE buffer supplemented with 1% agarose and 1 µL of RedSafe™ Nucleic Acid Staining

Solution (20.000x, SBS Genetech). The bands in the gel were visualized in a Molecular Imager Gel Doc XR (Bio Rad Laboratories, USA), by means of the Quantity One 4.6.7 software (Bio Rad Laboratories, USA). A homozygous mutant was considered in the absence of the wild type fragment.

The PCR protocol and the reaction mixture described were used for all cloning procedures, with two exceptions: i) step 4 in the PCR protocol; the annealing temperature and time were adapted for the melting temperatures of each set of primers used and the size of the fragment, respectively, and ii) a mixture of dreamTaq and Phusion, a High-Fidelity DNA Polymerase (error rate 50-fold lower than that of Taq).

3.2.1.2.1. mRNA isolation. mRNA was isolated from the T-DNA insertion homozygous plants of the four gene candidates. The WT plant was used as control.

The plant material was collected from leaves (> 50 mg). These were stored in a 1.5 mL centrifuge tube and frozen in liquid nitrogen. The samples were homogenized with a pestle, while the liquid nitrogen evaporated. The pestle was autoclaved before use. Then, 750 µL of TRI Reagent LS were added to each sample. Using the pestle, this compound was incorporated into the pulverized sample until its color changed from pink to light brown. The blending was continuous until the mixture defrosted. The mixture was pipetted into a 1.5 mL centrifuge tube, vortexed for a few seconds in order to separate the RNA from the associated proteins, and left to incubate at room temperature for 5 min. 200 µL of chloroform were then added to the mixture. It was vortexed and left to incubate at room temperature for approximately 15 min. The mixture was then centrifuged for 15 min at 10500 g. The aqueous fraction was transferred to a new 1.5 mL centrifuge tube and 400 µL of isopropanol was added. The mixture was left to incubate at room temperature for 20 min and then was centrifuged for 15 min at 10500 g. The pellet was then washed with 200 µL of 70% ethanol and was centrifuged for 15 min at 10500 g. This washing step was repeated. Finally, the pellet was resuspended in 50 µL H_2O MilliQ water and was incubated at 55 ºC for 5 min. The concentration of the RNA in solution was determined in a NanoDrop 1000 Spectrophotometer (Thermo Fisher Scientific, USA). The RNA stock solutions were stored at -80 ºC until use.

3.2.1.2.2. cDNA synthesis. 1 µg of total RNA was used in each sample to produce the cDNA. Prior to cDNA production, TURBO™ DNase method was used to remove any traces of genomic DNA in the RNA sample as follows: 0.1 volume 10x TURBO DNase Buffer and

1 µL TURBO DNase were added to the RNA, and gently mixed. The samples were incubated for 30 min at 37ºC. Then the samples were re-suspended and mixed in 0.1 volume of DNase Inactivation Reagent and incubated for 5 min at room temperature mixing occasionally. Finally, they were centrifuged at 10000 g for 2 min and the RNA transferred to a fresh tube.

The protocol was as follows:

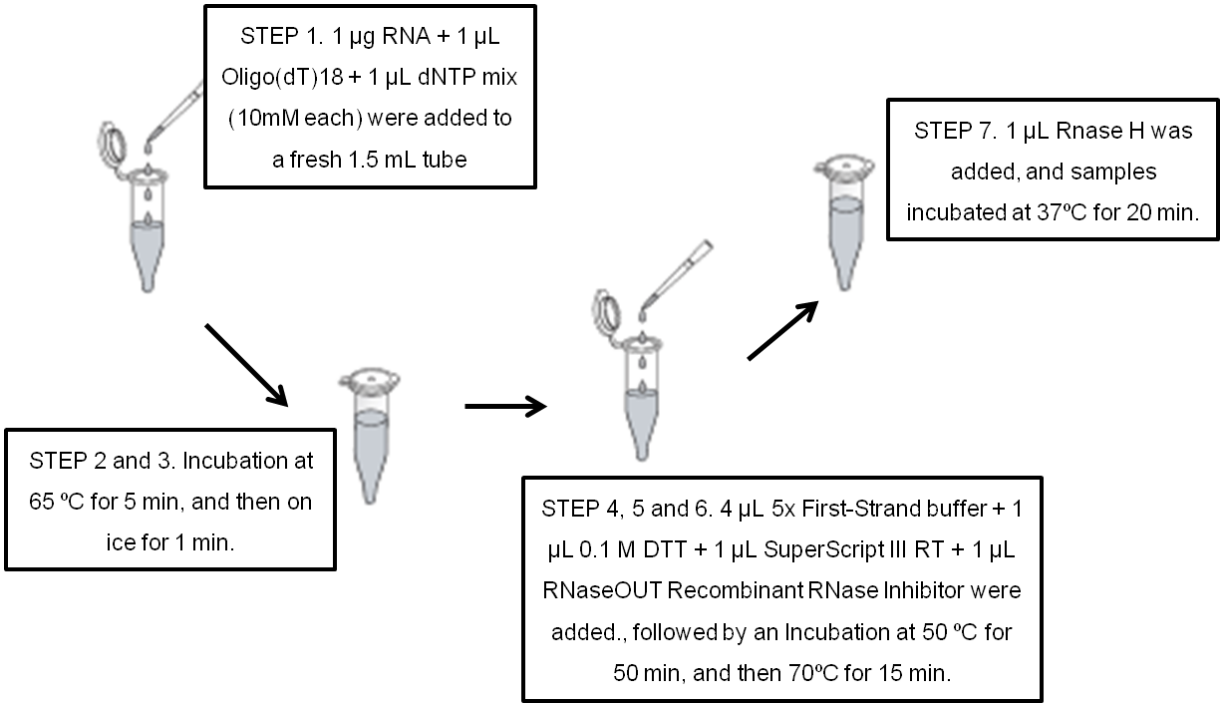

The incubation steps were performed in a Programmable Thermal Controller PTC-100 (MJ Research, Inc., USA). Immediately after the Reverse Transcription reaction, the resulting cDNA was used in a PCR, with the primers shown in Table 2. A genomic DNA sample was used in each PCR mix as a positive control for the primers, as well as a cDNA wild type sample, and the reaction mix. A negative control (sample without DNA) was also used. The Elongation-Factor α primers were used as a control for the quality of the cDNA samples. The PCR protocol is described above in 3.2.1.2. section. Two gene-specific primers were designed upstream and downstream the T-DNA insert, flaking the complete gene sequence. The PCR products were run in an agarose gel to check the absence of transcript.

Table 2. Primers used to analyze gene expression for each mutant line, and the respective combinations. A full knockout was considered in the absence of transcript.

Gene	Primer name	Direction	Sequence 5´ to 3'	Transcript Signal
At1g73020	AtTMEM-1F	Forward	ctgaaacttgacggcagagag	Absent

	AtTMEM-1R	Reverse	cctcctagccgagtgaggtac	
At1g30450	AtCCC_ATG	Forward	atggatagcggcgacattgaagaa	Absent
	AtCCC-RT	Reverse	cgcgaccaatgaggtaatatgg	
At4g17970	SLAH3_F	Forward	tcatagtaacggtccacaggc	Absent
	SLAH3_R	Reverse	aaagcggtaatggtgatgatg	
At5g24030	ALMT12_F	Forward	gttgtgcaaagggcttaatagag	Absent
	ALMT12_R	Reverse	caagaaggctcatgaaaagacag	
Elongation factor 1-α	EF1a_F	Forward	caattgtggacttaccagcat	
	EF1a_R	Reverse	cagttcctgatgagcaagaag	

Table 3. For the transgenic generation the following sequences were added to the primers in the Table: *attB1– ggggacaagtttgtacaaaaaagcaggcttc; attB2–ggggaccactttgtacaagaaagctgggtc, overlapping sequences were added to the forward and reverse sequence primers in the Table. For mammalian expression cloning the following linkers were added: ** Forward primer, aaaaTCTAGA- and Reverse primer, aaaaGCGGCCGC-

Gene	Primer name	Direction	Sequence 5´ to 3'	Transcript Signal
At1g73020	AtCaCC_ATG	Forward	atgaatgggagtaatggggagg	Absent
	AtCaCC_STOP	Reverse	tcaaaagcgctctgagtcttg	
At1g30450	AtCCC_ATG	Forward	atggatagcggcgacattgaagaa	Absent
	AtCCC-RT	Reverse	cgcgaccaatgaggtaatatgg	
At4g17970	SLAH3_ATG	Forward	atggaggagaaaccaaactatg	Absent
	SLAH3_STOP	Reverse	ttatgatgaatcactctcttgag	
At5g24030	ALMT12_ATG	Forward	atgtccaataaggttcacgtagg	Absent
	ALMT12_STOP	Reverse	tcattccgcggcaccgacac	
Elongation factor 1-α	EF1a_F	Forward	caattgtggacttaccagcat	
	EF1a_R	Reverse	cagttcctgatgagcaagaag	

3.2.2. Generation of transgenic *Arabidopsis* lines overexpressing the candidate genes.

The genomic sequence of the anionic channel/transporters candidates were amplified, from ATG to the STOP codons, with the primers shown in Table 3. The primers have an overlap sequence with the entry clone pDONR 207 vector (Table 3*). In particular, the *AtCCC* coding sequence was kindly sent by Colmenero-Flores et al., (2007). The Gateway® Cloning Protocols (Thermo Scientific™) was used.

First, the sequences were cloned into an entry clone pDONR 207 vector through a BP reaction as follows: in a 1.5 mL tube, 1-7 µL the attB-PCR product (150 ng/µL), 1 µL Donor vector (150 ng/µL) and TE buffer, pH 8.0 to 8 µl were added and mixed. Then 1 µL of BP Clonase™ II enzyme mix was added to each sample and vortexed. The reactions were incubated overnight at 25ºC, and inactivated in the following day at 37ºC for 10 min with

Proteinase K. Each reaction sample was transformed into 50 µL of competent *E.coli* cells (Strain: DH5α™), and plated onto selective plates with gentamicin (50 mg/mL, resistance present in the pDONR). Positive colonies were selected through single-colony PCR using a primer specific for the plasmid and another specific for the gene of interest; this procedure guaranteed that the fragment was correctly cloned.

Second, the fragment already enclosed in the pDONR vector was transferred into a destination vector (pk7fwg2, https://gateway.psb.ugent.be/vector/show/pK7FWG2/search/index/) through a LR reaction, in a similar way as the BP reaction, as follows: in a 1.5 mL tube 1-7 µL of entry clone (150ng) 1 µL destination vector (150 ng/µL) and TE buffer, pH 8.0 to 8 µl were added and mixed. To each sample 1 µL LR Clonase ™II enzyme mix was added and vortexed. The reactions were incubated overnight at 25ºC, and inactivated in the following day at 37ºC for 10 min with Proteinase K. Each reaction sample was transformed into 50 µL of competent DH5α *E.coli* cells, and plated onto selective plates with spectinomycin (100 µg/mL). The gateway destination vector used was, PK7FWG2 (ugent), which as GFP fused to the C-terminus. In addition, the Lat52 promoter was used, since its pollen specific (Twell et al., 1989). In both gateway reactions, the candidate gene was sequenced.

The transformation protocol used in all clonings was:

1. Competent *E.coli* (Strain: DH5α™) cells were thawed on ice.
2. The plasmid was added into the vial and mixed gently.
3. It was then incubated on ice for 30 minutes.
4. The cells were heat-chocked for 42 sec at 42°C without shaking in a Programmable Thermal Controller PTC-100 (MJ Research, Inc., USA). Then the tube was immediately transferred to ice.
5. 350 µl of room temperature Super Optimal Broth (S.O.C.) medium was added.
6. Cells were incubated at 37°C for 1 hour with shaking to recover.
7. 150 µl of bacterial culture was spread on a prewarmed LB agar plate containing the selective antibiotic; plates were then incubated overnight at 37°C.

The final construct was transformed into *A. thaliana* Col-0 plants via the *Agrobacterium tumefaciens*-mediated floral dip method (Clough & Bent, 1998), as follows: agrobacteria (Strain GV3101, which is resistant to gentamycin and rifampicin) was transformed, as described above for *E.coli* cells, with the destination vector with each gene candidate. Positive colonies were selected through single-colony PCR using a primer specific for the

plasmid and another specific for the gene of interest. The positive colonies were then grown in 10 mL of LB medium with gentamicin (50 mg/mL), rifampicin (50 mg/mL) and spectinomycin (100 mg/mL, resistance present in the destination vector) and for 48h. At this point a small volume is stored at -80ºC in 70% glycerol. From the 10 mL, 4 mL are dissolved in 400 mL of LB medium with the same antibiotics and left to grow for 24h. On the following day, the agrobacteria culture is pelleted in a Sorvall RC 5C plus centrifuge with the SLA 3000 rotor at 15000 rpm for 15 min at 4ºC. The cells are then re-suspended in 5% sucrose solution. Plants bolting with unopened flowers were transformed by dipping directly into the *A. tumefaciens* 5% sucrose solution supplemented with the Sylgard® 309 Silicone Surfactant (Dowcorning). Transformed plants were kept away from light and in a plastic dome for 24h, which increased humidity and bacteria transfer in the tissues. Transgenic plants were selected from plates with germination medium and kanamycin; positive plants were then transferred to soil and the pollen visualized in the Leica DMIRE2 inverted microscope, using the 20x 0.7NA objective, controlled with the MicroManager v1.14 software for GFP fluorescence.

3.2.3. Cell Line Cultivation and Transient Transfection

Human Embryonic Cells (HEK293) were acquired from American Type Culture Collection (ATCC: Manassas, USA, under the designation '293', accession code CRL-1573) and african green monkey kidney cells (COS-7) ATCC ® CRL-1651. The cultures were maintained in an incubator with an atmosphere of 5 % CO_2:95% air humidified in culture flasks with an area of 25 cm^2 (Corning®). The culture medium used was composed of D-MEM medium (Dulbeccos modified Eagle's medium with 4500 mg L^{-1} glucose +GlutaMax™ I, -piruvato, Biowest) FBS (fetal bovine serum) 10% (v/v), penicillin (50 $I.U.mL^{-1}$, Biowest) and streptomycin (50 $U.G.mL^{-1}$, Biowest). Before performing the passages of all solutions cultures (culture medium, phosphate buffer (PBS) and trypsin) was heated in a bath at 37°C. The passage of the HEK293 and COS-7 cultures was carried out under sterile conditions, at least twice a week. Cultures were grown until reaching a confluence of 70 to 100%, respectively, after which the culture medium was removed. Thereafter, the cells were washed with PBS and dissociated with a trypsin solution (0.05 % EDTA • 4Na, Biowest). The cells were re-suspended in about 3 mL of culture medium, which prevents the action of trypsin. For a better cell dissociation, the cell suspension is repeatedly pipetted with a plastic transfer pipette. A few µL of cell suspension were added to a new flask, previously

prepared with 5 mL of fresh culture medium. This flask is then kept in an incubator under the above conditions until the next passage (culture subdivision). HEK293 and COS-7 cells were maintained for 30 and 20 passages, respectively, before a new stock was thawed and regenerated, since their health (i.e. morphology, growth rate, and translational efficiency) deteriorates as the passage number increases.

3.2.3.1. Trasient Transfection, was performed in Petri dishes of Ø 3 cm (Sarstedt), previously filled with four plastic lamellae (VWR, Ø 13 mm). These were covered with 3 mL of fresh culture medium. Transfections were performed in the same day as the cells passage being used about 1 or 2 drops of the cell suspension. 2 µg of construct DNA were added (except for co-transfections wherein 0.7 µg of each plasmid was used) to a sterile 1.5 mL eppendorf and mixed with 6 µL of FuGENE® HD Transfection Reagent (Promega) and 150 µL of non-supplemented DMEM medium. The DNA added included the CD8 protein. The mixture was then added to the Petri dish's containing the cells, and these were grown in an incubator (37ºC, 5% CO_2). The patch clamp assays were performed 24 to 48h after transfection of the candidate protein, as follows: one lamellae was retrieved from the Petri dish and transferred to a new dish with 2 mL fresh bath solution (**B2**), and 1 µL of Dynobeads® CD8 (Invitrogen). The Petri dish was agitated for a few minutes, in order to disperse the microbeads and to promote their attachment to the transfected cells, and taken to the microscope for patch manipulation.

3.2.3.2. Constructs for heterologous expression. In order to transiently express the candidate genes in mammalian cells, the respective coding sequences were amplified, using the primers shown in Table 2 with extra sequences for double restriction enzyme digestion with *XbaI* and *NotI* (Table 2**, except for *CCC* since its electroneutral). The sequences were cloned into the pCI mammalian expression vector that holds a CMV promoter. The PCR was performed as described above, and the amplified fragments were double digested in CutSmart® Buffer at 37ºC, during at least 5 hours. The candidate DNA fragment with the correct size was then cut from the gel or treated with Alkaline Phosphatase, Calf Intestinal (CIP), and was then cleaned with Zymoclean™ Gel DNA Recovery Kit or DNA Clean & Concentrator™ (Zymo Research), according to the manufacturer instructions. Ligation with Quick T4 DNA Ligase was performed mixing the linearized pCI vector, restricted with the same enzymes, and with the candidate fragment for

6 min. The ligation was then transformed into DH5α™ *E.coli* cells and purified using Plasmid Midi Kit (Qiagen).

3.3. Live-Cell and Confocal Imaging

Images from A. thaliana Col-0 transgenic pollen tubes were acquired on an Applied Precision DeltavisionCORE system, mounted on an Olympus inverted microscope, equipped with a Cascade II 2014 EM-CCD camera, using the 100x UPlan SAPO 1.4NA Oil immersion objective, GFP and mCherry, for double labeling with FM® 6-64 Dye (N-(3-Triethylammoniumpropyl)-4-(6-(4-(Diethylamino) Phenyl) Hexatrienyl) Pyridinium Dibromide, Molecular probes^{TM}, Life technologies) fluorescence filter sets and DIC optics. Images were deconvolved with Applied Precision's softWorx software. For GFP and mCherry illumination, excitation wavelengths of 461-489 nm and 563-588 nm were used, respectively, and fluorescence emission was reflected via a filter cube (dichroic) 525/50 and 632/60 nm, respectively.

Confocal Z-series stacks were acquired on a Zeiss LSM 510 META, using a 63x 1.4NA and a 40x 1.3NA Oil immersion objectives, the 488nm and 543nm laser lines, and spectral detection adjusted for the emission of GFP.

3.4. Electrophysiology

3.4.1. Protoplast isolation

Arabidopsis thaliana pollen grains were isolated from freshly collected blossomed flowers, while *Lilium longiflorum* (Thunb.) pollen grains were collected from the anthers, aliquoted and stored at −20°C. On the day of the experiment, protoplast isolation was performed according to Tanaka et al., (1987); Fan et al., (2001); Mouline et al., (2002), with modifications.

The pollen grains were hydrated for 10 min at room temperature in 2 mL of standard solution: 1 mM KNO_3, 0.2 mM KH_2PO_4, 1 mM $MgSO_4$, 1 µM KI, 0.1 µM $CuSO_4$, 5 mM $CaCl_2$, 0.5 M glucose, 1 M sorbitol and 5 mM MES (2-(N-morpholino)ethanesulfonic acid), pH 5.8, adjusted with TRIS (tris(hydroxymethyl)aminomethane) (osmolarity = 1.5 $Osmol.kg^{-1}$). Hydrated pollen grains were centrifuged at 63 g for 5 min and the pellet was resuspended in 2 mL of enzyme solution: 1% (w/v) cellulase RS ‘Onozuka’ (Duchefa,

Haarlem, the Netherlands), 0.5% (w/v) macerozyme R-10 (Duchefa, Haarlem, the Netherlands), and 0.2% (w/v) BSA in standard solution, kept at -80º C until use.

Enzymatic digestion of the cell wall was performed for 110 min, at 30°C with mild agitation. The enzymatic solution was removed by centrifugation at 63 g for 5 min (supernatant), and the pellet was further washed twice with bath solution which osmolarity was adjusted to 1.5 Osmol kg^{-1} with sorbitol. The protoplasts were further resuspended in 1 mL of bath solution and the suspension was kept on ice for patch-clamp measurements for up to 8 h after isolation. For the germination assays, lily pollen grains were germinated for 40 min in 1.6 mM H_3BO_3, 1 mM KCl, 50 µM $CaCl_2$, 5% sucrose (w/v), and 50 µM MES, pH 6.3, after the hydration step and before the enzymatic digestion (which was reduced to c. 30 min). This procedure resulted in pollen grains with protruding pollen tubes (c. 200 µm in length) suitable for patch-clamp measurements.

3.4.2. Patch Clamp Set up

The set up consists of an inverted microscope mounted on top of a vibration isolation table (allows stable and clear electrical signals) and a headstage (which contains the pipette holder), that are located inside a Faraday Cage, which shields the sensitive headstage from electrical noise. The set up also integrates a patch clamp amplifier (to apply the electric stimulus and to amplify and record the received electric signal, since the currents measured are in the order of pA), a pulse generator, a micromanipulator and data-recording devices (Penner, 1995).

3.4.3. Patch Clamp Protocol

Currents from pollen protoplasts (c. 20 µm) were measured under voltage-clamp conditions with standard whole-cell recording technique as described by Hamill et al., (1981). Membrane potentials were controlled with a patch-clamp amplifier, Axopatch-1D or Axopatch 200A (Axon Instruments, Foster City, CA, USA) and visualized with a Digital to Analogue (D/A) converter, 1320A - 16 Bit Data Acquisition System (Axon Instruments, Foster City, CA, USA).

Petri dishes of 34 mm Ø with a 1 mL central chamber with glass bottom were used. The chamber was filled with 400 µL of bath solution and 100 µL of the protoplasts suspension and then placed in the microscope stage. After ~10 min (to allow the protoplasts to set) a smooth plasma membrane protoplast is chosen using an amplification of 200x in a Eclipse

TE300 inverted microscope (Nikon, Japan). A micropipette was then filled with the appropriate internal solution and introduced in the pipette holder, allowing the Ag/AgCl electrode to contact the pipette solution. Positive pressure was applied to the microelectrode through a syringe that is connected to the pipette holder, which closes the electric circuit. After introducing the micropipette in the bath solution, it was possible to measure the microelectrode resistance by applying a -40 mV pulse, and to position it above the chosen protoplast. The current generated by the difference of potential that was originated by the two different electrodes was corrected. Whole-cell recordings were performed by breaking the membrane with gentle suction and after the membrane resistance stabilized at > 0.5 GΩ. The outside-out recordings were obtained after whole cell was established by pulling the pipette away from the cell which allowed the membrane edges to close. A tight seal is achieved by consequent loss of current, consequence of the increase of resistance to the passage of ionic current between the external solution and the interior of the pipette, due to the approximation of the plasma membrane. After the cell stabilizes, the cellular parameters of access resistance (Ra), membrane resistance (Rm) and membrane capacitance (Cm) are registered, and the voltage protocols applied (Figures 6 and 7), first A and then B. Ra refers to the access to the cell's interior and dictates whether it is being completely clamped by the amplifier. Its value should always be kept low (Ra ≤ 10 MΩ, Penner, 1995). Rm refers to the integrity and permeability of the membrane (Rm ≥1 GΩ). Cm refers to the area of the membrane that is being clamped and its value is used to normalize the current values. The currents suffer a process entitled Rundown (monitored with protocol A, Fig. 6); then after the currents stabilize protocols A and B are applied and the inhibitor is applied. Again, after the currents stabilize protocol A and B are applied and the changes in the currents are monitored with the former protocol.

The electrical signal was sampled at 50 kHz and filtered at 5 kHz. Whole-cell and outside-out series resistance, and pipette and cell membrane capacitive transients were partially subtracted from the records by the amplifier circuitry before sampling. Clampex 8.0 software (Axon Instruments) and WinWCP V.4.9.3 were used to design the voltage protocols, to generate the command potentials, and to collect the current data.

Micropipettes, showing resistances of 5–9 MΩ (whole-cell) or 25 MΩ (outside-out patches) were pulled from a glass capillary with 1.5 mm external diameter and 0.86 mm internal diameter (GB150T-8P; Science Products, Hofheim, Germany) with a PB-7 vertical puller (Narishige, Tokyo, Japan). The reference electrode was an Ag/AgCl wire embedded in a 0.5 M KCl/agar bridge. The reference electrode with the saline bridge is mounted on the central

chamber and connected to the ground (earthed). The Ag/AgCl electrode permits a smooth transition between the electric current carried by electrons and the current carried by the ions in solution, reducing the contribution of possible junction potentials between the silver wire and the bath solution. All experiments were performed at 19ºC. Currents from germinated pollen were measured as described for pollen grain protoplasts, with P1/B1 solutions. The giga-ohm seals were formed 20–100 µm away from the tip.

3.4.4. Recording solutions

The solutions used in the electrophysiological assays were designed in order to have Cl^- as the main permeant ion.

3.4.4.1. Pollen protoplasts: Cells were maintained in 110 mM N-methyl-d-glucamine chloride (NMG-Cl), 5 mM NMG-NO3, 3 mM $CaCl_2$, 1 mM $MgCl_2$, 20 mM TEA-Cl, 1 mM $GdCl_3$ and 5 mM MES (**B1**). The pipette/internal solution had 135 mM NMG-Cl, 5 mM NMG-NO_3, 0.3 mM $CaCl_2$, 5 mM MgATP, 5 mM EGTA, and 5 mM HEPES (**P1**). The pH was adjusted to 7.2 (pipette) and 5.8 (bathing) with NMG and the osmolarity was adjusted with sorbitol to 700 mOsmol.kg^{-1} (*Lilium longiflorum*) and to 800 mOsmol kg^{-1} (*Arabidopsis thaliana*).

The equilibrium potentials for the permeable ions in solution, as predicated by the Nernst Equation: E_{Cl-}, -0.92; E_{NO3-}, 0.00; E_{Ca2+}, 165.01; E_{Mg2+}, 15.32 and E_{H+}, 81.11 mV.

The free $[Ca^{2+}]_{in}$ in the pipette solution was 6.04 nM. NMG^+ was used to replace the permeant cations Na^+ and K^+; tetraethylamonium (TEA^+), and gadolinium (Gd^{3+}) were used to block K^+ and Ca^{2+} currents, respectively (Fan et al., 2001; Dutta & Robinson, 2004; Wang et al., 2004). The inhibitory effect of NPPB, a known inhibitor anionic blocker (Gogelein, 1988) was tested on the currents. A stock solution in dimethyl sulfoxide (DMSO) was kept at 4°C (25 mM) and freshly dissolved in the bathing solution before use.

3.4.4.2. Mammalian Cells: Cells were maintained in 140 mM NMG-Cl, 2 mM $MgCl_2$, 2 mM $CaCl_2$, and 5 mM HEPES (**B2**). The pipette/internal solution used was, 140 mM NMG-Cl, 5 mM MgATP, 5 mM EGTA, 3,45 µM $CaCl_2$ and 5 mM HEPES (**P2**). The pH was adjusted to 7.4 (pipette) and 6.8 (bathing) with NMG and the osmolarity was adjusted with mannitol to 300 mOsmol.kg−1. The free $[Ca^{2+}]_{in}$ in the pipette solution was 250 nM. NMG^+ was used to

replace the permeant cations Na^+ and K^+. The inhibitory effect of NPPB was tested on the currents.

The internal solutions were complemented with EGTA as a Ca^{2+} and Mg^{2+} chelator, in order to maintain constant the free $[Ca^{2+}]_{in}$ in the pipette solutions. The free $[Ca^{2+}]_{in}$ was estimated using the software WEBMAXCLITE v1.15, available online from http://www.stanford.edu/~cpatton/webmaxc/ webmaxclite115.htm. ATP was added preventively to power any anionic transporters present in the membrane. The effect of the solvent DMSO and TEA in the anionic currents was tested in Tavares et al., (2011a); no differences were obtained.

3.4.5. Voltage Protocols

The voltage protocols applied to pollen protoplasts are shown in Figures 6 and 7 for pollen and mammalian cells, respectively.

In Figure 6, the cell membrane was kept at a holding potential of -100 mV. This potential was chosen because it maintains the seal stability between voltage jumps and it is similar to the physiological resting potential. The protocol was designed to study current activation. This protocol has voltage jumps with duration of 1 sec, in order to guarantee that the currents generated had time to stabilize (as in the voltage protocol used for mammalian cells, Figure 7).

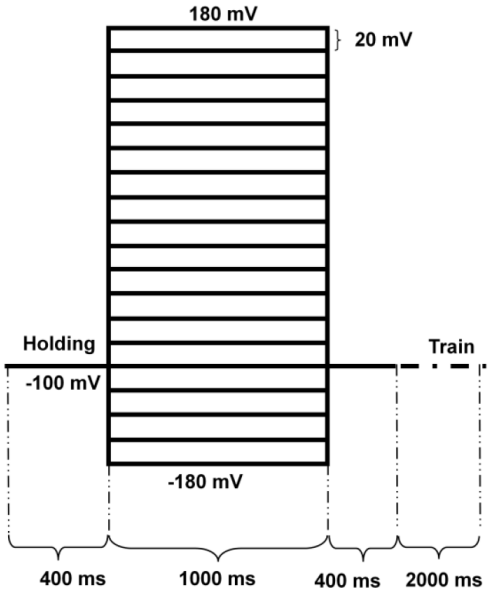

Figure 6. Voltage Protocols applied. A: Voltage protocol used to study current activation. During experiments, the cell membrane was kept at a holding potential of -100 mV, which was followed by a series of 1 sec voltage

jumps that ranged from -180 mV to +180 mV. The cell membrane was kept at -100 mV for 2 sec in between each voltage jump. (figure adapted from Tavares et al., 2011c).

Unitary currents were recorded from outside-out patches at fixed membrane voltage values ranging from −150 to +150 mV, for 20 s.

It was reported that *At*ALMT12 has higher conductivity at negative potentials (Meyer et al., 2010). Mammalian cells expressing ALMT12 were maintained at + 40 mV to ensure that the channels were in their minimum conductivity state (Figure 7).

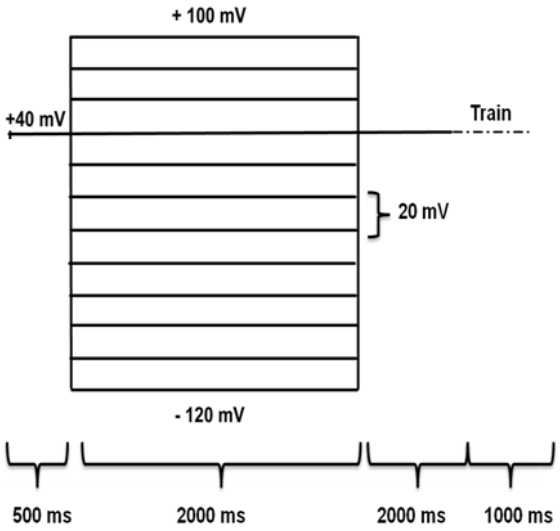

Figure 7. Voltage Protocol applied for mammalian cells. Voltage protocol used to study current activation. The membrane was kept at a positive potential, + 40 mV, which was followed by a series of 2 sec voltage jumps that ranged from -120 mV to +100 mV. The cell membrane was kept at +40 mV for 1 sec in between each voltage jump.

3.4.6. Data analysis

All the currents produced were acquired, recorded and analyzed with a computer, using pCLAMP software (version 8.0, Axon Instruments), on raw data for cells that had stable > 0.5 GΩ seals. Liquid junction potentials (difference of potential that arises at the interface between two different salt solutions and results from different anionic and cationic mobilities and from different solute concentrations (Halliwell et al., 1987)) were calculated with the Clampex 8.0 software (M Axon Instruments), and affects the potential that is being applied to the membrane during a patch clamp experiment, and therefore it was corrected for all recordings.

All linear and nonlinear data fitting was performed with the origin 6.1 software (OriginLab Corporation, Northampton, MA, USA). Statistical significances were determined using the Two-Sample t-Test comparison from OriginLab, and differences were considered significant

if $p < 0.05$. For each experimental condition, data from different cells were averaged. In particular, for the experiments with *Arabidopsis thaliana*, the intensity of the currents of each protoplast was normalized with the respective membrane capacitance (C_m), producing the current density values (pA/pF) used to build the Current – Potential (I/V) relationships, to gather information on the nature of the currents and the channels involved. The data shown are mean ± SE (n), where n is the number of cells obtained for a particular experiment. Asymptotic forward (outward) and backward (inward) conductances (determined for the most positive and negative portions of the Current–Voltage (I/V) relationship, respectively, where the current values are directly proportional to the electromotive force) were estimated using a least-mean-square linear fit. Equilibrium potentials for the ions in solution were calculated with the Nernst equation. Conductance–Voltage (G/V) curves were derived from I/V relationships according to the following equation:

$$G = \frac{I_{ss}}{V_m - E_{rev}} \qquad \textbf{Equation 1}$$

where Iss is the steady-state current at the end of the test potential Vm, and E_{rev} is the reversal potential of the current. Conductance values were normalized for the maximum response and fitted with a Boltzmann type equation:

$$\frac{G}{G_{max}}(V_m) = A_2 + \frac{A_1 + A_2}{1 + e^{\frac{V_m - V_h}{V_s}}} \qquad \textbf{Equation 2}$$

where A1 and A2 are the values for the minimum and maximum conductance, respectively, when this no longer varies with V_m, V_h is the potential for the half-maximal chord conductance and indicates at which V_m the transition between the two states of conductance occurs, and V_S is the slope of the $G/G_{max}(V_m)$ curve and a measure of the sensitivity of the currents to variations in V_m.

3.4.7. Anion-selective self-referencing probe

Extracellular anion flux measurements were performed as described in Gutermuth et al., (2013).

Arabidopsis pollen grains were collected from fresh flowers and germinated in liquid medium containing the following: 500 µM KCl, 500 µM $CaCl_2$, 125 µM $MgSO_4$, 500 µM H_3BO_3, 125 µM HEPES, and 15% of Sucrose at pH 7.5. After at least 3 h of incubation at

21.5°C, measurements were performed on growing pollen tubes that were at least 150 µm in length. The respective growth rate was evaluated simultaneously with the extracellular anionic fluxes, defined as the total length grown during the experiment divided by the amount of time spanned. Extracellular anionic flux at the pollen tube tip was estimated with the ion-selective vibrating probe (Kühtreiber & Jaffe, 1990; Shipley & Feijó, 1999). Anion-specific microelectrodes were fabricated from 1.5-mm borosilicate glass capillaries and pulled with a Sutter P-97 electrode puller (Sutter Instruments), baked at 230°C overnight and then internally covered with N,N-dimethyltrimethylethylsilamine for 40 min. Electrodes were backfilled with 100 mM KCl and subsequently front-loaded with a 30-µm column of the anion-selective liquid cocktail (chloride ionophore I cocktail A). A silver/silver chloride wire was inserted into the back of the electrode and a dry electrode (DryRef-2; World Precision Instruments) was used as a reference. Electrode calibration was performed by measuring the Nernst potential of three different Cl^- concentration solutions (0.1, 1, and 10 mM KCl). Electrode positioning and vibrating was performed with a stepper-motor–driven three-dimensional positioner. Data acquisition, setting of the voltage parameters, and the three-dimensional electrode micromanipulator were controlled via ASET software (Science Wares and Applicable Electronics). The ion-selective probe vibrated with an excursion of 5 µm, completing the cycle of acquisition in 4 s, which includes a tunable settling time after each move, two measurement periods, and the respective excursion time. All measurements were obtained as close as possible to the tip membrane without touching the tube. Background voltage values were taken after each measurement ~500 µm away from any other pollen grain or tube, and the values were subtracted from the millivolt differential recordings during data processing using a custom made Microsoft Excel sheet. Fluxes were calculated using Fick's law and the chloride diffusion coefficient in aqueous solution at 25°C (-2.03×10^{-5} $cm^{-2}.s^{-1}$) (information withdrawn from Gutermuth et al., 2013).

4. Results

4.1. Molecular Characterization of the Anionic Protein Transporters

4.1.1. Pollen expresses 4 anionic transporter proteins

A full search into the available transcriptomic datasets for *Arabidopsis thaliana* pollen grain (PG) and tube (PT) resulted in the selection of four candidate proteins that due to their known electrophysiological characteristics were strong candidates to account for the observed fluxes in the growing pollen tube (Table 5) (Pina et al., 2005; Wang et al., 2008). The four candidates chosen were AtCCC, SLAH3, ALMT12 and At1g73020 (AtTMEM16).

AtCCC was found to be highly expressed in pollen. For this reason, and because of its role in Na^+ and Cl^- transport in shoots and roots, it was chosen for further analyses. *SLAH3* is also present in high expression level in the grain and tube (Wang et al., 2008; Gutermuth et al., 2013). This channel was recently suggested to be important in the regulation of PT growth *via* a Ca^{2+}-dependent CPK2/CKP20 modulation (Gutermuth et al., 2013). In opposition, the transcripts of the last two proteins, At1g73020 and ALMT12, are detected at lower levels (Pina et al., 2005; Gutermuth et al., 2013). Based on sequence homology, the protein encoded by *At1g73020* belongs to the TMEM16 or anoctamin (ANO) protein family, and for this reason is here designated as AtTMEM16. Mammalian ANO1 and ANO2 have been identified as Ca^{2+}-activated Cl^- channels (mCaCC) (Yang et al., 2008; Schroeder et al., 2008; Caputo et al., 2008). SLAH3 and ALMT12 channels in guard cells, and CaCC in mammalian cells present strong voltage dependence, are activated by hyperpolarization and depolarization membrane potentials (V_m), and the amplitude of their current fluctuates with $[Cl^-]_{ext}$ (Yang et al., 2008; Schroeder et al., 2008; Caputo et al., 2008; Meyer et al., 2010; Geiger et al., 2011). These characteristics feature similarities with the currents found in hydrated pollen grain protoplasts and germinated tubes (Tavares et al., 2011a).

To test whether these proteins account for the anion conductances studied in *Lilium Longiflorum* and *A. thaliana* pollen protoplasts (Tavares, 2011; Tavares et al., 2011a), mutant pollen grain protoplasts from knock-out (KO) plants for all four candidates were obtained and characterized by means of electrophysiological techniques.

Table 4. Channel and Co-transporter candidates for the anionic fluxes found in the transcriptome of pollen grains from *Arabidopsis thaliana*.

Name of Protein and AGI ID	Additional Information
SLAH3 At5g24030	SLAC1 homologue 3; (Geiger et al., 2011).
ALMT12 At4g17970	Belongs to the Al^{3+}-activated Malate Transporter family. Responsible for the R-type currents found in guard cells (Meyer et al., 2010).
AtTMEM16 At1g73020	Mammalian TMEM16 family homologue.
AtCCC At1g30450	Member of Cation-Chloride Co-Transporter Family.

4.1.2. Expression validation of anionic channels and Mutant Genotyping

The transcription of each candidate gene was first verified and confirmed in wild type *A. thaliana* pollen by RT-PCR, using the primers in Table 2 (Materials and Methods (M.M.), page 45). cDNA produced from flowers was used as a control. We confirmed the transcriptional presence of all 4 target genes, ALMT12, SLAH3, AtTMEM16, and AtCCC, both in pollen grains and in flowers (Figure 8).

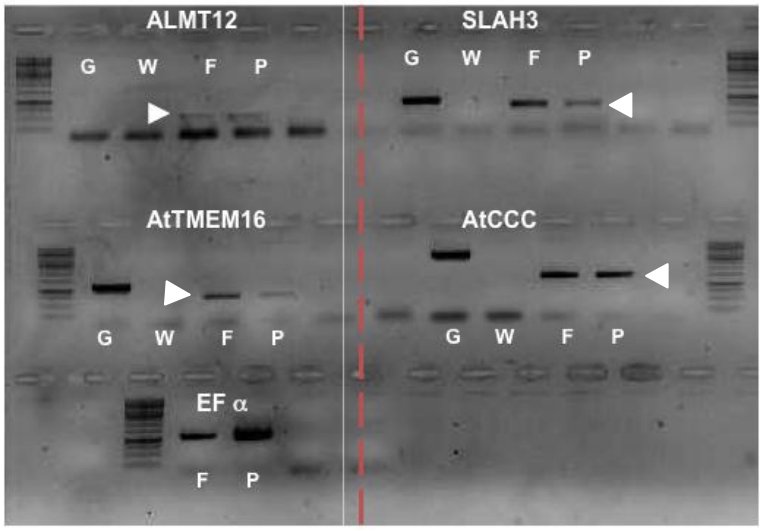

Figure 8. Validation of the transcripts of the candidate genes in tissues from flowers and pollen by RT-PCR. The transcripts of all 4 transporter proteins were detected in both pollen (P) and flowers (F). White arrow heads show the correct sized bands for ALMT12, SLAH3, AtTMEM16 and AtCCC. The elongation factor alpha (EFa) was used to evaluate sample quality. Amplification of the genomic sequence (G) was also performed. Water (W) was added has a negative control. Arrow head depicts the correct sized bands.

Plants homozygous for the T-DNA insertion were genotyped using the primers in Table 1 (M.M, Page 43). The KOs of the mRNAs were confirmed by RT-PCR. Each candidate transcript was only detectable in the Col-0 wild type plant, and absent from homozygous

mutant plants (Figure 9). The absence of transcripts could also be observed in the double mutant lines, *almt12*$^{-/-}$*;slah3*$^{-/-}$ and *attmem16*$^{-/-}$*;atccc*$^{-/-}$ (Figure 9).

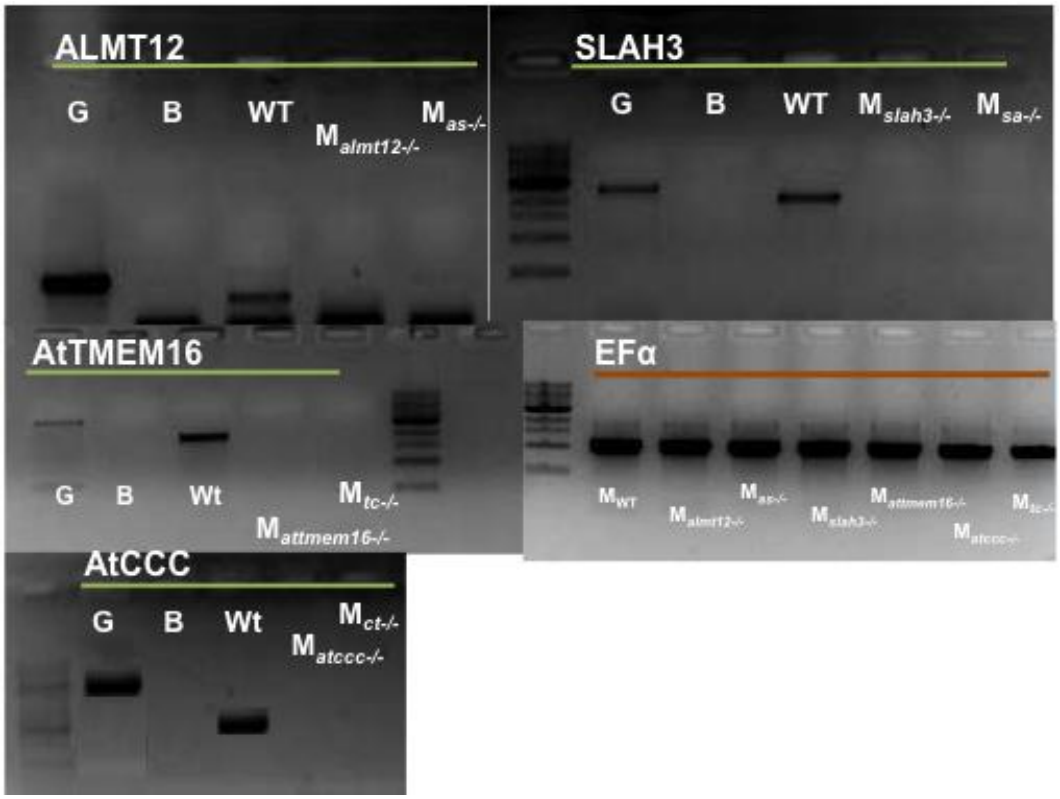

Figure 9. Gene expression of the candidate anionic transporters in leaves from wt and mutants (M) plants by RT-PCR. No transcript was detected in the mutants, confirming that the four homozygous mutant lines are true KO plants. Amplification of the genomic sequence (G) was performed as a control. Water (B) was added has a negative control, and the EFalpha was used to evaluate sample quality in the same PCR reaction. (as$^{-/-}$) is the double mutant *almt12*$^{-/-}$*;slah3*$^{-/-}$ plant, and (ac$^{-/-}$) is the double mutant *atccc*$^{-/-}$*;attmem16*$^{-/-}$.

4.1.3. Morphological Phenotype

No discernible phenotypical differences were observed for the single mutants *attmem16*$^{-/-}$, *slah3*$^{-/-}$ and *almt12*$^{-/-}$ seedlings and grown plants, when compared to the wild type (Figures 10 and 11). Nevertheless, the *atccc*$^{-/-}$ mutant, and the two double mutants *attmem16*$^{-/-}$*; atccc*$^{-/-}$ *and slah3*$^{-/-}$*;almt12*$^{-/-}$ displayed delayed growth (Figure 10 and 11). Additionally, we observed stunted growth, late flowering and bushy inflorescences, (Figure 11 and 12), as well as necrosis in the elongation zone of emerging inflorescence stems (Figure 12), in the mutant line *atccc*$^{-/-}$, in accordance with was previously reported for this mutation (Colmenero-Flores et al., 2007).

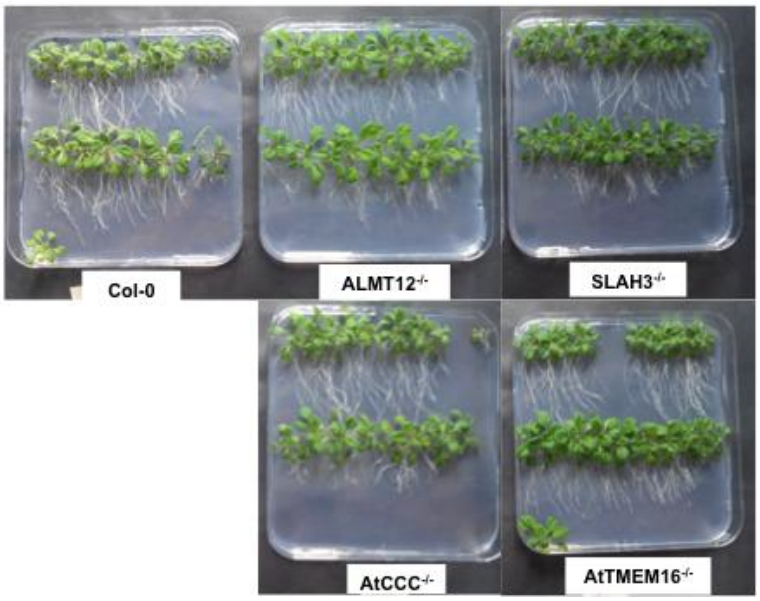

Figure 10. Two week old *Arabidopsis* plants grown in Short Day (SD) photoperiod, of the four anion transport proteins mutants (*almt12*$^{-/-}$, *slah3*$^{-/-}$, *atccc*$^{-/-}$ and *attmem16*$^{-/-}$) side by side with WT plants for comparison. No morphological differences were visualized at this stage.

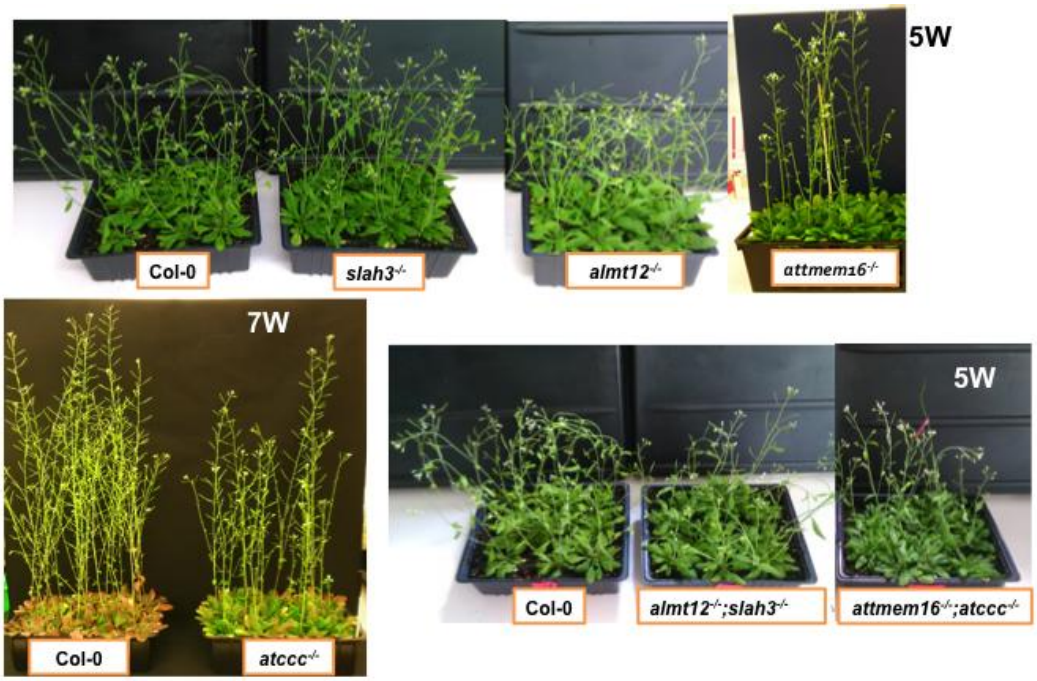

Figure 11. Four and seven week old *Arabidopsis* plants grown in Long-Day chambers (LD). The four anion transporter proteins mutants (*almt12*, *slah3*, *atccc* and *attmem16*) are shown side by side with WT plants for comparison. Crosses were performed to obtain the *slah3 x almt12* and *attmem16 x atccc* double mutant plants. A delay in plant growth is evident in the single *atccc* and the two double mutants *attmem16 x atccc* and *slah3 x almt12.*

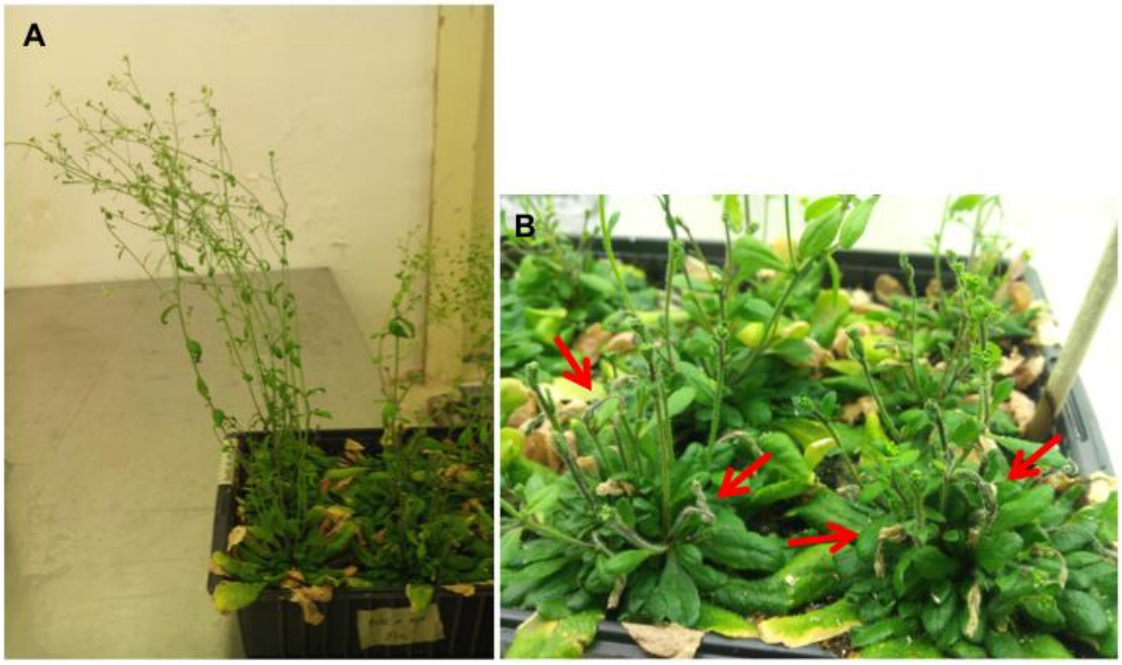

Figure 12. Seven week old *Arabidopsis* double *attmem16*$^{-/-}$*;atccc*$^{-/-}$ mutant plants grown in LD chambers showing **(A)** the whole plant, and **(B)** necrosis in the elongation zone of emerging inflorescence stems (red arrows). This phenotype was also reported for *ccc-1*$^{-/-}$ mutant plants (Colmenero-Flores et al., 2007).

4.2. Electrophysiological Characterization of the Anionic Transporters

4.2.1. Patch Clamp Analysis of the Anionic Currents in Pollen Grain Protoplasts from *Lilium longiflorum* and *Arabidopsis thaliana*

A first attempt to further investigate the nature of the Chloride (Cl^-) fluxes measured by Zonia et al., (2002) in pollen tubes was conducted by whole-cell measurements of Cl^- currents across the plasma membrane of hydrated pollen protoplasts from *Lilium longiflorum* (Tavares, et al., 2011a) and from *Arabidopsis thaliana* (Tavares, 2011), by means of the patch-clamp technique. We applied the whole-cell patch-clamp configuration to protoplasts of pollen grains from both species using symmetrical Cl^- concentrations ($[Cl^-]$) in the bath and pipette solutions. The symmetrical $[Cl^-]$ was chosen in order to eliminate the chemical potential, while isolating the dependence of the currents on the variation of the membrane potential (V_m). These currents were studied by clamping the cell membrane at a holding potential of -100 mV, followed by test membrane potentials (V_m) ranging from -180 mV to +180 mV, with 20 mV increments (M.M., Figure 6, page 54). This voltage protocol triggered steady-state currents showing outward rectification, with the positive currents (anions entering the cell) being greater than the negative currents (anions exiting the cell). The reversal potential of the majority of the Current-Voltage (I/V) curves was close to the

expected equilibrium potential for Cl^- (E_{Cl-} = -0.92 mV). In all protoplasts, a gradual decrease in the maximum amplitude of the currents after breaking into the whole-cell configuration was observed. The rundown of the current is a common feature of channels showing intracellular regulation by effectors, probably because of their dilution during the period required to equilibrate the cytoplasmic content of the cell with the solution from the pipette (Marty & Neher, 1995), a phenomenon already described for anionic channels (Becq, 1996; Binder et al., 2003; Tavares et al., 2011a). The gradual removal of a modulating factor could affect the conductance of all channel populations in the membrane by altering their open probability, thereby impacting steady-state currents at any given voltage(Tavares et al., 2011a).

Overall, under the same experimental conditions both species presented three different conductances of steady-state anion currents, in overall showing outward rectification, i.e., promoting Cl^- influx. The three activities were also shown to be differently regulated by $[Ca^{2+}]_{in}$ (Tavares et al., 2011b). The current lost by rundown (I_{LostRd}; Figure 16A4) may be attributed to a population of channels present in the plasma membrane that are sensitive to intracellular effector(s). After complete rundown, a stable level of current is achieved (I_{Final}, Figure 16A2) (Tavares et al., 2011b). NPPB, a known inhibitor of anion channels, shown to block tobacco and lily pollen tube growth (Zonia et al., 2002; Breygina, et al., 2009a) and Cl^- release from tobacco pollen grain (Breygina et al., 2009a), was then tested on the remaining anionic current. The application of NPPB allowed us to discriminate between two additional populations of anionic currents, one that was insensitive to the inhibitor ($I_{afterNPPB}$, Figure 16A3) and one that was completely abolished in the presence of the inhibitor ($I_{LostNPPB}$, Figure 16A5) (Tavares et al., 2011a).

4.2.1.1. Anionic single-channel currents across the plasma membrane of *Lililum longiflorum* pollen protoplasts

To demonstrate the individual existence of anionic fluxes across channels in the plasma membrane of ungerminated grains, we observed single-channel events from outside-out patches in *L. longiflorum* (Easter lily or Lily). Lily was initially chosen because of the facility in obtaining large quantities of pollen that could be preserved at -20ºC and latter used, unlike the pollen from *Arabidopsis* that had to be collected fresh. In addition, Lily has been regularly used in sexual plant reproduction studies, namely in the study of pollen tube

growth and development (e.g. Rathore et al., 1991; Obermeyer & Kolb, 1993; Zonia et al., 2002; Tavares, 2011; Su et al., 2012).

Single-channel anionic currents were measured from isolated outside-out membrane patches of pollen grain protoplasts with the same intra- and extracellular solutions as those used for whole-cell currents (P1/B1 solutions, M.M., page 53). Before the measurement of single-channel currents, we confirmed the outside-out configuration by measuring the currents in response to the application of the activation voltage protocol (M.M., Figure 6, Page 54). Figure 13A, shows a typical set of currents measured at different membrane potentials (from x to y), jumping from a holding potential of −100 mV. These currents, although much smaller in amplitude than those obtained with the whole-cell configuration, showed the typical outward rectification. To study single-channel events we used longer recordings and higher sampling rates. Figure 13B shows the currents measured from an outside-out patch measured at different membrane potential values (+150, 0 and −150 mV). For potentials ≥ +50 mV we systematically observed bursts of activity with flickering, which displayed greater amplitude with increasing positive potential values (increasing electrochemical gradient for Cl^-). This behavior was consistent during the 20 sec of the recordings and was observed in all the tested cells (n = 38). For negative potentials, we observed a noisier baseline for membrane potentials ≤ −100 mV, which was probably an indication of channel activity. In two cells, we detected single-current events for membrane potentials ≤ −100 mV. We observed only two or three longer opening events per 20 sec recording, while positive currents were active during the entire measurement period. The measured currents displayed opposite directions for positive and negative potentials, according to the applied electrochemical gradients. Concurrently, we never observed unitary currents at 0 mV, which is the reversal potential expected for the currents if they correspond to the equilibrium potentials for Cl^- and NO^{3-}, the two anions present in solution.

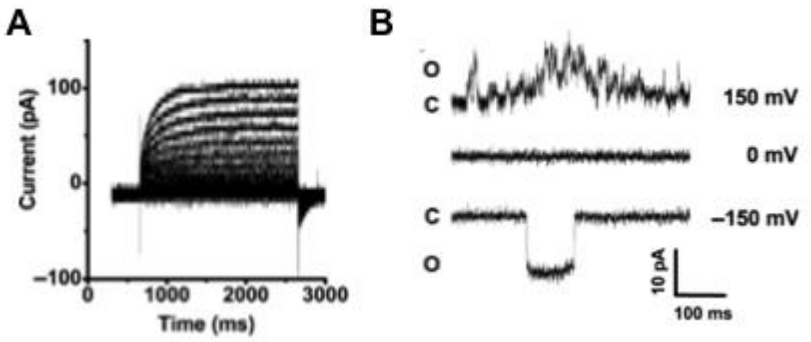

Figure 13. Typical anionic currents from an excised outside-out patch of a pollen grain protoplast of *Lilium longiflorum* (B1/P1, nM Ca^{2+}), measured with P1/B1 solutions. (a). The currents were measured as described

in Fig. 6, (b). Single-channel events acquired at −150, 0 and +150 mV membrane potentials. C, closed state of the channel; O, open states of the channel.

The anionic nature of the unitary currents was confirmed by the use of NPPB (n = 2), a known inhibitor of chloride channels which inhibited a population of the whole-cell currents ($I_{LostNPPB}$). Figure 14 shows currents measured from one cell in the absence (control) and the presence of 500 µM NPPB. The inhibitor caused a shift of the baseline towards values closer to zero for both positive and negative membrane potentials, consistent with an inhibitory effect. This result suggests the presence of small conductance constitutive channels that maintain constant macroscopic levels of anionic current across the plasma membrane of pollen grain protoplasts. We could on occasion observe single-channel events resulting from the inhibition. NPPB induces a flicker type block (e.g. Dreinhöfer et al., 1988), meaning that NPPB enters the channel opening and briefly blocks ion conductance causing the single channel recordings seen in Figure 14B.

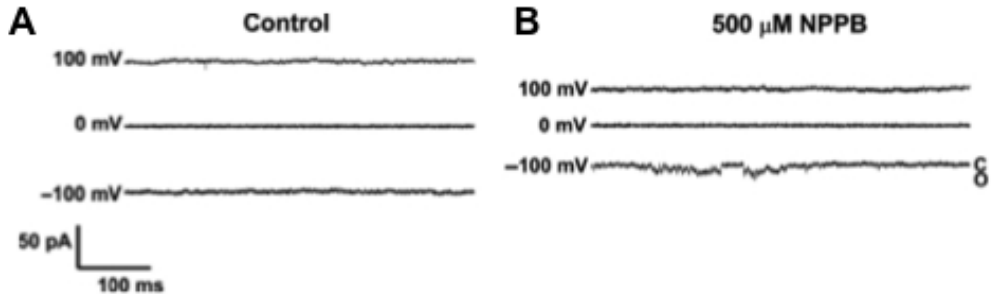

Figure 14. Outside-out anionic currents recorded at -100, 0 and +100 mV membrane potentials before (A) and after the application of 500 µM 5-nitro-2-(phenylpropylamino)-benzoate (NPPB) to the extracellular side (B). The inhibitor reduces the overall amplitude of the current baseline, and exposes single-channel events. C, closed state of the channel; O, open state of the channel.

Although the electrical signals were not suitable for an open probability analysis of the currents, we were still able to detect unitary currents showing different levels of conductance. Figure 15 shows one such recording. As the simultaneous opening of three channels is an improbable occurrence, it is likely that these levels of current represent different conductance sub-states from the same channel (C → O3). This also holds for the simultaneous double closure (O2 → C).

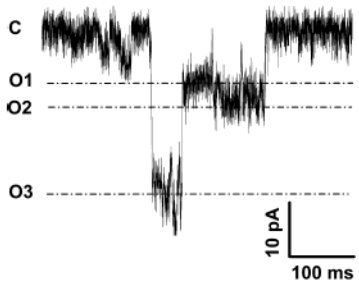

Figure 15. An example of a burst of channel activity showing three conductance states. The currents were measured from an outside-out excised patch held at -100 mV. C, closed state of the channel; O, open states of the channel.

4.2.1.2. Lily pollen tubes presents similar current activities to those measured in hydrated pollen protoplasts

To gain access to the PT plasma membrane, germinated grains were submitted to enzymatic digestion of the cell wall for a short incubation period of 40 min, and protoplasts corresponding to the pollen tube zone were selected on the basis of their smaller size in relation to the sporoplast. However, this protocol does not allow discrimination between the membrane from the sides of the tube and from the tip. The protocol for the isolation of the anionic currents was the same as previously described, and the currents observed were overall similar (n = 4). Figure 16 shows the anionic currents measured with P1/B1 solutions (M.M., page 53). The three detected anionic activities showed strong outward rectification, and the current–voltage relationships reversed near 0 mV, as expected for anionic currents measured with symmetric Cl^--based solutions. Table 5 contains the normalized current values for each population; it also contains the conductance and the Boltzmann parameters calculated for these currents. The values are shown for -160 and 160 mV, here used as representative of the V_m applied. These values were not significantly different from those obtained for the currents measured from Lily pollen grains, suggesting that the same putative channels are responsible for the currents, both in the grain and in the tube.

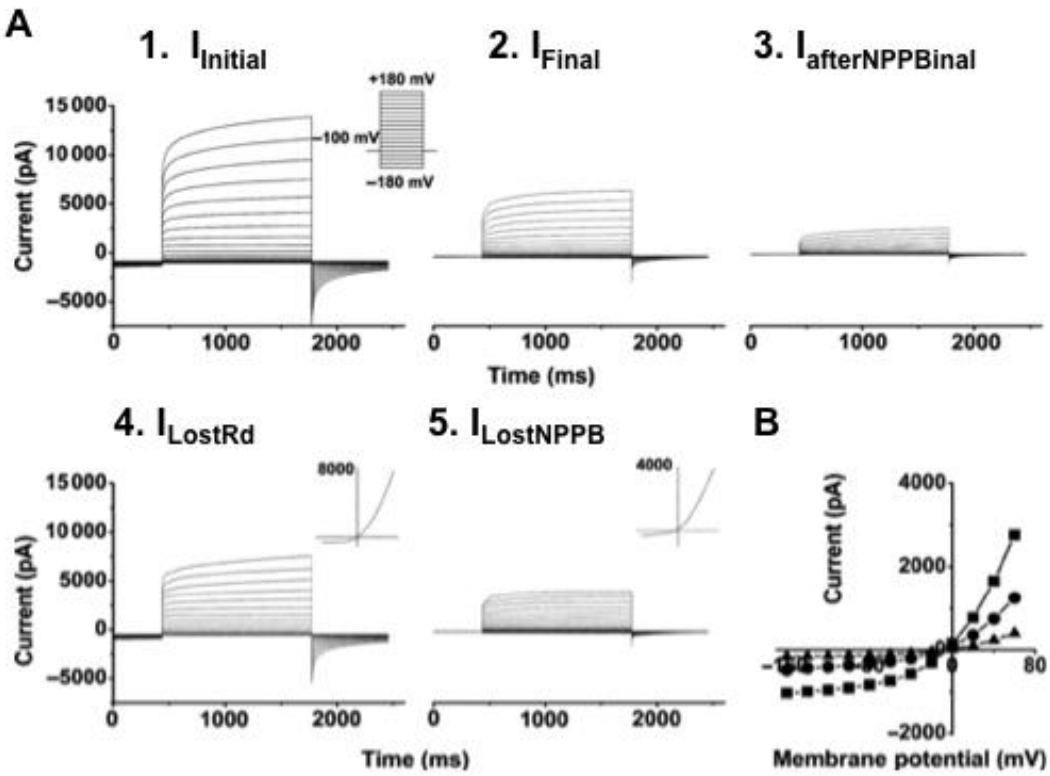

Figure 16. Typical chloride whole-cell currents from a germinated pollen tube of *Lilium longiflorum*, measured with P1/B1 solutions adjusted to 700 mOsmol.kg^{-1}. Currents were triggered from a holding potential of −100 mV with the voltage protocol depicted on the insert of (A1). (A1) The initial current recorded immediately after entering the whole-cell configuration ($I_{Initial}$). (A2) Current recorded after rundown (I_{Final}). (A3) Current recorded after inhibition by 500 µM NPPB ($I_{afterNPPB}$). (A4) Current lost during rundown (I_{LostRd}) obtained by subtraction of $I_{Initial}$ and I_{Final}. (A5) Inhibited current ($I_{LostNPPB}$) obtained by subtraction of I_{final} and $I_{afterNPPB}$. (B) Current–potential (I/V) relationships of $I_{Initial}$ (squares), I_{Final} (circles) and $I_{afterNPPB}$ (triangles) (Tavares et al., 2011a).

Table 5. Steady-state chloride currents' parameters obtained from germinated *L. longiflorum* pollen with B1/P1 solutions. $I_{(-160\ mV)}$ and $I_{(+160\ mV)}$ correspond to the current density (pA/pF) elicited by *Vm* of -160 mV and +160 mV respectively. g_B, g_F, and g_F/g_B refer to the backward conductance, the forward conductance and their ratio, respectively (g_B and g_F are in nSiemmens/pF). V_h is the potential for the half-maximal chord conductance and indicates at which V_m the transition between the minimum and maximum states of conductance occurs, and V_s is the slope of the $G/G_{max}(V_m)$ curve and a measure of the sensitivity of the currents to variations in V_m. (V_h and V_s are in mVolts). V_{rev} refers to the reversal potential and is in mVolts. $I_{Initial}$, I_{Final}, I_{LostRd} and $I_{LostNPPB}$ refer to the current obtained right after entering whole-cell, the current after Rundown, the current lost during Rundown, the current inhibited by NPPB, respectively. %Rundown refers to the percentage of current lost during rundown for V_m = -160 and +160 mV. %Inhibition refers to the percentage of inhibited current for those same V_m. $[NPPB]_{max}$ refer to the maximal [NPPB] needed for maximal inhibition. Data are represented as mean ± SE.

Germinated Lily Pollen

	$I_{(-160\ mV)}$ (pA/pF)		$I_{(+160\ mV)}$ (pA/pF)	n
I_{LostRd}	53 ± 23		247 ± 48	4
$I_{afterNPPB}$	10 ± 1		147 ± 25	4
$I_{LostNPPB}$	7 ± 3		78 ± 30	3
%Rundown	72 ± 9		55 ± 4	
%Inhibition	43 ± 12		37 ± 14	
	g_B (nS)	g_F (nS)	g_F/g_B (nS)	n
I_{LostRd}	2.48 ± 0.78	41.38 ± 8.89	62 ± 50	4
$I_{afterNPPB}$	0.58 ± 0.12	36.14 ± 5.92	66 ± 11	4
$I_{LostNPPB}$	0.94 ± 0.24	17.64 ± 4.86	21 ± 7	3
	V_h (mV)		V_s (mV)	n
I_{LostRd}	7.6 ± 34.0		48.8 ± 10.3	4
$I_{afterNPPB}$	103.8 ± 9.5		63.8 ± 5.2	4
$I_{LostNPPB}$	87.7 ± 15.8		59.0 ± 7.9	3

Table 5 contains values of the percentage of Rundown (%RD) and of Inhibition (%I). The values obtained for RD were 72 ± 9 % (−160 mV) and 55 ± 4 % (+160 mV) (Table 5). The values for %RD are similar to those obtained in hydrated pollen protoplasts measured with higher intracellular $[Ca^{2+}]$ (in the µM to mM range). Conversely, the currents $I_{afterNPPB}$ and $I_{LostNPPB}$ obtained from germinated pollen reached values that approximate those obtained from a hydrated grain with the lowest $[Ca^{2+}]_{in}$ tested (6.04 nM). This result suggests that the relative contributions of I_{LostRd}, $I_{afterRd}$ and $I_{LostNPPB}$ to the total current crossing the cell membrane at a given time may differ between the hydrated grain and tube growth, probably as a consequence of regulatory mechanisms other than Ca^{2+} or due to the presence of different channels in the plasma membrane. Consistent with this finding, the percentages of inhibition with a maximum of 500 µM NPPB were 43 ± 12% (−160 mV) and 37 ± 14% (+160

mV), were significantly different from the values obtained with hydrated pollen protoplasts (Table 5).

4.2.1.3. The absence of AtTMEM16 and SLAH3 channels, but not ALMT12, generates higher $I_{Initial}$

The AtTMEM16, SLAH3 and ALMT12 transporters that are expressed in pollen from *Arabidopsis thaliana*, were further characterized by determining the anionic currents of the respective KO pollen grain protoplasts. Unlike AtTMEM16, SLAH3 and AtALMT12, which present electrogenic transport, (i.e., they generate net charge across the membrane), the AtCCC co-transporter is electroneutral, and for this reason its electrophysiological role in pollen germination and growth can only be described through the use of the vibrating probe system.

Before a more thorough analysis was performed, the intensity of the currents of each protoplast was normalized with the respective membrane capacitance (C_m), resulting in current density values (pA/pF) that were used to build the Current – Potential (I/V) curves (Figures18 and 19). All V_m applied were considered for comparative analysis, but to simplify, only the average values for the V_m -160 mV and +160 mV are shown as representative. Figure 17 and 18, and Table 6 and 7, depict the I/V curves values of the measured normalized currents and the parameters obtained from them. Taken together with the values for the current density, it is possible to confirm that the channels responsible for the measured currents in *A. thaliana* protoplasts show strong outward rectification, but allows the passage of current in both directions.

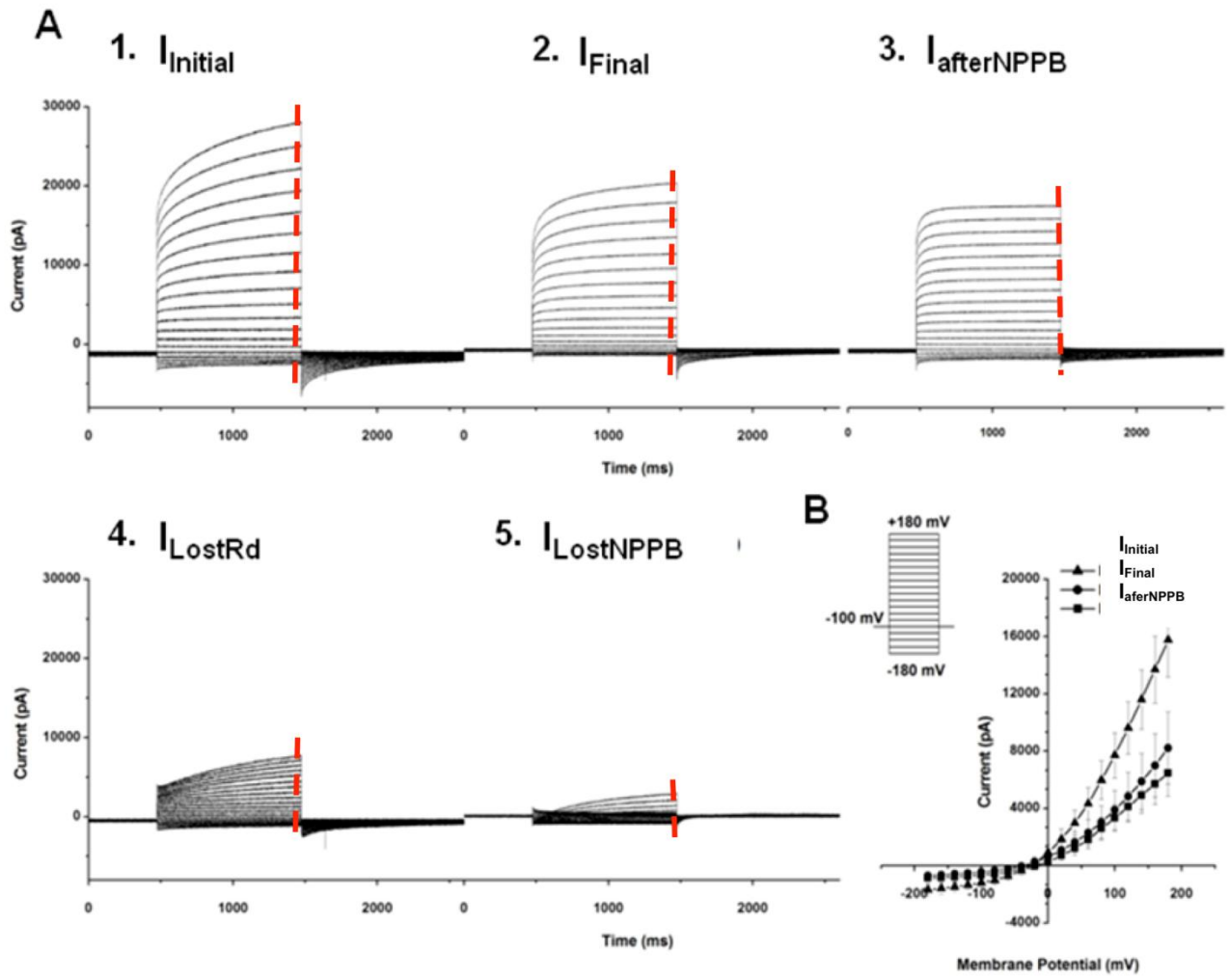

Figure 17. Typical chloride whole-cell currents from a pollen grain protoplast of the mutant KO line *slah3*, measured with B1/P1 solutions adjusted to 800 mOsmol.kg^{-1}. The currents were elicited from a holding potential of -100 mV with the voltage protocol depicted in B. A1 - 5 portray the raw data obtained for these currents: A1 represents the Initial current recorded immediately after entering whole-cell configuration ($I_{Initial}$); A2, the current recorded after Rundown (I_{Final}); A3, the current recorded after inhibition by 100 µM NPPB ($I_{afterNPPB}$); A4, the current lost during rundown (I_{LostRd}) obtained by subtracting $I_{Initial}$ and I_{Final}; A5, the Inhibited Current ($I_{LostNPPB}$) obtained by subtracting I_{Final} and $I_{afterNPPB}$. B, represents the average Current-Potential (I/V) relationships of $I_{Initial}$ (▲), I_{Final} (●), and $I_{afterNPPB}$ (■) obtained for all *slah3* pollen protoplasts tested (n = 13). The data to construct this curve was averaged from the last 100 ms of the respective raw data for each protoplast (red dashed lines).

Figure 17A represents the raw data of the anionic currents obtained from one *slah3*$^{-/-}$ mutant protoplast, using B1/P1 solutions. They represent, from A1 to A5, $I_{Initial}$, I_{Final}, $I_{afterNPPB}$, I_{LostRd} and $I_{LostNPPB}$, respectively. Figure 17B shows the average Current - Voltage (I/V) relationships obtained by plotting the elicited steady-state (non-normalized) currents from all mutant protoplasts measured (average of the points from the final 100 ms of each pulse – red dashed line) against the corresponding V_m. These curves refer to $I_{Initial}$ (▲), I_{Final} (●), and $I_{afterNPPB}$ (■). In Figure 17B, it is possible not only to observe the decrease in the current's amplitude before and after rundown, but also a slight reduction caused by the

inhibitor NPPB. Similarly, $I_{Initial}$ reductions were obtained from WT protoplasts, but when NPPB was applied, a higher % of current loss was obtained for all V_m tested (Table 6). From the present WT data it is not possible to determine whether I_{LostRd}, $I_{afterNPPB}$ and $I_{LostNPPB}$ are the result of three different conductance states of one channel or of three different channels. Therefore, I_{LostRd} and $I_{LostNPPB}$ are addressed as current populations and will be considered so for analysis. In addition, $I_{Initial}$ will be also analyzed, in order to fully visualize the differences between KO protein mutants and WT (Control). The raw data obtained for the two mutants, *attmem16*$^{-/-}$ and *almt12*$^{-/--}$ (Figure 23A), depicted a similar electrophysiological behavior as to the measured for both *slah3*$^{-/-}$ and *wt*. (Figure 17 and 18): a strong outward rectification and current loss by rundown. For this reason only traces of a *slah3*$^{-/-}$ protoplast are shown (Figure 17).

The expected result for the mutant lines would be an overall reduction of the anion currents. Surprisingly, *attmem16*$^{-/-}$ and *slah3*$^{-/-}$ protoplasts elicited higher $I_{Initial}$ (currents measured after entering WC) than those obtained for WT. The I_{Inital} values for *wt* are: 467 ± 65 and -105 ± 12 pA/pF for +160 mV and -160 mV, respectively (Table 6). These values were then compared with those obtained from mutant protoplasts. Specifically, the absence of AtTMEM16 protein produced a statistically significant increase in $I_{Initial}$ for all V_m tested by an average of 63% and 45%, for -160 mV (-171 ± 37 mV) and +160 mV (678 ± 93 mV), respectively. Similarly, *slah3*$^{-/-}$ protoplasts elicited a significantly higher $I_{Initial}$ for the positive V_m, increasing on average 94% (+160 mV; 907 ± 127 pA/pF). On the other hand, *almt12*$^{-/-}$ protoplasts produced on average 22% less $I_{Initial}$, when negative V_m were applied (-160 mV; -81 ± 15 pA/pF).

The reversal potential (V_{rev}) measured right after entering WC for *wt*, and *attmem16*, *almt12* and *slah3* mutant protoplasts was -1.3 ± 0.7, -0.3 ± 1.4, -0.3 ± 0.3 and -10 ± 5.6 mV, respectively. The V_{rev} in the first 2 mutants was similar to the equilibrium potential of Cl^- (E_{Cl-}), confirming that the $I_{Initial}$ measured are due to the passage of Cl^- ions. However, $I_{Initial}$ from *slah3*$^{-/-}$ presented a significant shift towards more negative V_m than WT and the other two mutants analyzed. This result is suggestive that SLAH3 channel activity impacts other transporters, like for e.g. Ca^{2+} channels that would shift the V_{rev} towards more negative V_m. This shift was lost after the current stabilized.

4.2.1.4. Disruption of AtTMEM16 and SLAH3 channels generates higher current loss by Rundown for depolarizing V_m

Figure 18A depicts raw data obtained from a WT protoplast right after entering whole cell; the dashed red line indicates the timing (last 100 ms), where an average of the current was performed from the respective test potential. The average normalized I/V curves produced from these points for each raw data and test group, are shown in Figure 18B. Figure 19, illustrates in greater detail the data summarized in Figure 18, in order to better observe the currents obtained in the negative V_m range.

As mentioned, a gradual decrease of the currents' intensity after breaking into the WC configuration was observed in all protoplasts. This loss of current can be observed in both Figure 18 and in Figure 19. Under WT conditions, the percentage of anionic current lost during rundown (%RD) increased in in the mutants in a statistically significant manner for negative V_m, and was constant for positive V_m. To simplify the comparative analysis of this factor in different experimental groups, only the %RD obtained for representative V_m (-160 mV and +160 mV) are shown. The values of this parameter in *wt* protoplasts are 55 ± 5 % and 46 ± 4 % for -160 and +160 mV, respectively. This difference is indicative of the loss of an intracellular effector during RD, which regulates these currents, and its absence seems to impact stronger at negative transmembrane potentials.

The values of %RD parameter for -160 and +160 mV obtained for the three mutant groups are: *almt12*$^{-/-}$, 63 ± 9 % and 52 ± 9 %; *attmem16*$^{-/-}$, 63 ± 4 % and 65 ± 5 %; and *slah3*$^{-/-}$ 53 ± 13 % and 52 ± 11 %, respectively (Table 6). *Wt* and *almt12*$^{-/-}$ protoplasts presented a non significant difference of the %RD values for the positive V_m tested. In opposition to the *wt* group, *attmem16*$^{-/-}$ protoplasts depicted a statistically significant increase in the %RD for positive V_m, and constant %RD values for negative V_m. Moreover, %RD measured from *slah3*$^{-/-}$ protoplasts exhibited a constant non-significant increase for all V_m tested. Both *attmem16*$^{-/-}$ and *slah3*$^{-/-}$ protoplasts presented a similar non-significant increase for the negative V_m,. Despite the statistical non-significance of these increases, the data warrants further investigations, as it may reveal a similar mechanism of regulation. Specifically, when AtTMEM16 or SLAH3 channels are not present, the intracellular effector is unable to actuate, which strongly suggests that the same intracellular effector regulates both channels in the negative V_m. Similarly, *almt12*$^{-/-}$ also elicited a significantly higher %RD in this V_m range, in relation to the WT. Interestingly, this increase was constant with the applied V_m which might imply that different types of intracellular effectors regulate these channels.

The significant increase in %RD observed for *attmem16*$^{-/-}$ and *slah3*$^{-/-}$ protoplasts for the positive V_m resulted in a statistical loss of current due to RD (I_{LostRD}) for the same V_m. For +160 mV, *attmem16*$^{-/-}$ and *slah3*$^{-/-}$ protoplasts elicited 95% and 142% more I_{LostRD} than that measured in WT protoplasts (Table 6). Interestingly, after the currents stabilized (I_{Final}), *attmem16*$^{-/-}$ continue to elicit significantly more current than the WT (> 70%), while *almt12*$^{-/-}$ elicited significantly less current (< 55%), when negative V_m were applied. Additionally, the I_{Final} elicited from *slah3*$^{-/-}$ and WT became comparable for all V_m tested. The average I_{Final} values obtained from *slah3*$^{-/-}$ and WT for +160 and -160 mV are, 350 ± 95 and 247 ± 45 pA/pF, and -48 ± 9.1 and -54 ± 7 pA/pF, respectively.

As expected, V_{rev} for I_{Final} (-4.3 ± 1 mV, 0.5 ± 2.4, -5.5 ± 0.9 and 3.2 ± 2.3 for *wt*, *attmem16*$^{-/-}$, *almt12*$^{-/-}$ and *slah3*$^{-/-}$, respectively) are similar to E_{Cl-} (-0.92 mV), which further confirms the nature of these anionic currents (Table 6). Interestingly, V_{rev} obtained for the I_{LostRd} in the WT group is 18 ± 0.7 mV. The discrepancy from the E_{Cl-} was significantly more positive for the WT group when compared to the *attmem16*$^{-/-}$, *almt12*$^{-/-}$ and *slah3*$^{-/-}$ groups (4.4 ± 3.8 mV, 3.7 ± 1.4 mV and -4.5 ± 2.3 mV, respectively). This shift can be explained by: 1) the passage through the membrane of other permeable intracellular ions during the process of current stabilization (rundown), which would cause a shift of V_{rev} to more positive values; 2) it can also be explained by the leakage of cations, such as Ca^{2+} (E_{Ca}^{2+} = 165.01), Mg^{2+} (E_{Mg}^{2+} = 15.32) or H^+ (E_{H}^{+} = 81.11 mV), from the pipette into the bath solution, or by the passage of H^+ through transporters such as H^+ - anion antiporters, or of other cations thought cationic transporters; and 3) since the three mutant groups do not depict the same positive V_{rev} shift measured for the WT, one can speculate that AtTMEM16, SLAH3 and ALMT12 channels may directly or indirectly regulate the passage of H^+ through transporters. The cation leakage suggestion, although more common, is less likely to occur in this system, since the majority of the seals obtained had a resistance > 500 MΩ.

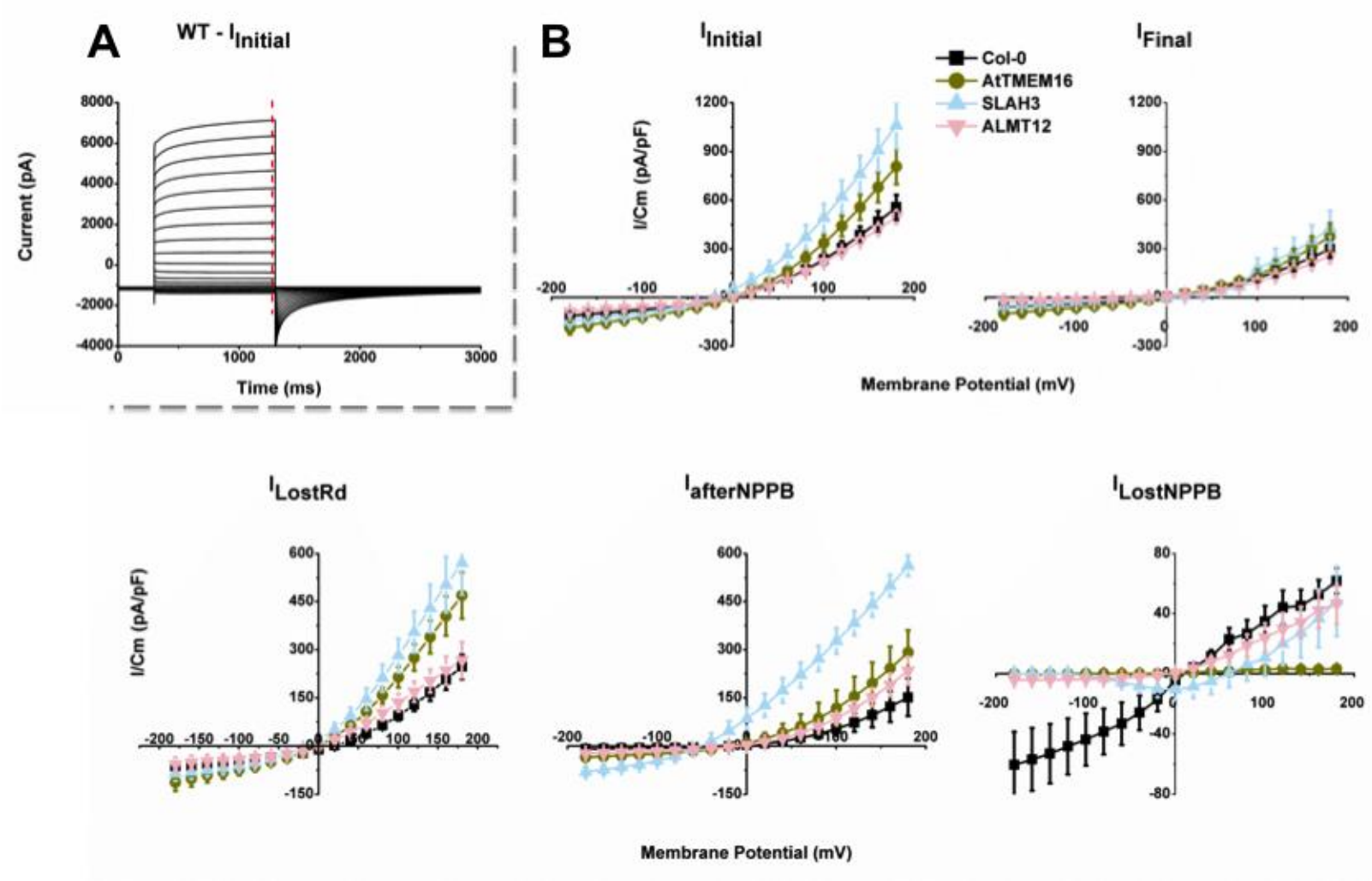

Figure 18. Chloride WC currents from WT and mutant pollen grain protoplasts of *A.thaliana*, measured with B1/P1 solutions. The currents were elicited from a holding potential of -100 mV with the voltage protocol in M.M., page 54. A, represents a typical WT initial current recorded immediately after entering whole-cell configuration ($I_{initial}$). The data to construct the I/V curves shown in B were averaged from the last 100 ms of the each respective raw data point (red dashed line). B, represents the average normalized Current-Potential (I/V) relationships of $I_{initial}$, the current after Rundown (I_{Final}), current lost by Rundown (I_{LostRd}), current acquired after application of NPPB ($I_{AfterNPPB}$) and inhibited current ($I_{LostNPPB}$), obtained from pollen protoplasts of WT and the mutant lines, *attmem16*$^{-/-}$, *slah3*$^{-/-}$ and *almt12*$^{-/-}$.

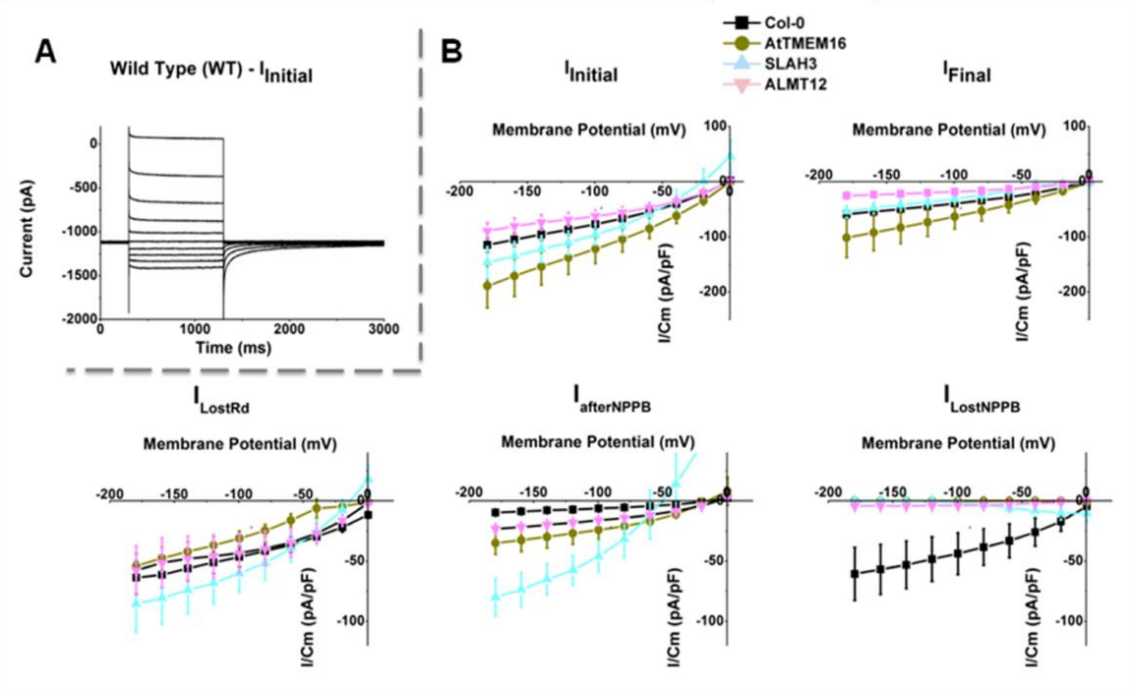

Figure 19. Expanded view of the negative currents shown in Figure 18 elicited for negative V_m..

4.2.1.5. AtTMEM16, SLAH3 and ALMT12 channels are sensitive to NPPB

After the stabilization of the rundown, the anion channel inhibitor NPPB was tested on the remaining current. A maximum inhibition of the Cl^- currents was obtained for a NPPB concentration ([NPPB]) of 300 µM. Unlike the %Rundown, the percentage of inhibited current (%Inhibition) was constant for all V_m for both positive and negative V_m in the WT group. This can indicate that the inhibition process is independent from changes in the transmembrane portential. Inhibition by NPPB in a voltage-independent manner has been previously demonstrated in such anionic channels as the volume-activated Cl^- channel (Schmid et al., 1998; von Weikersthal et al., 1999), and the mammalian Ca^{2+}-activated Cl^- channel (Hartzell et al., 2005).

The %Inhibition obtained for the three mutant groups was significantly different when compared to the *wt* group. The %Inhibition values for -160 and +160 mV were: 48 ± 21 % and 38 ± 8.4 % for WT and 14 ± 7 % and 18 ± 4.2 % for *almt12*$^{-/-}$, respectively (Table 6). Surprisingly, both *attmem16*$^{-/-}$ and *slah3*$^{-/-}$ currents suffered a minor inhibition on positive V_m (> + 20 mV); for +160 mV the values were: 4.7 ± 2.5 % and 6 ± 2.7 %, respectively, which could help explain the non-significant change obtained for the reverse potentials in $I_{LostNPPB}$. These

results imply that both AtTMEM16 and SLAH3 belong to the population of anionic channels that show higher sensitivity to NPPB. In addition, *almt12*$^{-/-}$ I_{Final} inhibition by NPPB was partial (when compared to the WT), suggesting that NPPB causes a low-effect block on ALMT12 channels.

Table 6. *A.thaliana* steady-state chloride currents' parameters calculated for WT and for the different mutant lines, *attmem16*, *almt12* and *slah3* obtained in B1/P1 solutions adjusted to 800 mOsmol.kg^{-1}. Parameters $I_{(-160\ mV)}$, $I_{(+160\ mV)}$, V_{rev}, $I_{Initial}$, I_{Final}, I_{LostRd}, $I_{LostNPPB}$, %Rundown, and %Inhibition as described in Table 5. $[NPPB]_{max}$ was 300 µM. Data are represented as mean ± SE. *, refer to significant differences between comparable elements in the same experimental group. ¥, refer to significant differences between comparable elements in different experimental groups ($p < 0.05$).

	WT (Control)				***attmem16*$^{-/-}$**				***almt12*$^{-/-}$**				***slah3*$^{-/-}$**			
	$I_{(-160\ mV)}$ (pA/pF)	**$I_{(+160\ mV)}$ (pA/pF)**	**V_{rev} (mV)**	**n**	**$I_{(-160\ mV)}$ (pA/pF)**	**$I_{(+160\ mV)}$ (pA/pF)**	**V_{rev} (mV)**	**n**	**$I_{(-160\ mV)}$ (pA/pF)**	**$I_{(+160\ mV)}$ (pA/pF)**	**V_{rev} (mV)**	**n**	**$I_{(-160\ mV)}$ (pA/pF)**	**$I_{(+160\ mV)}$ (pA/pF)**	**V_{rev} (mV)**	**n**
$I_{Initial}$	-105 ± 12	467 ± 65	-1.3 ± 0.7	27	-171 ± 37¥	678 ± 93¥	-0.3 ± 1.4	21	-81 ± 15¥	421 ± 29	-0.3 ± 0.3	5	-135 ± 26	907 ± 127¥	-10 ± 5.6¥	13
I_{Final}	-54 ± 7	247 ± 45	-4.3 ± 1	27	-92 ± 33¥	307 ± 71	0.5 ± 2.4	20	-24 ± 4.3¥	210 ± 37	-5.5 ± 0.9	4	-48 ± 9.1	350 ± 95	3.2 ± 2.3	13
I_{LostRd}	-61 ± 11	207 ± 32	18 ± 0.7	27	-102 ± 25	404 ± 61¥	4.4 ± 3.8¥	20	-51 ± 20	235 ± 45	3.7 ± 1.4¥	4	-80 ± 22	502 ± 88¥	-4.5 ± 2.3¥	13
$I_{LostNPPB}$	-56 ± 21	53 ± 9.8	-7.6 ± 13	5	-1.7 ± 0¥	13 ± 10¥	3 ± 6.8	3	-4 ± 2¥	42 ± 12	-4.3 ± 1.4	3	2.6 ± 3.2¥	36.8 ± 19	49.7 ± 27.5	4
%Rundown	54.6 ± 5	46 ± 3.6*		27	63 ± 4¥	65 ± 5*¥		20	63 ± 9¥	52 ± 9*		4	62 ± 6.7¥	62 ± 6.4¥		13
%Inhibition	48 ± 21	38 ± 8.4		5	-	4.7 ± 2.5¥		3	14 ± 7¥	18 ± 4.2¥		3	-	6 ± 2.7¥		4

Table 7. *A. thaliana* steady-state chloride currents' parameters calculated for WT and for the different mutant lines, *attmem16*, *almt12* and *slah3* obtained in B1/P1 solutions adjusted to 800 mOsmol.kg^{-1}. Parameters g_B, g_F, g_F/g_B, V_h, V_s, $I_{Initial}$, I_{Final}, I_{LostRd}, and $I_{LostNPPB}$, obtained from the respective normalized currents described in Table 6. The parameters were used as described in Table 5. Data are represented as mean ± SE. *, refer to significant differences between comparable elements in the same experimental group. ¥, refer to significant differences between comparable elements in different experimental groups ($p < 0.05$).

	WT (Control)				***attmem16*$^{-/-}$**				***almt12*$^{-/-}$**				***slah3*$^{-/-}$**			
	g_B (nS/pF)	**g_F (nS/pF)**	**g_F/g_B**	**n**	**g_B (nS/pF)**	**g_F (nS/pF)**	**g_F/g_B**	**n**	**g_B (nS/pF)**	**g_F (nS/pF)**	**g_F/g_B**	**n**	**g_B (nS/pF)**	**g_F (nS/pF)**	**g_F/g_B**	**n**
$I_{Initial}$	0.5 ± 0.006	4.3 ± 0.6	16 ± 3	27	0.9 ± 0.2¥	6 ± 0.8¥	16 ± 3	21	0.4 ± 0.08	3.7 ± 0.5	12 ± 3.4	5	0.6 ± 0.1	7 ± 0.9¥	23 ± 8.7	13
I_{Final}	0.24 ± 0.03	2.5 ± 0.4	15 ± 3	27	0.5 ± 0.2	3.3 ± 0.7	23 ± 7	20	0.08 ± 0.02¥	2.2 ± 0.3	31 ± 7¥	4	0.3 ± 0.08	3.6 ± 0.6	17.5 ± 3	12
I_{LostRd}	0.3 ± 0.07	2 ± 0.4	12 ± 3	27	0.4 ± 0.2	3 ± 0.6	10 ± 3	20	0.24 ± 0.08	1.6 ± 0.7	10 ± 5	4	0.4 ± 0.1	4 ± 0.7	17 ± 4.6	12
$I_{LostNPPB}$	0.08 ± 0.05	0.5 ± 0.04	5.6 ± 8	5	-	0.2 ± 0.1	-	3	-	0.3 ± 0.09	-	3	-	0.4 ± 0.2	-	4
	V_h (mV)	**V_s (mV^{-1})**		**n**	**V_h (mV)**	**V_s (mV^{-1})**		**n**	**V_h (mV)**	**V_s (mV^{-1})**		**n**	**V_h (mV)**	**V_s (mV^{-1})**		**n**
$I_{Initial}$	93 ± 3	73 ± 2		27	92 ± 3	68 ± 2		21	81 ± 3	64 ± 2		5	71 ± 3	68 ± 3		12
I_{Final}	172 ± 7	93 ± 2		27	191 ± 23	87 ± 6		21	122 ± 5¥	74 ± 3¥		4	240 ± 31¥	96 ± 6		12
I_{LostRd}	81 ± 3	61 ± 2		27	80 ± 3	71 ± 2		20	55 ± 5¥	57 ± 4		4	45 ± 3¥	54 ± 3		12
$I_{LostNPPB}$	153 ± 48	103.7 ± 20		5	-17 ± 3¥	7 ± 3¥		3	30 ± 5¥	45 ± 5¥		3	-31 ± 17¥	62 ± 23¥		4

4.2.1.6. The absence of ALMT12 channel causes a significantly decrease in the backward conductance

The asymptotic forward and backward conductances, g_F and g_B, respectively, and the respective ratio g_F/g_B, are other important parameters used to characterize a ionic channel. Table 7, depicts the values for all *wt* and mutant groups analyzed. The $I_{Initial}$ measured from *attmem16*$^{-/-}$ and *slah3*$^{-/-}$ show a significantly higher g_F (6 ± 0.8 nS/pF and 7 ± 0.9 nS/pF, respectively), when compared to the *wt* (g_F 4.3 ± 0.6 nS/pF). The g_B from $I_{Initial}$ of *attmem16*$^{-/-}$ protoplasts (0.9 ± 0.2 nS/pF) also depict a statistically significant difference with the g_B measured for *wt* (0.5 ± 0.006 nS/pF). These differences illustrate that the anionic channels present in *slah3*$^{-/-}$ and *attmem16*$^{-/-}$ are more conductive than the anionic channels present in the *wt* protoplasts. Specifically, *slah3*$^{-/-}$ elicited more current for depolarizing V_m, while *attmem16*$^{-/-}$ elicited more current for all V_m tested. After rundown, no significant differences were detected for *slah3*$^{-/-}$ and *attmem16*$^{-/-}$ (Table 7). Surprisingly, *almt12*$^{-/-}$ currents obtained after Rundown (I_{Final}) present a significantly higher g_F/g_B ratio, 31 ± 7, than that of *wt*, *attmem16*$^{-/-}$ and *slah3*$^{-/-}$ groups, 15 ± 3, 23 ± 7 and 17.5 ± 3, respectively. A higher ratio indicates stronger rectification, in this case caused by a significant reduction of g_B shown by *almt12*$^{-/-}$, when compared to the WT (g_B = 0.08 ± 0.02 pA/pF and 0.24 ± 0.03 pA/pF, respectively). This result suggests that the lack of ALMT12 channels in *almt12*$^{-/-}$ protoplasts caused a decrease in the global ion conductivity in the negative V_m range tested. In opposition, an increase was observed in *slah3*$^{-/-}$ and *attmem16*$^{-/-}$ mutants.

In order to study the variation of the conductance with the applied V_m, the values for the current intensity were converted into their respective cord conductances (G) by applying Equation 1 (M.M., page 56). They were then normalized and plotted against V_m. The data were fitted with Equation 2 (M.M., page 56), and the characterizing parameters V_h – potential corresponding to the half-maximal chord conductance, indicating at which V_m the transition between the two states of conductance (minimum and maximum) occurs; and V_s – the slope of the $G/G_{max}(V_m)$ curve and a measure of the sensitivity of the currents to variations in V_m for all test groups were also included in Tables 6 and 7. Experimentally it was not possible to elevate V_m to values higher than +200 mV.

Nevertheless, at V_m ≈ +200 mV the maximum conductance had not been achieved and its variation was still dependent on the potential. Therefore, the values of V_s and V_h for the analyzed currents (especially for I_{Final}) depicted in Table 7 are an approximation. According to these data, all test groups suffered subtle variations in both fitting parameters, and were more evident after Rundown occurred (I_{Final}). The V_h obtained from I_{Final} *almt12*$^{-/-}$ and *slah3*$^{-/-}$ protoplasts, presented different sensitivities to variations in V_m, when compared to the WT group; the transition between the minimum and the maximum conductance states occurred at significantly smaller or higher V_m, 122 ± 5 mV and 240 ± 31 mV, respectively. Given that V_h specifies the potential to which the channels reach 50% of their maximum conductivity, the data are suggestive that the shifts measured in both mutants are due to the absence of the AtALMT12 and AtSLAH3 proteins and the lack of each contribution to the overall current. Moreover, the sensitivity (V_s) of the *almt12*$^{-/-}$ currents, but not *slah3*$^{-/-}$ currents, significantly shifted to less depolarizing potentials, from 93 ± 2 (WT) to 74 ± 3 mV^{-1}. This shift indicates that the absence of this channel alters the sensitivity to V_m of the population of channels present in *almt12*$^{-/-}$ protoplasts.

As already seen, the current sensitive to NPPB measured from the three mutant protoplasts varied significantly (Table 6), and as a result so did V_h and V_s Boltzmann fitting parameters (Table 7). When compared to *wt* value V_h = 153 ± 48 mV, the transition between the minimum and the maximum conductance states observed in *attmem16*$^{-/-}$, *almt12*$^{-/-}$ and *slah3*$^{-/-}$ protoplasts are significantly altered towards less depolarizing and hyperpolarizing V_m, with V_h = -17 ± 3, 30 ± 5 and -31 ± 17 mV, respectively. This dramatic shift towards less depolarizing and hyperpolarizing V_m, strongly indicates that the measured NPPB sensitive currents from WT are significantly reduced in *attmem16*$^{-/-}$, *almt12*$^{-/-}$ and *slah3*$^{-/-}$ protoplasts. In addition, the sensitivity of the currents to variations in V_m, measured for the three mutants, is also significantly altered towards lower depolarizing V_m. These results suggest that AtTMEM16, SLAH3 and ALMT12 channels are sensitive to NPPB, as previously stated, and that their individual absence affects the remaining sensitivity of the currents to variations in V_m.

4.2.1.7. The double mutant *almt12*$^{-/-}$;*slah3*$^{-/-}$ causes a significantly decrease in all currents analyzed

Table 8 depicts the same parameters shown in Table 5, for the data obtained from the double mutant *almt12*$^{-/-}$;*slah3*$^{-/-}$. Several distinctions from the single mutants and WT are evident and statistically significant. The first major difference was observed in the current obtained right after entering WC for the negative V_m (-49 ± 10.2 pA/pF), which showed a reduction almost by half in relation to *almt12*$^{-/-}$ (-81 ± 15 pA/pF) and more than half than WT (-105 ±12 pA/pF) and *slah3*$^{-/-}$ (-135 ± 26). Surprisingly, the $I_{Initial}$ obtained for the double mutant for the positive V_m did not differ from the WT (460 ± 32.5 and 467 ± 65 pA/pF, respectively), and the I_{Final} was more similar to that of *almt12*$^{-/-}$ (211 ± 26 and 210 ± 37, respectively). This tendency was maintained after RD (Table 8). As a consequence, the %RD was much higher for the negative V_m, and the g_F/g_B ratio was significantly higher (81 ± 18.6, Table 8), depicting strong outward rectification.

Interestingly, the V_{rev} for $I_{Initial}$ was close to the one obtained for the single *slah3*$^{-/-}$ (-9.5 ± 2.5 and -10 ± 5.6 mV, respectively). In addition, the reduced $I_{Initial}$ and I_{Final} and respective backward conductance (0.04 ± 0.01 nS/pF, Table 8) observed in the double mutant define these channels as major contributors to the overall current, especially at the physiological negative membrane potentials. Again, after the current stabilized, a maximum of 300 µM NPPB was added to the bath medium. The *almt12*$^{-/-}$;*slah3*$^{-/-}$ presented a slightly higher $I_{LostNPPB}$ for the negative potentials tested, -1.1 ± 0.4 pA/pF, in relation to the single *slah3*$^{-/-}$, 2.6 ± 3.2 pA/pF, but lesser than that of *almt12*$^{-/-}$, -4 ± 2 pA/pF. The lack of complete inhibition presented by the double mutant, as seen in the single's *almt12*$^{-/-}$ and *slah3*$^{-/-}$, could imply that other mechanisms of regulation and/or other channel populations might contribute to the overall current, which would help explain the different sensitivities to NPPB. This hypothesis is supported by the values obtained for V_h parameter acquired from $I_{Initial}$ and $I_{LostNPPB}$. The V_h of *almt12*$^{-/-}$;*slah3*$^{-/-}$ protoplasts show a similar potential (101 ± 2.8 mV) when compared to the WT, but not with the single *almt12*$^{-/-}$ and *slah3*$^{-/-}$ mutants (93 ± 3, 81 ± 3 and 71 ± 3 mV, respectively), suggesting that a higher or different channel populations are contributing to the overall measured

currents (Table 7 and 8). Furthermore, the V_s from $I_{Initial}$, was significantly altered to less depolarizing V_m (60.5 ± 1.6 mV), in relation to the WT (73 ± 2). This tendency was maintained after RD (I_{Final}) (Table 8).

After applying NPPB, the V_h calculated from $I_{LostNPPB}$ in *almt12*$^{-/-}$;*slah3*$^{-/-}$ protoplasts, presented a significant shift towards more positive potentials (112 ± 19 mV) when compared to the single mutants *almt12*$^{-/-}$ and *slah3*$^{-/-}$ (30 ± 5 and -31 ± 17 mV, respectively), and a significant shift towards less depolarizing potentials in relation to the WT (153 ± 48 mV).

Table 8. Same as Table 6 and 7, but now comparing currents' parameters calculated for the double mutant *almt12$^{-/-}$;slah3$^{-/-}$*. Parameters $I_{(-160\ mV)}$, $I_{(+160\ mV)}$, g_B, g_F, g_F/g_B, V_h, V_s, V_{rev}, $I_{Initial}$, I_{Final}, I_{LostRd}, $I_{LostNPPB}$, %Rundown and %Inhibition as described in Tables 6 and 7. Data are represented as mean ± SE. *, refer to significant differences between comparable elements in the same experimental group. ¥, refer to significant differences between comparable elements in different experimental groups ($p < 0.05$).

almt12$^{-/-}$;slah3$^{-/-}$

	$I_{(-160\ mV)}$ (pA/pF)	$I_{(+160\ mV)}$ (pA/pF)	V_{rev} (mV)	n
$I_{Initial}$	-49 ± 10.2¥	460 ± 32.5	-9,5 ± 2.5¥	5
I_{Final}	-10.8 ± 2.6¥	211 ± 26	-6.2 ± 7	5
I_{LostRd}	-38 ± 9.6¥	248.9 ± 52.8	-12 ± 1.6¥	5
$I_{LostNPPB}$	-1.1 ± 0.4¥	11.9 ± 2.9¥	-19.8 ± 14	5
%Rundown	76.5 ± 6¥	52 ± 8*		5
%Inhibition	10 ± 1.2	6.4 ± 2.1		5
	g_B (nS/pF)	g_F (nS/pF)	g_F/g_B	n
$I_{Initial}$	0.2 ± 0.04¥	4.8 ± 0.2	25.4 ± 4.2	5
I_{Final}	0.04 ± 0.01¥	2.8 ± 0.4	81 ± 18.6¥	5
I_{LostRd}	0.2 ± 0.04	2 ± 0.4	14 ± 3.4	5
$I_{LostNPPB}$	0.004 ± 0.006¥	0.13 ± 0.02	0.13 ± 6.6	5
	V_h (mV)		V_s (mV^{-1})	n
$I_{Initial}$	101 ± 2.8		60.5 ± 1.6¥	5
I_{Final}	136 ± 1.5		54 ± 0.6¥	5
I_{LostRd}	59 ± 1.5¥		53.4 ± 1.3	5
$I_{LostNPPB}$	112 ± 19¥		53.7 ± 10.5¥	5

4.2.1.8. Mutating different anionic channels results in different biophysical properties in the overall current

By employing the outside-out and single cell configurations of the patch clamp technique with Cl^- based bath and pipette solutions, we were able to detect pulses of current corresponding to a channel with a major conductivity (I_{Inital}) state and two sub-states (I_{LostRd} and $I_{afterNPPB}$) (Figure 18), which could account for the populations of whole-cell macroscopic currents. From the results here described, one might infer that the observed currents crossed the membrane through three different channels, namely AtTMEM16, SLAH3 and ALMT12 transporters.

Overall, the currents measured from mutant protoplasts presented differences to those measured for the WT group. From Tables 6, 7 and 8 we can observe that:

i. the $I_{initial}$ (current obtained right after entering WC) was statistically higher for *slah3*$^{-/-}$, when positive V_m were applied, and for *attmem16*$^{-/-}$, for all V_m tested;
ii. the high level of current measured in *slah3*$^{-/-}$ and *attmem16*$^{-/-}$ protoplasts for the positive V_m was statistically significantly lost during RD;
iii. during Rundown the current from the *wt* group showed a shift in V_{rev} towards more positive V_m, but not on the mutant groups, a strong indicator of the existence of an intracellular effector that regulates these channels, which is lost during RD and is sensitive to changes in the transmembrane potential;
iv. the inhibition by NPPB was significantly reduced for all V_m for all three mutant groups and nonexistent for the negative V_m for *attmem16*$^{-/-}$ and *slah3*$^{-/-}$ protoplasts, strongly suggesting that AtTMEM16, SLAH3 and ALMT12 belong to the population of channels sensitive to this inhibitor; in addition NPPB may also inhibit ALMT12 channels by inducing a low-effect block;
v. *almt12*$^{-/-}$ presented a weak rectification in the negative V_m range, resulting in statistically reduced g_B, which implicates that ALMT12 channels are more active in the negative V_m;
vi. statistically significant shifts in the V_m and of the sensitivity of the currents to variations in V_m were obtained, indicating that the absence of each channel influenced the remaining population of channels.
vii. double mutant *almt12*$^{-/-}$*;slah3*$^{-/-}$ analysis strongly suggests that ALMT12 and SLAH3 channels are major contributors to the overall current, specifically in the physiological negative V_m.

The patch clamp data here described is suggestive that, (1) in a system so dependent of ion exchanges as the pollen tube, the lack of one or two anionic channels is insufficient to abolish growth, and (2) that effective compensation may exist, either by activation of remaining channels or by induction of transcription of other channels.

4.3. Regulation of Anionic Currents by GABA

One of the possible mechanisms behind anion-driven PT growth may have GABA as an upstream effector. This hypoyhesis emerges not only from the knowledge of equivalent data from animal cells, but also on the recent finding that ALMT protein family has been reported to be regulated by this amino acid (Ramesh et al., 2015). In our contribuition to this paper, we have generated data showing that pollen tubes of *Arabidopsis* were in fact affected by GABA specific pharmacology. To test this hypothesis mecahnistically, we further applied the patch-clamp technique to wild type and *almt12*$^{-/-}$ mutant *Arabidopsis* pollen protoplasts in the presence of different GABA concentrations and muscimol.

4.3.1. Muscimol reduces tube elongation in vitro, and bicuculline antagonizes muscimol regulation

To analyze the effect of GABA and its analogue muscimol, experiments on *Arabidopsis* pollen germination and pollen tube growth were conducted. In the control condition (col-0) more than 36 ± 4% of pollen germinated after 3 hours, while in the presence of GABA (different concentrations, not significantly different) and 20 µM muscimol, a reduction in germination of 20 ± 1% and 27 ± 1% respectively, was observed (n = 350 and n = 440). This effect was not recovered when bicuculline, a GABA antagonist, was added (3h, 27 ± 1.61% less, n = 480).

The data shown in Figure 20 were collected after 1 and 3 hours of pollen germination. The average PT elongation was reduced in the presence of 20 µM muscimol, and enhanced in the presence of different GABA concentrations, at 1 and 3h post germination (Figure 20). The muscimol effect on PT elongation was rescued to control values by 200 µM bicuculline (Figure 20). Similar tests done in *Vitis vinifera* also showed a reduction in pollen tube elongation by muscimol, and the rescue of the muscimol effect by bicuculline antagonization (Ramesh et al., 2015). After 3 h of germination, PT lengths were in the same range of the control, with the exception of the groups treated with muscimol and with 10 mM GABA, which were significantly smaller and larger, respectively. In 2003 Palanivelu et al., showed pollen tube growth stimulation by GABA. This

response is conserved in other plant species, namely in pollen from *Nicotiana tabacum* and *Lilium concolor* (Yu et al., 2014).

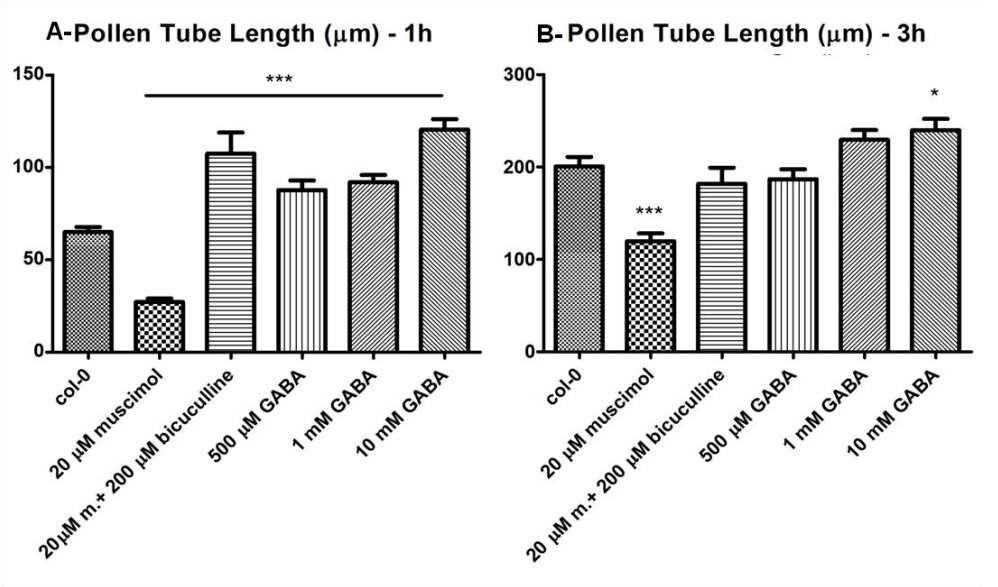

Figure 20. Length of *in vitro* grown *Arabidopsis* wild-type pollen tubes, in the absence (col-0) and presence of 200 µM bicucculline and/or 20 µM muscimol, and different GABA concentrations, 500 µM, 1 and 10 mM. (A) after 1 hour of germination ± treatments (n = 876), and (B) after 3 hours of germination ± treatments (n = 1106). Data obtained from at least three independent experiments. m. stands for muscimol. Data are represented as mean ± SEM, *, *** refers to statistical significant differences with Col-0 test $P < 0.05$ and < 0.0001.

4.3.2. 500 µM GABA reduces anionic currents in the wild type, but not in the mutant line *almt12*$^{-/-}$

GABA was first tested and added in the bath solution with no visible effect in the overall patch clamp currents. The GABA analogue muscimol is a powerful GABA agonist with 3 to 11 times greater affinity for GABA binding sites than GABA (Krogsgaard-Larsen & Johnston, 1978; Nicholson et al., 1979). A similar response is reported in the present study (Figure 21, Figure 22 and Figure 23). When 500 µM of GABA or 10 µM muscimol were applied to the intracellular medium in the wild type, both outward and inward anionic currents were drastically reduced, and the strong outward rectification was abolished (Figure 21 and Figure 23). Current reduction occurred within 5 to 10 minutes, an indication that GABA and muscimol directly interact with the anionic transporters present in the plasma membrane of pollen protoplasts. As muscimol presented such a strong effect on the currents, it was tested in the single mutant line *almt12*$^{-/-}$ by adding 10 µM muscimol to the pipette solution.

Strinkingly, its effect was completely absent on the single mutant (Figure 22 and Figure 23). These results show that GABA regulates directly ALMT12 and is suggestive that anion current modulation in pollen by GABA is primarily effected by its direct interaction with ALMT12.

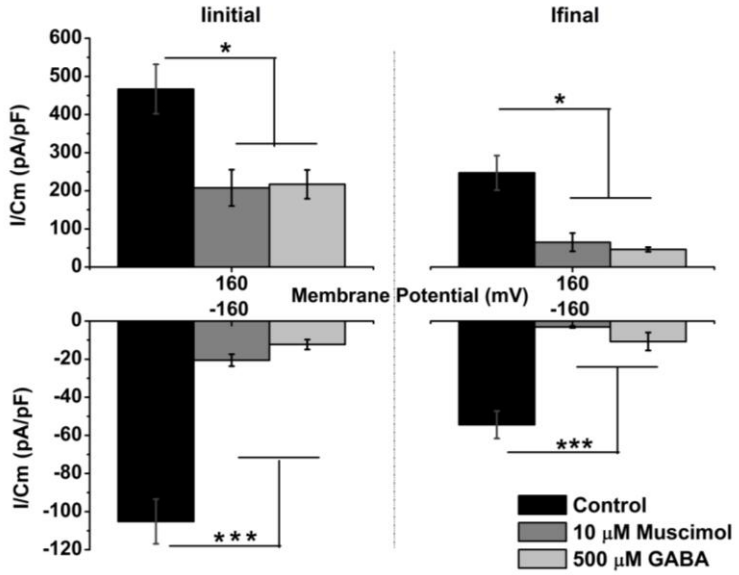

Figure 21. *Arabidopsis thaliana* wild type average normalized (pA/pF) steady state anionic currents for the control (Ø), $[500\mu M]_{in}$ GABA and $[10\mu M]_{in}$ muscimol tests. Current acquired 10 min after entering whole cell configuration, Iinitial, and after rundown, Ifinal, measured at ±160 mV. Data is represented as mean ± SE. *, *** refers to statistical significant differences, P < 0.05 and *** < 0.0001.

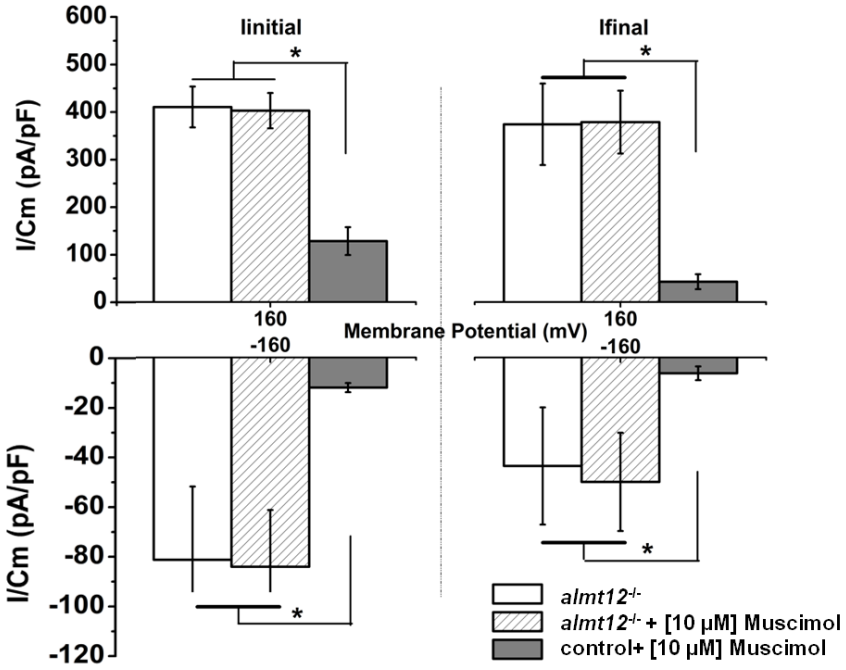

Figure 22. *Arabidopsis thaliana* average normalized (pA/pF) steady state anionic currents. Current acquired 10 min after entering whole cell configuration, Iinitial, and after rundown, Ifinal, measured at ±160 mV. The KO mutant line *almt12*$^{-/-}$ was challenged with $[10\mu M]_{in}$ muscimol;

currents acquired with and without muscimol for the At*almt12* and for wild type are also depicted for comparison, respectively. Data is represented as mean ± SE. *, refers to statistical significant differences, by Two-Sample t-Test ($p < 0.05$).

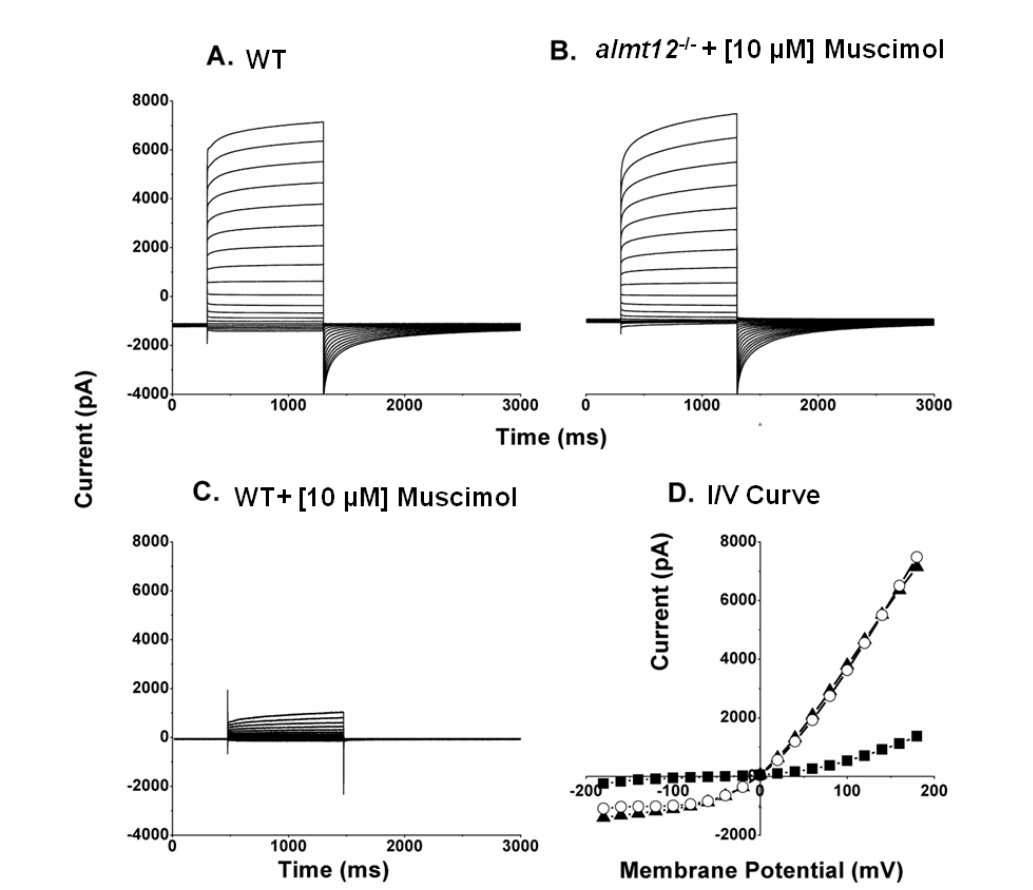

Figure 23. *Arabidopsis thaliana* steady state anionic currents acquired 10 min after of entering whole cell, I_{inital}. Panel A, B and C show whole cell currents elicited with the activation protocol, denoting a strong outward rectification for A and B, and a loss of rectification in C. Currents from Panel A and C were obtained from Col-0 wild type plants in the absence (control) and presence of $[10\mu M]_{in}$ muscimol, respectively; B, shows currents obtained from the KO mutant line At*almt12*. D, I/V curves of the relationship seen in Panel A (▲), B (O) and C (■).

Figure 24 depicts normalized average chord conductance (G/G_{max}) curves in response to pulse potentials, obtained from steady state currents immediately after entering whole cell ($I_{initial}$), and after rundown (I_{final}). The currents analyzed came from wild type Col-0 protoplasts in the absence and presence of $[10\mu M]_{in}$ muscimol; and from *almt12*$^{-/-}$ mutant protoplasts in the presence of $[10\mu M]_{in}$ muscimol. The curves were fitted with a Boltzmann equation in order to analyze the biophysical properties of the anionic channels before and after rundown. The *almt12*$^{-/-}$ mutant currents obtained 10 min after entering whole cell ($I_{initial}$) showed a higher conductivity for the more depolarizing potentials, with a decrease in the hyperpolarizing range. The latter result indicates that the

ALMT12 channel is more active in this V_m range. As expected, the muscimol treatment in the *wt* resulted in a loss of channel conductivity in all potentials measured. After entering whole-cell the Boltzmann fitting parameters, V_h and V_s, for the control (Col-0) conditions were 93 ± 3 mV and 73 ± 2 mV^{-1}, respectively (Table 9).

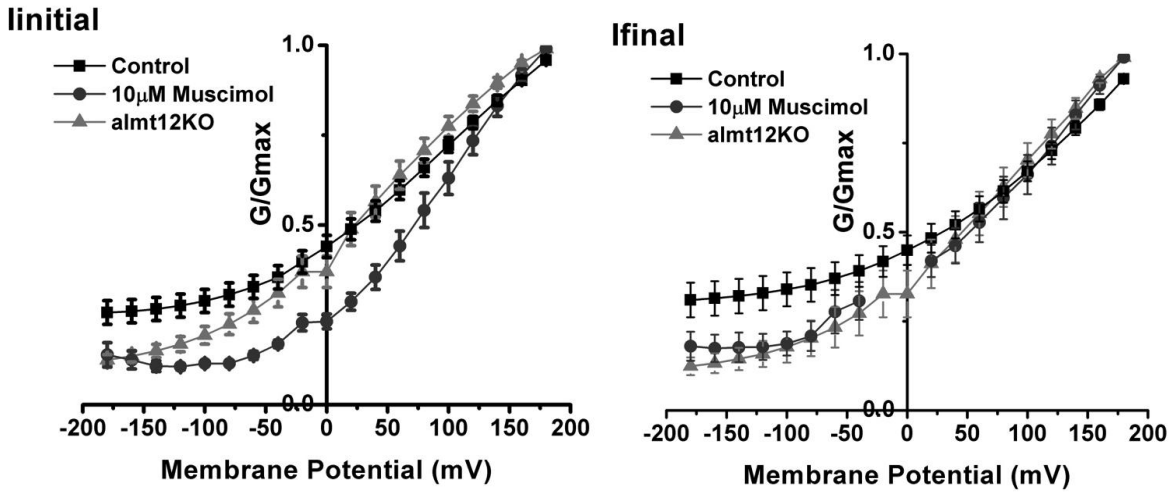

Figure 24. Normalized average chord conductance curves in function of pulse potentials, obtained from steady state currents right after entering whole cell (Iinitial), and after rundown (Ifinal). (■) and (●) shows Col-0 wild type currents in the absence (control) and presence of $[10\mu M]_{in}$ muscimol, respectively. (▲), depicts *almt12*$^{-/-}$ mutant in the presence of $[10\mu M]_{in}$ muscimol. Data is represented as mean ± SE.

The presence of $[10\ \mu M]_{in}$ muscimol in wild type pollen protoplasts shifted the sensitivity (V_s) of the currents to a significant less depolarizing potential, from 73 ± 2 mV^{-1} to 52 ± 4.5 mV^{-1}, while in the *almt12*$^{-/-}$ mutant, this sensitivity remained unchanged (72.3 ± 3.2 mV^{-1}). This shift indicates that muscimol alters the gating of the sensitive population of channels present in the plasma membrane of pollen protoplasts. Interestingly, the mean half-maximal activation potential (V_h) of the channels from the muscimol treatment was not altered in the *wt* (97.2 ± 10.0 mV), but it shifted towards a less depolarizing potential in the mutant *almt12*$^{-/-}$ (74.1 ± 3.6, Table 9). Given that V_h specifies the voltage at which half the channels are open, one can hypothesize that the shift measured in the mutant is due to the absence of the ALMT12 protein and the lack of its contribution to the overall current. After the rundown, both treatments showed similar fitting parameters (V_h and V_s) values, but different from the control.

Again, the results strongly suggest that the GABA analogue (and consequently GABA itself) binds to and inhibits the ALMT12 channel.

Table 9. Normalized chord conductance Boltzmann fitting parameters obtained from *Arabidopsis* Col-0 steady state currents. V_h is the potential for the half-maximal chord conductance and indicates at which membrane potential the transition between the maximum and minimum states of conductance occurs, V_s is the slope of the G/Gmax curve and a measure of the sensitivity of the currents to variations in membrane potential. Data is represented as mean ± SE. *, refers to statistical significant differences, by Two-Sample t-Test ($p < 0.05$), with the control.

		Control (col-0)	Col-0 + 10µM Muscimol	*almt12*$^{-/-}$ + 10µM Muscimol
$I_{initial}$	**Vh**	93 ± 3	97.2 ± 10.0	74.1 ± 3.6*
	Vs	73 ± 2	52 ± 4.5*	72.3 ± 3.2
I_{final}	**Vh**	172 ± 7	133.3 ± 27.9	110.6 ± 7.9*
	Vs	93 ± 2	84.1 ± 11.9*	82.7 ± 4.3*

The application of 500 µM of GABA in the intracellular medium increased the %RD both for negative and positive potentials in relation to the WT (Table 10). These results seem to suggest that GABA could bind to specific anionic channels, like ALMT12, causing a deactivation through time. In addition, GABA may also regulate other anion transporters through downstream signal molecules, like Ca^{2+}.

Furthermore, the single mutant *almt12*$^{-/-}$, tested with $[10\ \mu M]_{in}$ muscimol, showed a similar %Inhibition to the control. This result, taken together with the global anionic currents obtained for the *almt12*$^{-/-}$ mutant line (Figure 23B) immediately after entering whole-cell ($I_{initial}$) and after rundown (I_{final}), strongly suggests that the absence of ALMT12 channels is being compensated by other different anionic transporter populations. Interestingly, the %RD for GABA and muscimol was significantly higher for the negative potentials, implicating that GABA binds to channels that are more active in this potential range. One other possible candidate would be SLAH3 channels, since the negative currents, elicited right after entering WC and after RD, in the double mutant *almt12*$^{-/-}$*;slah3*$^{-/-}$, presented a significant decrease in relation to WT currents, suggesting that both channels are more active in this V_m.

Table 10. Mean percentage of current lost by rundown and by 300 µM NPPB. Data is represented as mean ± SE. *, refers to statistical significant differences, $p < 0.05$.

V_m (mV)	Control (Col-0, WT)	WT+ 500 µM GABA	WT + 10µM Muscimol	*almt12*$^{-/-}$	*almt12*$^{-/-}$ + 10µM Muscimol
			% Rundown		
-160	55 ± 5	74.8 ± 4.1*	72.1 ± 7.4	63 ± 9*	60.7 ± 7.4
160	46 ± 3.6	75.1 ± 3.4*	41.4 ± 15.5	52 ± 9	48.8 ± 7.2
			% Inhibition		
-160	48 ± 21	28.3 ± 8.3	12 ± 2.1*	14 ± 7*	29.8 ± 10.1
160	38 ± 8	21.1 ± 8.8	9.26 ± 0.64*	18 ± 4*	25.3 ± 12.9

In the presence of 300 µM NPPB, pollen protoplasts from all tested groups, with the exception of "WT + 10µM Muscimol" and *almt12*$^{-/-}$, showed a comparable loss of current at both ±160 mV potentials, when compared with the control (Col-0, WT) (Table 10). These observations suggest that ALMT12 channel passes currents sensitive to NPPB. In addition, the similar loss of current measured in *almt12*$^{-/-}$ and *wt* implies that the absence of ALMT12 channels, is being compensated by other of anionic transporters.

The currents from *wt* pollen treated with muscimol were nearly insensitive to NPPB, indicating that the GABA agonist may have a higher affinity to the GABA biding site than GABA itself, as previously reported (Krogsgaard-Larsen & Johnston, 1978; Nicholson et al., 1979). The insensitivity to NPPB also implies that GABA deactivates most of the sensitive channels prior to NPPB application.

4.3.3. Anionic currents showed higher inhibition between 200 µM to 500 µM GABA

To further improve on the relationship between GABA and the anionic currents, we have generated a dose-response curve for current parameters in *wt*. Figure 25 depicts measured steady state anionic currents after 10 min of entering whole cell ($I_{initial}$), after Rundown (I_{final}) and after applying NPPB ($I_{afterNPPB}$) in the absence (control, Ø GABA) and presence of increasing [GABA]: 80 µM, 200 µM, 500 µM and 5 mM. The curve describes a non-linear U-shaped dose-response relationship, meaning that the response was not directly proportional to the dose. In addition, the graph shows that the GABA effect on the currents is

biphasic, with moderate levels inhibiting the activity of the channel(s) (80 µM – 500 µM) while with the highest concentration (5 mM) the channels seem to lose sensitivity to the amino acid.

Interestingly, application of 300 µM NPPB to the extracellular solution did not block the anion currents, in the presence of either 200 µM or 500 µM of GABA (intracellular solution), when compared with the control situation (Ø GABA). On the other hand, the lowest and highest [GABA] tested, 80 µM and 5 mM still showed currents sensitive to NPPB. These results suggest that a range of GABA concentrations, between 80 and 500 µM, are sufficient to inhibit other channel populations that are sensitive to NPPB. Interestingly, the results suggest a second type of transporters that are insensitive to NPPB, and are activated by GABA for lower concentration (80 µM and 200 µM). In the presence of 500 µM a loss in sensitivity to GABA occurs. For higher concentrations, the elicited currents from these transporters increase in the presence of 5 mM GABA. These results suggest a bi-phasic dose-response, describing two points of inflection due to two inhibition levels by GABA.

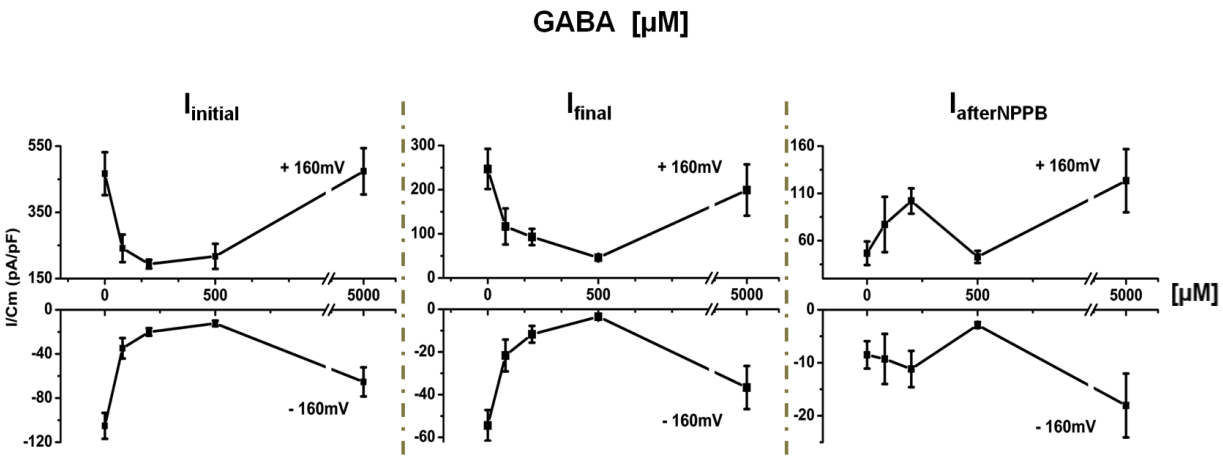

Figure 25. Dose-response curves describing the correlation between *Arabidopsis thaliana* steady state anionic currents acquired 10 min after entering whole cell (I_{inital}), after Rundown (I_{final}) and after 100 µM NPPB application ($I_{afterNPPB}$) and increasing GABA concentrations, 80 µM, 200 µM, 500 µM and 5 mM, and its absence (control, Ø GABA).

4.5. Heterologous expression of *Arabidopsis* ALMT12 transporter protein in the COS-7 mammalian cell line

4.5.1. ALMT12 transporter shows inward and outward currents in COS-7 cells.

The heterologous expression of ALMT12 and its electrophysiological characterization was conducted in animal cell lines HEK293 and COS-7. Unlike expression in COS-7 cells, no anionic currents were detected in HEK293 cells transformed with *ALMT12*, so this cell line was no longer used. Several quantities of the ALMT12 construct were transfected into COS-7 cells (0.5 µg, 1 µg, 1.5 µg and 2 µg), with cell death increasing with increasing plasmid quantities, which could indicate that the ALMT12 protein is toxic for these cells. To continue this line of research, we decided to use lower construct quantities, which resulted in low expression levels (3 out of 12 cells show expression) and a variable density of channels. The health of the cells was also affected by ALMT12 as shown in Figure 26B, which depicts a transfected cell showing fluorescent protein aggregation (*ALMT12* tagged with GFP at the C-terminus) and altered morphology. We chose the best looking cells to perform patch clamp studies and it was possible to elicit anion currents through the ALMT12 channel (n = 8), using P2/B2 solutions (M.M. page 53). A pCMV-GFP construct was used as a negative control. Figure 26A depicts two cells expressing GFP throughout the cytoplasm.

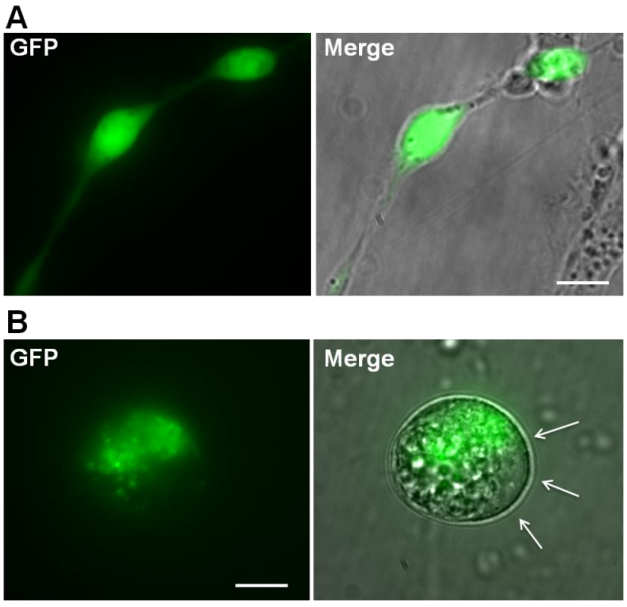

Figure 26. Co-Transfected COS-7 cells with pCMV-*GFP* alone (**A**) or pCMV-*ALMT12::GFP* (**B**) plasmids. Merged images between brightfield/DIC and GFP channels. The arrows depict an unclear plasma membrane location. Scale bar, 10 µm.

Figure 27 illustrates endogenous currents from CD8 transfected COS-7 cells. In these cells, the ALMT12 currents are mainly inward (Figure 27 and 28); the mean average I/V curves can be observed in Figure 27 (Right Panel). This feature was also observed by Meyer et al. (2010) in mesophyll protoplasts and in Xenopus oocytes expressing ALMT12. The same study showed that the activity of heterologously expressed ALMT12 increased with higher extracellular malate (mal^{2-}) concentrations, displaying R-type channel gating characteristics, which result in a bell-shaped I/V curve. In order to test whether our currents were due to the ALMT12 channel, the dependence on mal^{2-} was also verified in pollen grain protoplasts. The substitution of Cl^- ions by 5 mM of mal^{2-} in the extracellular solution did not elicit the characteristic bell-shaped I/V curve, but the positive currents were inhibited and the inward currents were maximized (Tavares, 2011). In pollen, ALMT12 channels have a low expression level, and for this reason, it might produce weaker voltage dependence than the one seen in guard cells. Furthermore, as discussed, the overall currents, both inward and outward, measured in pollen protoplasts and tube, are due to a population of different anionic transporters that might be masking the expected bell-shaped I/V curve from the ALMT12 channel.

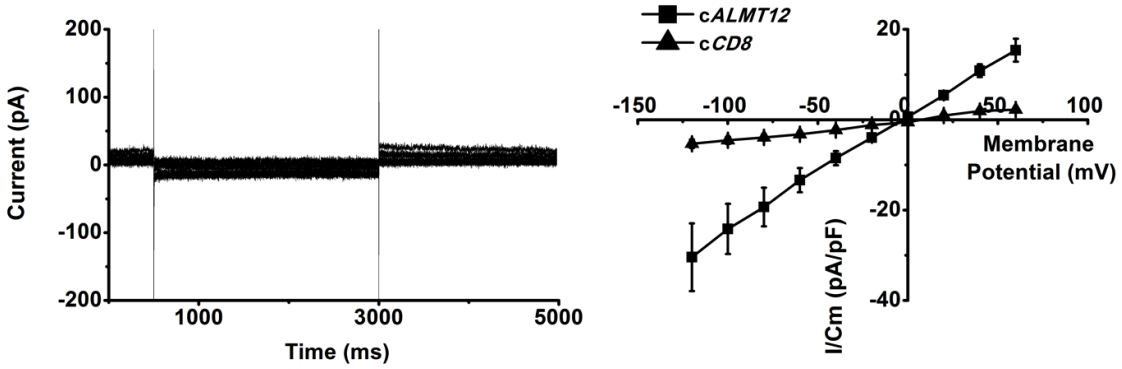

Figure 27. Left Panel: Traces of current acquired from a co-transfected COS-7 cell with *CD8* with using P2/B2 solutions (M.M. page 53). Right Panel: I/V curve obtained from mean normalized currents of cells transfected with *CD8* (▲, n = 4) and cells transfected with *CD8* and *ALMT12* (■, n = 8) elicited with the "+40 mV protocol" (M.M., Figure 7, page 55).

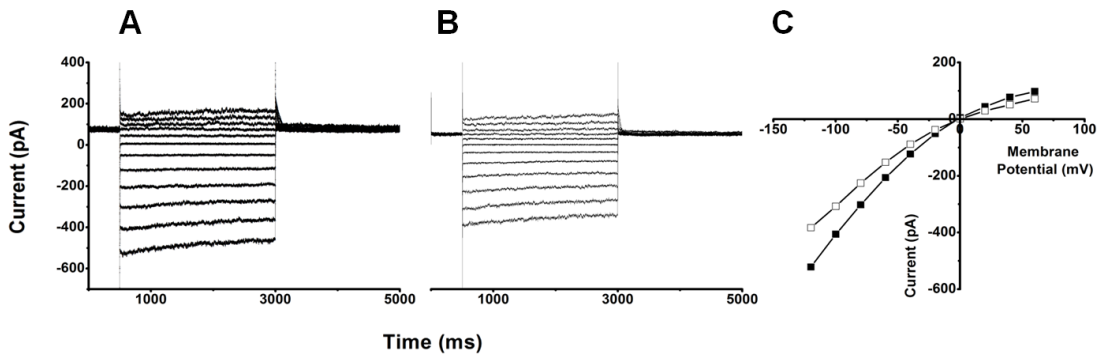

Figure 28. Traces of a representative individual COS-7 cell after 3-day of transfection with CD8, and ALMT12 cDNAs. Raw data currents obtained before (A) and after (B) adding 100 µM of IAA-94, a potent Cl^- channel blocker. The currents were elicited with the "+40 mV protocol" (M.M., Figure 7, page 53). C) depicts I/V curves obtained for each cell from A (■) and B (□) currents.

4.5.2. GABA regulates ALMT proteins activity in COS-7 cells

To verify if the regulatory mechanism of ALMT12 by GABA is similar to that of $GABA_A$, 500 µM GABA was applied to the extracellular side during a whole cell configuration assay with a *ALMT12* transfected COS-7 cell. Since the quantity of construct used in the transfection was low, it was possible to observe single channel activity in the WC configuration. Hyperpolarized potentials, between -120 and – 60 mV, after a positive pre-pulse (+ 40 mV), elicited openings and closings of single channels, which resembled a flickering channel behavior (Figure 29). In addition, at least three levels of channel conductive states were detected for these potentials when GABA was added to the bath solution. Nevertheless, there was a slight decrease in the mean current density after 5 min of adding GABA (Figure 29). Both channel flickering and the decreased current response can be interpreted in terms of a channel blocking mechanism. Flickering occurs when molecules other than the permeating ion enter the channel opening and briefly block ion conductance.

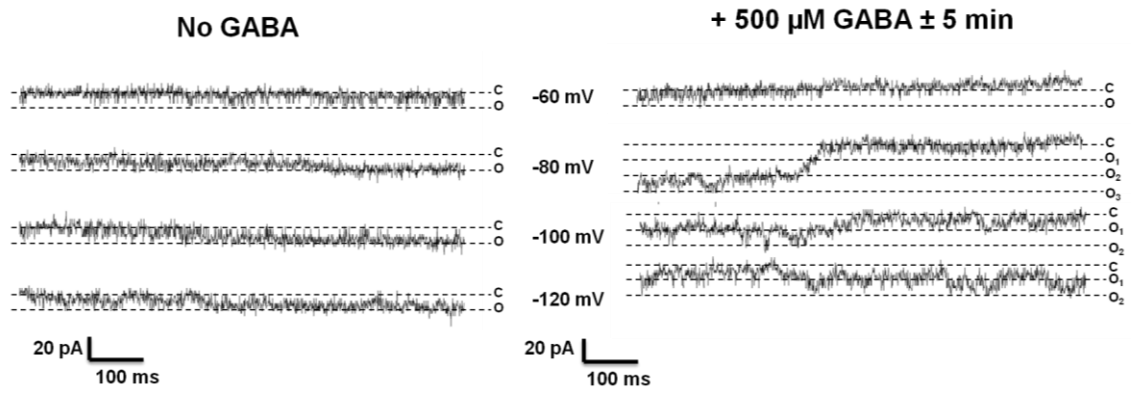

Figure 29. Whole cell currents acquired from a 3-day COS-7 cell transfected with *CD8*, At*ALMT12* cDNAs, in the absence and presence of 500 µM GABA in the extracellular side using the B2/P2 solutions (n = 2). Currents were elicited in the hyperpolarized voltage range, between -120 and – 60 mV, after a positive pre-pulse (+ 40 mV) was applied, to close the channels. After > 2-5 min in the presence of GABA, current fluctuations resembling a flickering behavior, with openings and closings of single channels, start to appear. C, closed; O_1 open state 1, O_2 open state 2, O_3 open state 3.

4.6. Vibrating Probe Analyses of the 4 anion transporter mutants

To complement the patch clamp data, extracellular anionic fluxes at the pollen tube tip were estimated with the ion-selective vibrating probe (M.M., page 56). The vibrating probe measures differences in voltage between two points, one very close to the tip and the other positioned 10 µm from the previous point. Given that the electrode is filled with a anion specific ionophore cocktail, these differences are indirect measures of minute extracellular gradient of anions. These gradients form as a result of ion fluxes through the membrane and thus allow their estimation by applying Nernst and Fick's law.

We have measured the growth rate (Figure 30A) and the anion fluxes at the tip of growing pollen tubes (Figure 30B) for *wt*, single and double mutants for anion transport candidates. The anion fluxes obtained from the single gene mutation of, *atccc*$^{-/-}$ and *slah3*$^{-/-}$, show a significant reduction in relation to *wt*, while the *almt12* and *attmem16* showed a slight non-significant reduction. Interestingly, the anion fluxes measured from the double mutant *attmem16*$^{-/-}$;*atccc*$^{-/-}$ are comparable to the fluxes measured in the *wt*, and present a significant recovery in relation to the single mutant *atccc*$^{-/-}$ but not to *attmem16*$^{-/-}$. Similarly, the double mutant *almt12*$^{-/-}$;*slah3*$^{-/-}$ anion fluxes were comparable to the *wt*, and statistically higher than the fluxes measured in the single mutant *slah3*$^{-/-}$.

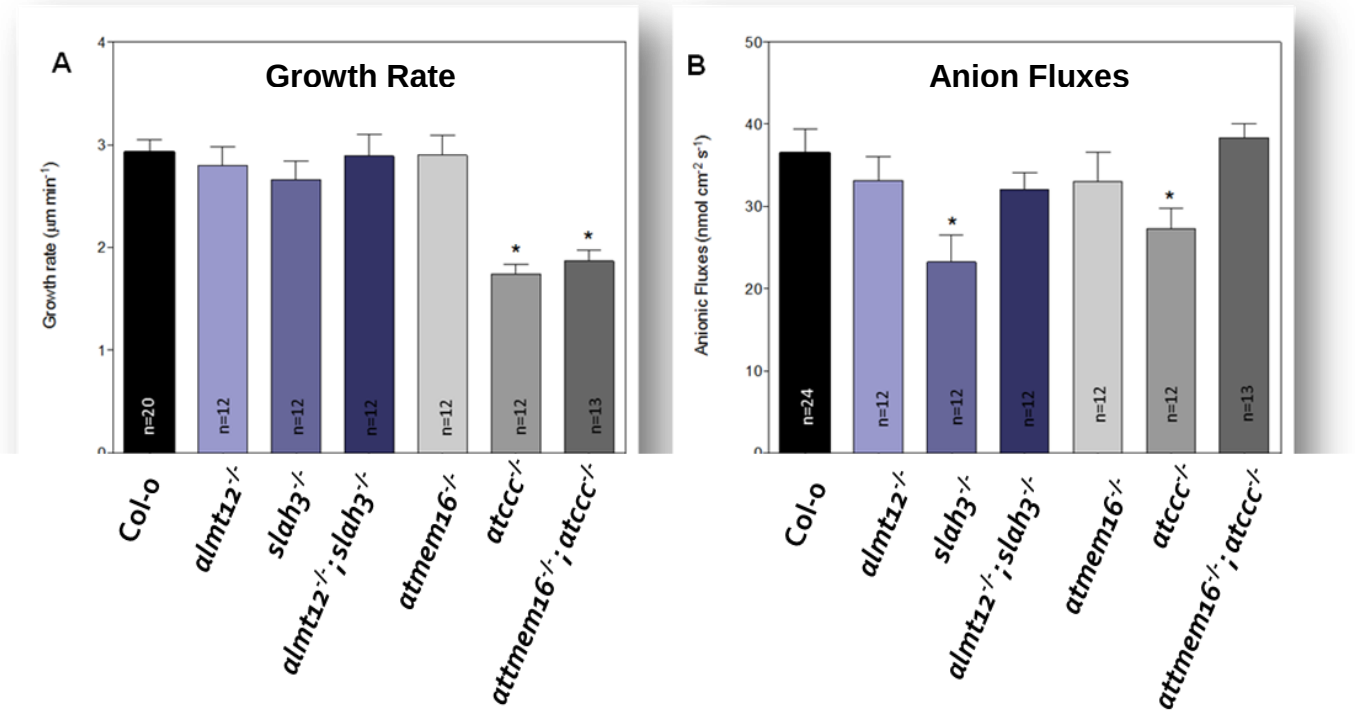

Figure 30. Anion fluxes measured with anion-selective vibrating microelectrodes. In PTs from different mutant *Arabidopsis* lines. (**A**) Growth rate of the PTs measured for the fluxes in the respective genetic background. (**B**) Anion fluxes at the PT tip of wild-type (n = 24, Col-0), *almt12*$^{-/-}$ (n = 12), *slah3*$^{-/-}$ (n = 12), *attmem16*$^{-/-}$ (n=12), *atccc*$^{-/-}$ (n=12), *almt12*$^{-/-}$;*slah3*$^{-/-}$ and *attmem16*$^{-/-}$;*atccc*$^{-/-}$ PTs. Data are represented as mean ± SE. *, refer to significant differences between comparable elements in the same experimental group, p ≤ 0.05.

Furthermore, growth rate was significantly affected in the single *atccc*$^{-/-}$ and double *attmem16*$^{-/-}$;*atccc*$^{-/-}$ mutants. Curiously, *attmem16*$^{-/-}$;*atccc*$^{-/-}$ significant increase in the measured fluxes was not accompanied by an increase in growth. The reduced growth rate obtained for *atccc* may explain the development of shorter siliques, with reduced seed set, described by Colmenero-Flores et al., (2007). This phenotype is probably a result of shorter PTs, and their inability to reach and fertilize ovules. To verify this, *atccc*$^{-/-}$ pollen grains were germinated in liquid germination medium (M.M., page 41), and the length of *atccc*$^{-/-}$ PTs measured after 1h and 3h of germination. Figure 31A depicts three independent pollen germination assays; after 1h of germination *wt* PGs germinated 38% more than *atccc*$^{-/-}$. In addition, the length of *atccc*$^{-/-}$ PTs was significantly affected when compared to *wt*. The significant difference between *atccc*$^{-/-}$ and *wt* PTs was maintained after 3h of germination. This result may account for the increase number of unfertilized ovules illustrated in the *atccc*$^{-/-}$ silique shown in Figure 31B.

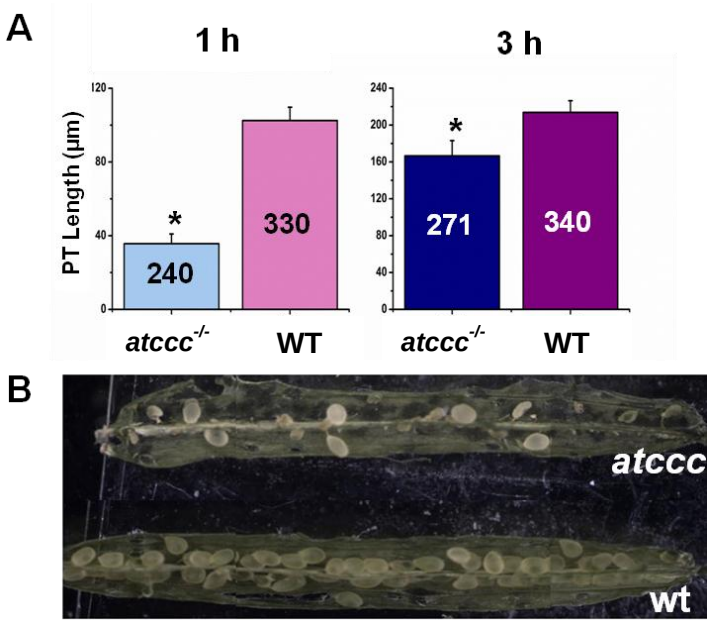

Figure 31. A. Pollen tube Length assays. Three independent analyses were performed and the length of the tube measured using the ImageJ tool, NeuronJ. The measurements were executed in PGs with visible cytoplasmatic extensions. B. Comparison of a WT silique with a *atccc* silique; an increase number of unfertilized and aborted ovules is evident in the *atccc* silique.

4.7. Anionic Transporter Localization

The molecular identity of the transport proteins responsible for the anionic fluxes remains elusive. After identifying four candidate genes for anionic channels/transporters that show expression in pollen and could account for the observed fluxes, we investigated their subcellular localization. In order to do this, the green fluorescence protein (GFP) was fused to the C- terminus of the coding sequence of *AtCCC* and genomic sequences of *ALMT12*, S*LAH3* and *AtTMEM16*. In general most channels are present only at very low protein numbers, and can therefore hardly be visualized using their own promoter. We thus generated transgenic *Arabidopsis* (Col-0) plants expressing the *gene*-GFP construct under the control of the pollen-specific promoter Lat52. Confocal and Widefield microscopy analysis of the generated overexpression lines show, GFP fluorescence of each anion channel/transporter candidate located in different portions along the pollen tube.

Figure 32, shows confocal images of three overexpressing Lat52::*SLAH3*-GFP pollen tubes; flurescence can be visualized in the pollen tube periphery, which confirms the plasma membrane localization seen by Gutermuth et al., (2013) in

tobacco. Figure 32D shows SLAH3 channel localized in the plasma membrane (PM) at the tip, though obviously more concentrated in spaced speckles. Interestingly, it seems that the channel is being constantly carried and delivered by an intense movement of vesicles along the pollen tube through cytoplasmatic streaming (Figure 32A, B and C).

The overexpressing Lat52::*At*CCC-GFP fusion presented a clear plasma membrane localization in the shank of pollen tubes with a decreasing and more diffuse signal towards the tip (Figures 33A and B). From Figure 33A and B, it appears that AtCCC is completely absent from the tip plasma membrane. Double labeling with FM 4-64 dye confirmed the PM localization of this co-transporter at the shank of the growing tube (Figure 33B).

Similarly to AtCCC, AtTMEM16:GFP overexpressing pollen tubes also depicted a strong signal intensity at the shank of the pollen tube, but presented no signal at the tip region (Figure 34A and B). Observing the Z-stack sequence shown in Figure 34A it appears that this protein is localized along the small secretory vesicles or vacuoles that are strongly carried through the cytoplasmic streaming flow. The dynamics of GFP signal in the form of strings appears to fit Cheung et al., (2008) analysis of actin derived movement. The authors, through fluorescent protein labeled actin-binding proteins in elongating tobacco and lily pollen tubes, described long, streaming actin cables along the shank, and a subapical structure made of shorter actin cables. In certain regions, PM localization becomes evident (Figure 35A and B). Recently, the CaCC activity in murine portal vein cells was shown to be modified by the interaction of TMEM16A with abundant actin cytoskeleton; actin disruption by cytochalasin D did not affect the current density (Ohshiro et al., 2014). One can hypothezise a similar dependence between AtTMEM16 channel activity and the cytoskeleton during pollen tube growth.

Two rounds of experiments were performed to produce the transgenic line overexpressing AtALMT12 channel, also under the Lat52 promoter. Two *Agrobacterium* transformations were executed first in the presence of the surfactants Silwet and a second try with Sylgard; neither resulted in positive resistant transgenic plants. As a last resort, transgenic plants produced by Meyers et al., (2010), designed with the stomata specific promoter for Myb60,

were requested. Myb60 is transcription factor shown to play a crucial role in stomatal movement (Oh et al., 2011). Since it was found to have expression also in pollen (Pina et al., 2005), the seeds were requested and germinated. The signal observed is weak (Figure 36A and B). A similar vesicle localization to the one seen with SLAH3 protein was observed, but without a clear PM localization.

Taken together, the results identify for the first time, 3 channels and a co-transporter that possibly account for the anionic efflux and influx described at the tip and shank of a growing tube. Namely, at the shank the co-transporter AtCCC (Colmenero-Flores et al., 2007) and channel AtTMEM16 proteins may mediate the majority of the inward-directed anion transport process. Additionally, AtSLAH3 also seems to participate on the uptake of anions in this region, but more strikingly to be the channel responsible for the efflux of anions observed at the tip, confirming earlier results (Guttermuth et al. 2013). Biolistic transformation of *N. tabacum* pollen with AtSLAH3:YFP from *Arabidopsis* showed a uniform plasma membrane fluorescence at the shank of the tube, and a decrease of signal towards the apex, and only when AtSLAH3:YFP was transiently co-expressed with YFP:CPK2, using the Bimolecular Fluorescence Complementation (BiFC) method, did the signal appear exclusively at the plasma membrane at the tip (Gutermuth et al., 2013). Both BiFC expression and the stable transgenic line produced in the present work, Lat52::*Slah3*-GFP, robustly imply SLAH3 is the main channel responsible for the massive efflux measured at the tip.

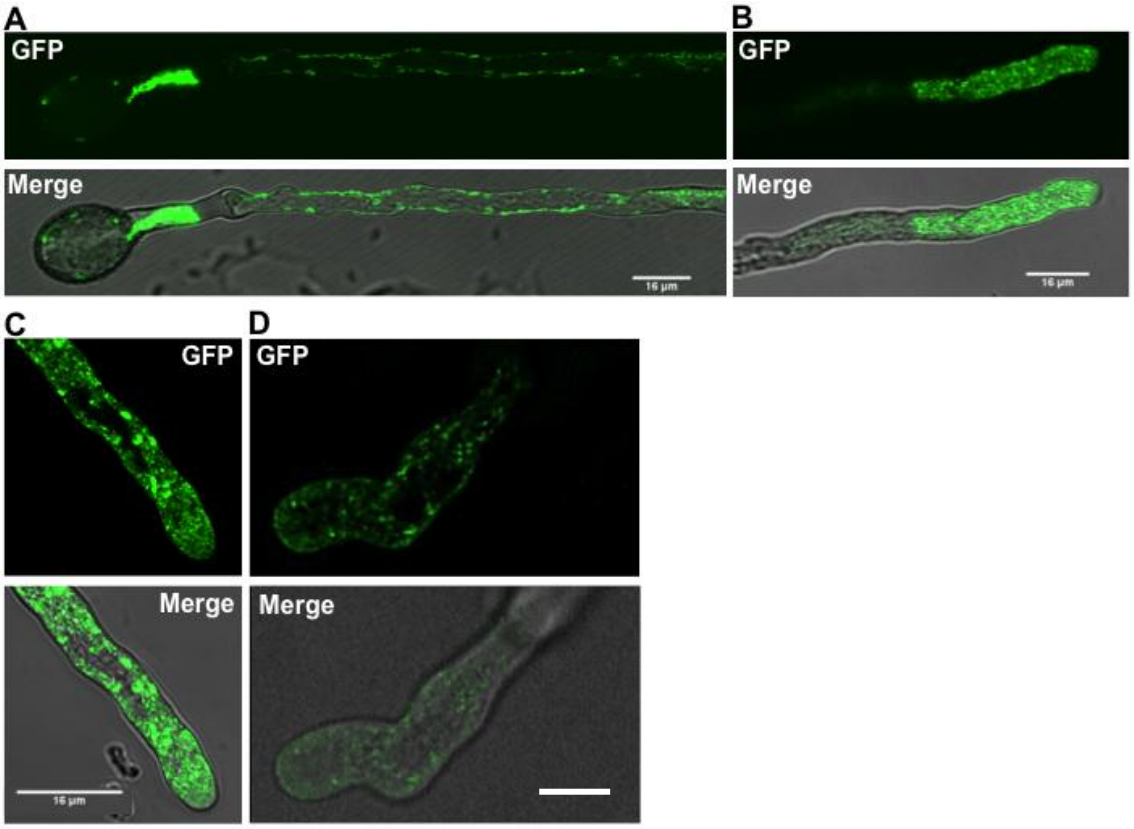

Figure 32. Confocal and Widefield images of two overexpressing Lat52::*SLAH3*-GFP pollen tubes. **A, B and C** were acquired on a Zeiss LSM 510 META, using a 40x 1.3NA (A and B) and a 63x 1.4NA (C) Oil immersion objectives. Images "Merge" are the merge between the DIC reference and GFP channels. **D**. Widefield image acquired on an Applied Precision DeltavisionCORE system, using the 100x UPlan SAPO 1.4NA Oil immersion objective. SLAH3 protein appears to be packed in small vesicles and delivered to the plasma membrane along the shank to the tip of the growinf tube; GFP signal reveals a likely plasma membrane location in D. Scale bar, 16 µm and 10 µm (D).

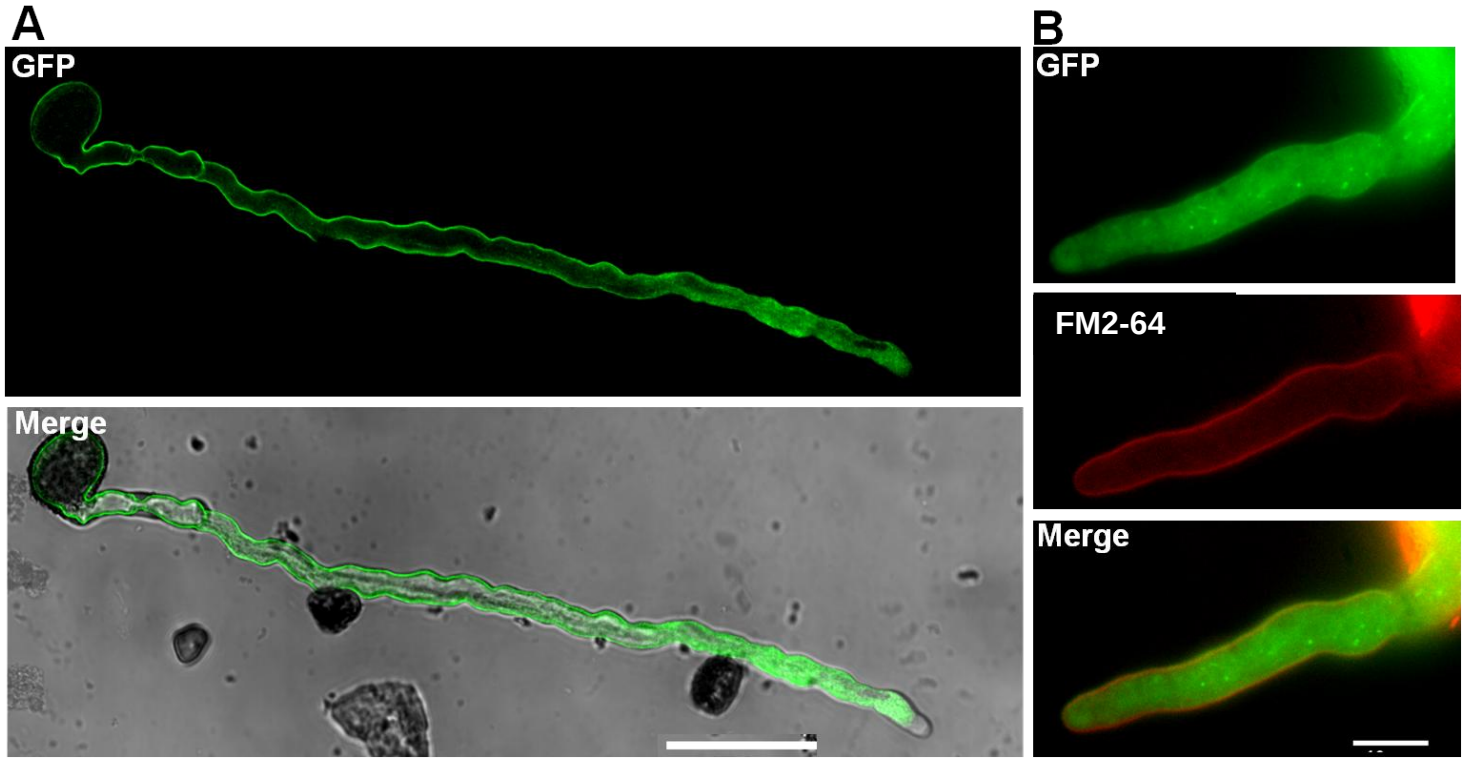

Figure 33. Images of two overexpressing Lat52::c*AtCCC*-GFP pollen tubes. **A**, Confocal image acquired on a Zeiss LSM 510 META, using a 20x 0.75NA objective; GFP signal reveals plasma membrane localization. “Merge” image is the merge between the DIC reference and GFP channels. **B**, Widefield image acquired on an Applied Precision DeltavisionCORE system, using the 100x UPlan SAPO 1.4NA Oil immersion objective; the use of the FM2-64 marker confirmed plasma membrane localization. Scale bar A, 47 µm and B, 10 µm.

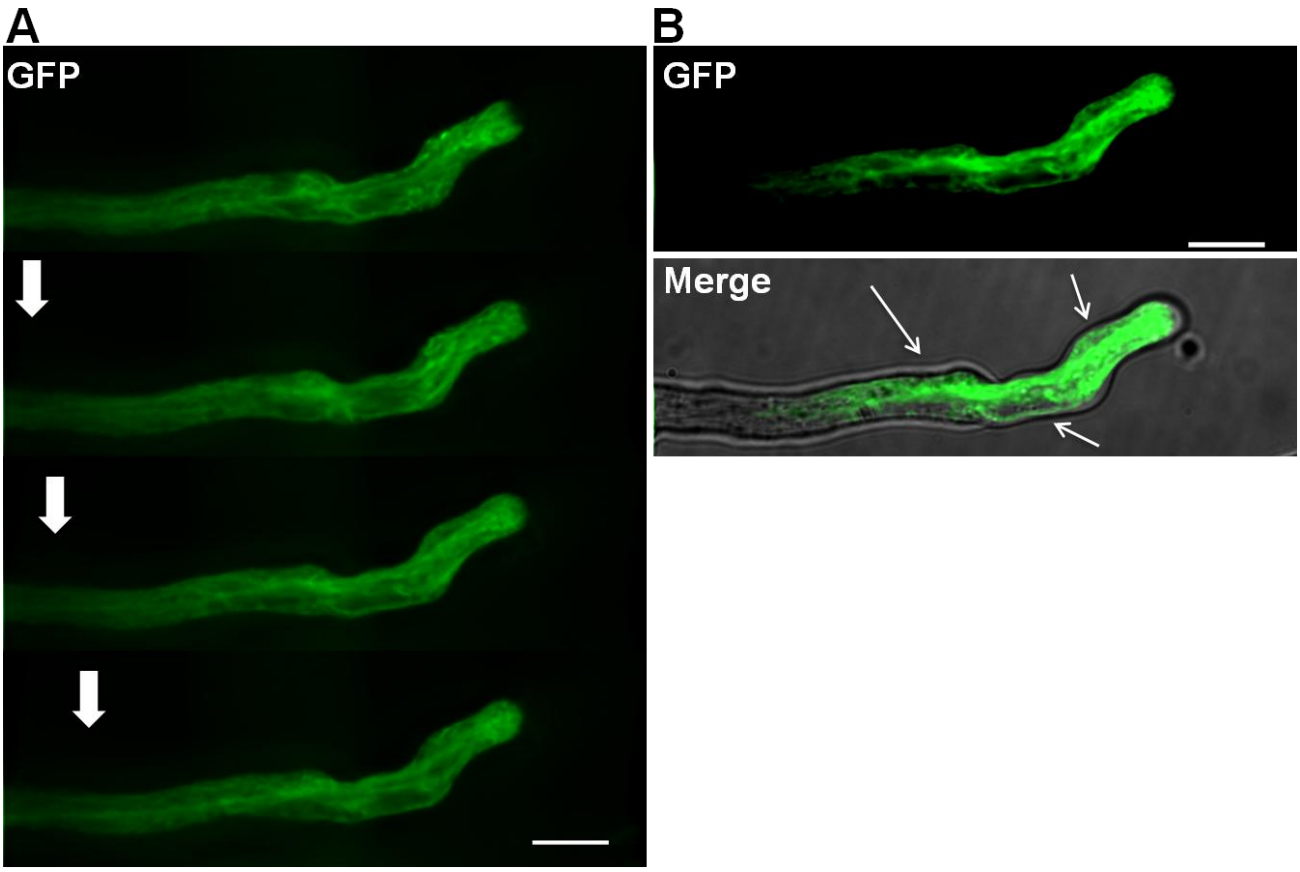

Figure 34. Images of an overexpressing Lat52::*AtTMEM16*-GFP pollen tube, acquired on an Applied Precision DeltavisionCORE system, using the 100x UPlan SAPO 1.4NA Oil immersion objective. **A**. Z-stack sequence (large arrows) projection deconvolved with the Huygens software. **B**. The lower panel image is the Merge between the differential interference contrast (DIC) reference and GFP channels (middle panel, deconvolved image from A with altered brightness and contrast parameteres). GFP signal reveals a likely cytoskeleton location. The lean arrows may depict plasma membrane location. Scale bar, 10 µm.

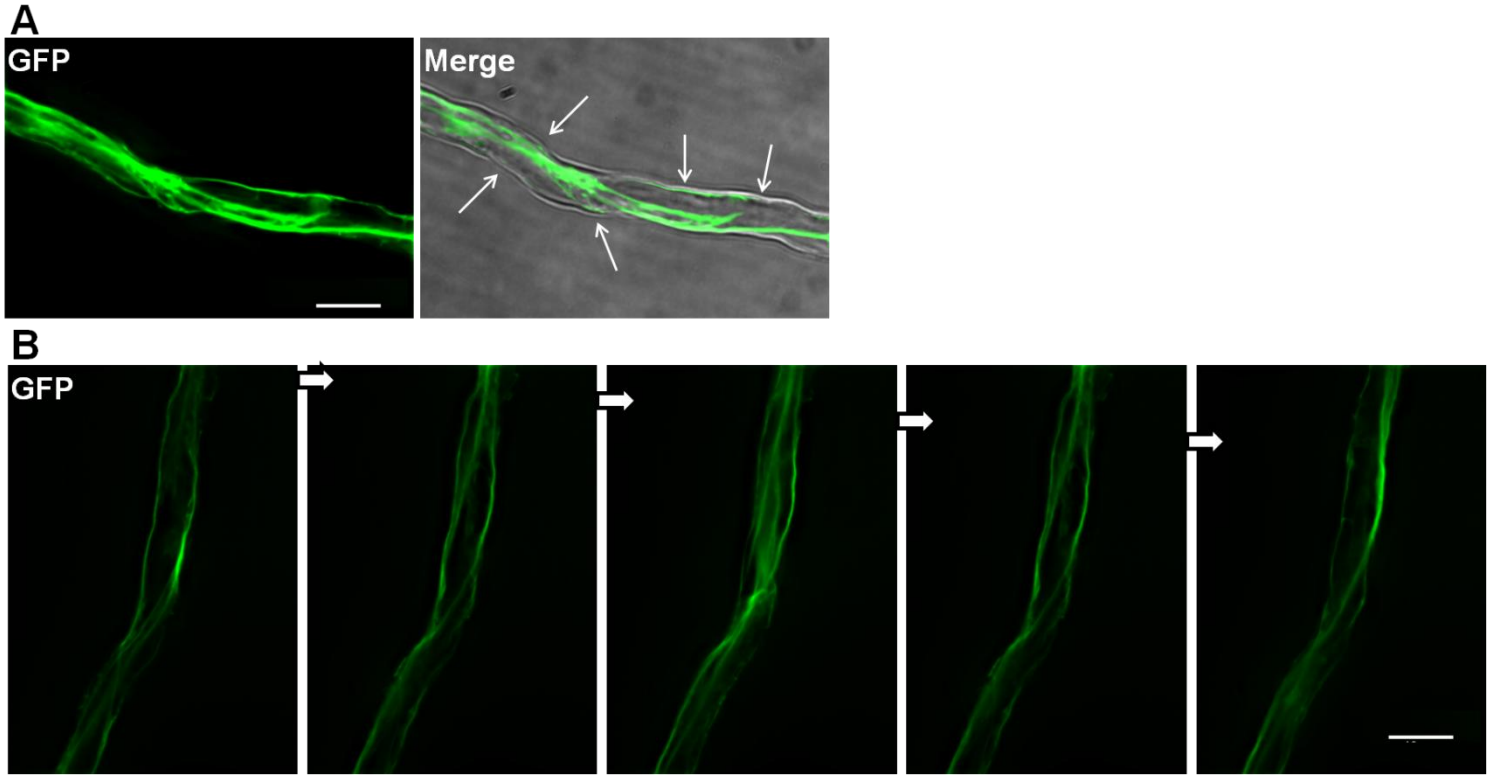

Figure 35. . Images of an overexpressing Lat52:: *AtTMEM16*-GFP pollen tube shank, acquired on an Applied Precision DeltavisionCORE system, using the 100x UPlan SAPO 1.4NA Oil immersion objective. **A.** The right panel image is the Merge between DIC reference and GFP channels. **B.** Z-stack sequence projection deconvolved with the Huygens software. GFP depicts PM and intracellular location. The arrows depict plasma membrane location. Scale bar, 10 µm**.**

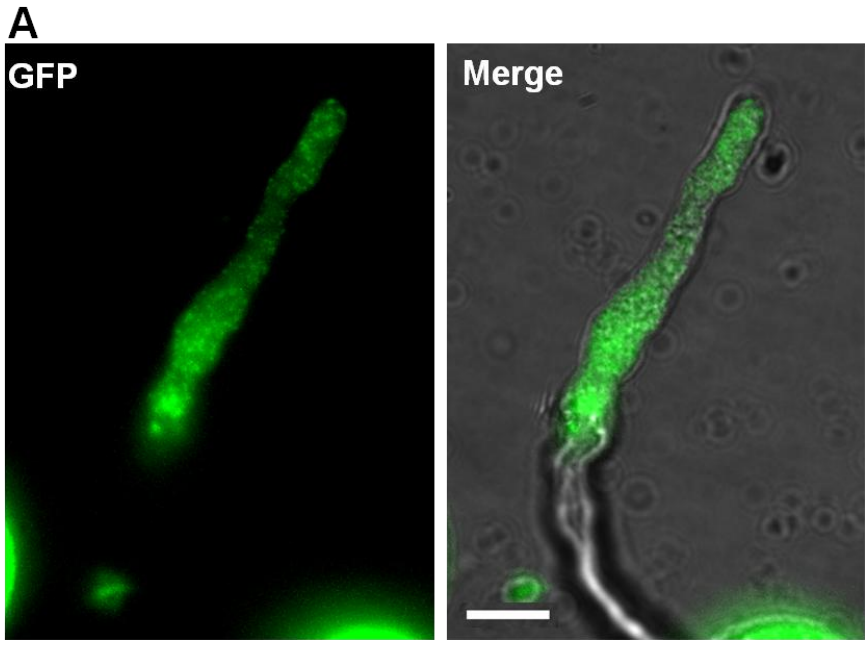

Figure 36. Images of an overexpressing Myb60::*ALMT12*-GFP pollen tubes, acquired on an Applied Precision DeltavisionCORE system, using the 100x UPlan SAPO 1.4NA Oil immersion objective. The right panel image is the Merge between the differential interference contrast (DIC) reference and GFP channels. Similarly to SLAH3, ALMT12 protein appears to be packed in small vesicles. Scale bar, 10 µm.

5. Discussion

To some extent, the physiological role of Cl^- in pollen tube growth remains and controversial. The fact that the molecular nature and mechanisms of the pollen tube anion transporters and regulators is mostly unknown contributes to the perpetuation of this conundrum. In an attempt to address the functional role of anions, namely Cl^-, we have postulated four possible anionic transporter as candidates for being responsible of the bulk of anion fluxes currents described in these cells. We characterized them by electrophysiological methods, and established their localization in the growing pollen tube. In addition, we showed that GABA regulates anionic currents elicited from *wt* hydrated pollen protoplasts, by applying the patch clamp technique. In a nutshell, all four candidate genes seem to play relevant roles, and may well explain the bulk of properties associated with physiology of Cl^- in growing pollen tubes. The physiological implications of the present findings are here discussed.

5.1. Electrophysiological characterization of *atccc*$^{-/-}$, *almt12*$^{-/-}$, *slah3*$^{-/-}$, *and attmem16*$^{-/-}$ single mutants, and *almt12*$^{-/-}$*; slah3*$^{-/-}$ double mutant

The currents reported on this thesis were measured in protoplasts of hydrated pollen grains of *Arabidopsis thaliana* before the onset of germination. These results, together with the single channel currents previously characterized in *Lilium longiflorum* under the same experimental conditions (Tavares et al., 2011a) demonstrate the existence of anionic currents across channels in the plasma membrane of un-germinated grains, probably due to AtTMEM16, SLAH3 and ALMT12 channels.

While not physiological, in this study we used a broad range of V_m values for scrutinizing the currents, a common procedure in this kind of patch-clamp approaches. The extreme positive values are necessary to attain linearity of the currents with the applied potentials, a strategy that allowed us to latter determine the conductance ratios and the respective Boltzmann parameters. These parameters were used to compare experimental groups (Tavares et al., 2011a). However, whole cell currents elicited in *wt* protoplasts do not allow us to

determine which anionic currents belong to which anionic channels. To do that we used the available mutant lines *almt12$^{-/-}$, slah3$^{-/-}$, and attmem16$^{-/-}$*.

Interestingly, the currents measured from the three mutant protoplasts presented significant specific key differences to those measured for the WT group, namely:

i) a higher elicited $I_{Initial}$ from *slah3$^{-/-}$ and attmem16$^{-/-}$* protoplasts;
ii) *almt12$^{-/-}$* elicited reduced $I_{Initial}$ and I_{Final} for the negative V_m tested;
iii) increased %RD specifically for the negative V_m;
iv) a higher loss of I_{LostRd} in *slah3$^{-/-}$ and attmem16$^{-/-}$* protoplasts;
v) different sensitivities to NPPB in the three mutants and
vi) different sensitivities and conductive states to V_m variations.

In addition, the currents elicited from the double mutant line, *almt12$^{-/-}$; slah3$^{-/-}$*, also presented key differences when compared to the WT, and to the respective single mutants, namely:

i) a significant decrease in $I_{Initial}$, I_{Final} and I_{LostRd},
ii) a higher %RD for the negative V_m,
iii) a higher %Inhibition in relation to the *slah3$^{-/-}$* single mutant.

Different $I_{Initial}$ and I_{Final} amplitudes were measured from the single mutant lines and the double mutant line. It appears likely that Cl^- transport regulation is very complex and involves several regulatory loops, suggesting different types of compensation. An hypotheses was thus drawn to explain the patch clamp results. We hypothesize that all three channels interact and modulate with each other, and/or other transporters present in each mutant background (e.g. Ca^{2+} channels, Cl^-/H^+ antiporters) in a feedback loop. Several compelling evidences support this claim, namely:

i) the increase in $I_{Initial}$ observed in *slah3$^{-/-}$ and attmem16$^{-/-}$* mutants, could be explained by a stimulation of the activity of specific transporters due to the absence of the regulatory function of either SLAH3 and AtTMEM16 channels;
ii) the $I_{Initial}$ V_{rev} obtained in *slah3$^{-/-}$* was significantly shifted towards more negative V_m to that measured for the WT, suggesting that SLAH3

could be modulated by an intracellular effector or other transporters, namely ALMT12;

iii) the double mutant, *almt12*$^{-/-}$*; slah3*$^{-/-}$ did not generate the same shift in V_{rev} as the observed for the single *slah3*$^{-/-}$, which implies a possible SLAH3 channel regulation by ALMT12; and

iv) the $I_{Initial}$ and I_{Final} elicited in the negative V_m in the double mutant *almt12*$^{-/-}$*; slah3*$^{-/-}$ was significantly lower than those measured in the single mutants, *almt12*$^{-/-}$ and *slah3*$^{-/-}$, implying that both channels might regulate the activity of each other.

In mammalian cells, one of the best recognized functions of CFTR is the ability to modulate the functioning of other transporters. Subsequently, CFTR has been reported to affect the activity of a large number of other ion channels and solute transporters (e.g. Greger, (1996). For e.g in salt-absorbing sweat ducts, activation of CFTR caused ENaC (epithelial Na^+ channels) stimulation (Schwiebert et al., 1999). Another level of regulation can be observed from the high %RD observed for the negative V_m in the three mutants (in opposition to WT), which not only implies the presence of intracellular effectors that modulate the three channels, but also that each channel is being differently regulated by those effectors. Last but not least a possible common denominator could be at the level of the modulation of plasma membrane potential.

To conclude on the contribution of each channel for the overall *wt* current, using the obtained currents from the mutant lines is not an easy achievable task. Nevertheless, one can speculate that these three channels are activated in hyperpolarizing conditions, but each contributes in different ways. In particular, ALMT12 channels seem to have a higher contribution in the negative V_m than AtTMEM16 channels, since on its absence the currents were weaker and therefore there was no compensation. In addition, SLAH3, in coordination with ALMT12 channels, might also show a similar contribution in the same V_m range. As for the positive V_m, SLAH3 and AtTMEM16 channels seem to be more sensitive to these potentials and are very likely to be the main contributors of the strong outward rectification observed in WT currents. Finally, AtTMEM16, SLAH3 and ALMT12 channels were shown to be sensitive to NPPB, despite the lower affinity for the blocker shown by ALMT12, indicating that the current

insensitive to NPPB can only be attributed to one or more further uncharacterized electrogenic anionic transporter(s) (e.g. Cl^-/H^+ antiporters). Surprisingly, the AtTMEM16 transporter was recently shown to be sensitive to pH changes, indicating that it could be in fact an anion/H^+ co-transporter (Dias P, unpublished data). The effect of extracellular pH was analyzed in *wt* and the *atmem16*$^{-/-}$ single mutants protoplasts, and we were able to observe that: 1) the currents were not largely affected in *atmem16*$^{-/-}$; 2) conductances had slight changes but rectification was unaffected; and 3) the reversal potential did not follow the changing H^+ gradient in the instantaneous component of the measured current.

The data collected for extracellular fluxes, also suggest another level of compensation. The anion fluxes from the double mutants *almt12*$^{-/-}$*;slah3*$^{-/-}$ and *attmem16*$^{-/-}$*;atccc*$^{-/-}$ were stronger than the fluxes measured in the *slah3*$^{-/-}$ and *atccc*$^{-/}$ single mutants, respectively. These differences could be explained through transcriptional regulation in the mutant backgrounds. Furthermore, no correlation was observed between growth rate and anion fluxes, suggesting that other compensation mechanisms are set into play on the absence in each mutanted channel line. Similar effects are obtained for Ca^{2+} and H^+ fluxes measured from different *glr* (glutamate-like receptor) and *aha* (*Arabidopsis* H^+-ATPase) double mutants family members in relation to their single counterparts *and wt*, where some double mutants show significantly higher fluxes than the respective single mutants (Portes T.M. and Wudick M. personal communication). To complicate matters, in plants most ions can be transported by distinct non-related carriers (Barbier-Brygoo et al., 2011; Ayadi et al., 2015).

Somehow pollen tubes, and possibly other cells with strong dependance on ion physiology for their functions, have evolved redundancy and sophisticated compensation mechanisms to increase robustness to point mutations that could jeorpadize their function. Being the male gametophyte, and therefore carrying the potential for Darwinian sexual selection, individual pollen grains should under very strong pressure, especially on any mechanism that affects growth, as this would be the most obviously parameter to affect the fitness of individual pollen tubes. In accordance with this hypothesis, evolutionary trends within Gymno and Angiosperms seem to obviously favour faster pollen tube growth

rates. Genetic redundancy is a common feature in flowering plants, and it is responsible for the absence of a phenotype associated with a vast majority of single loss-of-function mutation compensated by homologous genes (Simillion et al., 2002; Ayadi et al., 2015). A striking >80% of the *Arabidopsis* genome is duplicated, which is linked to the need of plants to adapt to different conditions (Simillion et al., 2002; Ayadi et al., 2015).These numbers obviously hide an even complex picture arising from multiple levels of functional redundancy encoded on regulatory networks.

5.2. Currents of Lily germinated pollen

We also found similar anionic currents from germinated pollen from *Lilium longiflorum*, which are most likely due to the same kind of putative channels. A possible explanation for this result could lie on the fact that many of the channels already present in the plasma membrane of the grain protoplasts may suffer a spatial redistribution to specific regions of the membrane during pollen tube germination and growth or that they undergo recycling. Previous studies in the growing pollen tube showed proton fluxes per area unit similar to those detected in the hydrated grain, probably attributable to relocation/recycling of the transporters, or de novo synthesis, balancing transporter concentrations (Feijó et al., 1999; Certal et al., 2008). The results presented here seem to confirm that the same putative channels could be responsible for the currents measured from hydrated pollen and during pollen tube growth, but responding to the natural spatial and temporal variation of $[Ca^{2+}]_{in}$ and other factors. At this point we cannot discriminate between a re-distribution of the channels initially present in the membrane and the *de novo* synthesis of these membrane proteins. We observed a great variation in current density between cells, probably reflecting differences in the number of active channels in the membrane. The error associated with the mean I/V curves obtained with the measured currents normalized to their respective capacity values was greater than the error associated with the non-normalized currents, but for comparison purposes only the normalized values were shown and used. In addition, our group was able to estimate the equivalent ionic fluxes to the Cl^- currents measured with nM Ca^{2+}, by assuming a spherical shape for the membrane

surface and calculating the corresponding current density (pA cm^{-2}). For the negative membrane potential values (−160 to −60 mV), we obtained values for the fluxes ranging on average from 300 to 4000 pmol cm^{-2} s^{-1}, according to a given radius (10 to 3 µm, respectively). These values were estimated from $I_{Initial}$ and are comparable to those reported by Zonia et al. (2002) which were measured with vibrating probes and which showed an oscillatory efflux that ranged from 50 to 8000 pmol cm^{-2} s^{-1}, under a low extracellular Cl^- concentration (c. 1.1 mM).

Ca^{2+} has emerged as a central and crucial modulator that not only regulates but also integrates the coordination of several processes essential for directed apical growth, including the regulation of ion transport during pollen tube growth (Steinhorst and Kudla, 2013). As described in this thesis, $[Ca^{2+}]_{cyt}$ activated Cl^- currents were measured in Lily grain and tube protoplasts, and in pollen protoplasts of *Arabidopsis*. The effect of Ca^{2+} over time in chloride currents led us to conjecture that this stimulation is likely to be due to indirect rather than a direct binding of Ca^{2+} to the anionic channels. Interestingly, a link between Ca^{2+}-dependent protein kinases, CPK2 and CPK20, and the anion channel SLAH3 was proposed to regulate pollen tube growth at the tip (Gutermuth et al., 2013). Several findings supported this claim:

i) both CPKs tagged with YFP localized strictly at the tip of the plasma membrane (but not SLAH3:YFP that was shown to be widespread along the pollen tube and diffuse ate the tip) ;
ii) expression of SLAH3 with either CPK2 or CPK20 *Xenopus laevis* oocytes elicited S-type anion channel currents;
iii) bimolecular fluorescence complementation confirmed interaction assays of SLAH3 with CPK2/CPK20
iv) extracellular anion fluxes from *slah3-1* and the double mutant *cpk2-1 cpk20-2* were reduced when compared with wild-type tube tips

Most of the cellular processes discussed above for anions are physiological effectors of the Ca^{2+} gradient (Roy et al., 1999; Parton et al., 2003; Becker et al., 2004; Hwang et al., 2005; Helling et al., 2006) and a temporal correlation between anions and Ca^{2+} homeostasis was also recently observed by Gutermuth et al. (2013). By expressing $[Ca^{2+}]_{cyt}$ reporter Yellow-Cameleon

YC3.6 in tobacco pollen it was possible to measure pronounced growth alterations and tip-focused oscillatory $[Ca^{2+}]_{cyt}$ if changes in the extracellular Cl^- concentration exceeded 10 mM. A consequent increase in growth rate correlated with an increase in $[Ca^{2+}]_{cyt}$ and simultaneous reduction in cytosolic anion concentration. Moreover, both the cytosolic anion and Ca^{2+} gradients were eliminated by the application of NPPB, which resulted in pollen tube growth arrest. The authors hypothesized that $[Ca^{2+}]_{cyt}$-dependent anion release at the pollen tube tip generates a cytosolic anion concentration gradient (Gutermuth et al., 2013), most probably through CPK regulation.

5.3. Localization of the 4 anionic transporters in the tube

Anion fluxes form a closed loop in the apical domain of lily and tobacco, with pronounced oscillatory efflux at the tip, and a steady and nonoscillatory anion influx behind the tip (Zonia et al., 2001, 2002). Moreover, growing pollen tubes have a cytosolic anion concentration negative gradient. By expressing the genetic anion-sensitive probe *Chloride-Sensor* in *N. tabacum* pollen tubes Gutermuth et al., (2013) were able to monitor changes in anion levels by increasing extracellular Cl^- concentrations. At standard growth conditions with 0.4 mM Cl^-, low and high anion concentrations were visualized in the tip and subapical region (0 to 10 µm behind the tip), as well as the base of the tube (≥50 µm behind the tip), and in the region 20 to 50 µm behind the tip, respectively. Noticeably, an increase in the overall ratio was observed with each increase in external $[Cl^-]$, but the distribution was unaltered. Curiously, after applying ≥ 10 mM Cl^-, the authors observed pronounced growth oscillations, that were always accompanied by a decrease in anion concentration in the pollen tube tip (Gutermuth et al., 2013). The conclusions are in agreement with the previous vibrating probe data, which shows that the oscillatory efflux at the tip is most pronounced when the outburst of a growth cycle begins (Zonia et al., 2002; Gutermuth et al., 2013). In addition, here we show that the anion fluxes from the tip in the *slah3*$^{-/-}$ mutant are reduced when compared with the *atccc*$^{-/-}$ mutant. Since there is an uneven distribution of $[Cl^-]_{cyt}$ along the pollen tube, an also uneven allocation of anion channels and transporters has to exist in order to guarantee the tube polarization. The presence of a channel(s) at the tip

explains the rapid efflux fluctuations observed; whereas, the more stable non-oscillatory influx and gradient behind the tip (20 to 50 µm) can be explained through a carrier-driven transport. Moreover, upon extracellular Cl^- elevation a subsequent rise in cytosolic anion concentrations in the region ~20 to 40 µm behind the tip is also a hint for an active inward-directed anion translocation process (Gutermuth et al., 2013). By overexpressing the candidate channels and co-transporter under the control of the Lat52 pollen specific promoter, we were able to successfully confirm the previous assumptions in *A. thaliana*. GFP fluorescence, which represents protein localization, in the transgenic lines, showed that the SLAH3 channel localizes preferentially at the tip of the tube, and the co-transporter AtCCC and the AtTMEM16 transporter, are preferentially localized at the shank and grain (Figure 38). Thus, SLAH3 may be responsible for the the rapid efflux fluctuations at the tip, along with ALMT12 channels, while AtCCC and AtTMEM16 transporters may account for the non-oscillatory influx measured in the shank of the tube. To our knowledge, AtCCC transporter is the first positive molecular localization of an anion transporter at the plasma membrane in the pollen tube shank.

The presence of AtCCC in the plasma membrane of the pollen tube shank Recently, a study in Grapevine and *Arabidopsis* localized AtCCC, using fluorescent tagging with YFP, to the Golgi and trans-Golgi network. A possible PM localization was discarded, making it impossible for the co-transporter to directly mediate ion transfer with the xylem or have a direct role in salt tolerance (Henderson et al., 2015). Nevertheless, others have already observed AtCCC localization in the PM of arabidospis vasculature at the xylem/symplast boundary, and of rice root cells (Colmenero-Flores et al., 2007; Kong et al., 2011). Intracellular vesicular localizations are always possible on over-expressing conditions, so these two results are not necessarily contradictory.

With defined subcellular localizations of the pollen channels/transporter candidates, it is tempting to discuss possible functional roles for each. Overall, there is a substantial amount of evidence pointing to the importance of Cl^- efflux in the germination of pollen grains and in the growth of pollen tubes, specifically in the regulation of cytoplasm compartmentalization, membrane potential regulation, and to a smaller extent mitochondrial regulation (Zonia et al., 2002;

Matveyeva et al., 2003; Breygina et al., 2009a,b; Breygina et al., 2010). By applying the Cl^- channel blockers DIDS, NA and NPPB, and Ins(3,4,5,6)P_4, a known Ca^{2+}-activated Cl^- conductance blocker, Zonia et al., (2002) showed that they not only completely abolished tip anion efflux and tobacco pollen tube growth, but also induced an increase in apical volume, indicating an anion flux driven balance of the osmotic pressure. In guard cells a similar correlation is present and well established. The movement of guard cells is associated to variations in its turgor pressure, which are regulated by the flow of K^+, Cl^- and organic anions in and out of the cells. Specifically, R- and S-type channels drive the exit of anions, which leads to membrane depolarization and consequent activation of plasma membrane K^+ channels. Anions and cations then decrease turgor pressure by driving water across the cell. There is abundant evidence of the importance of the regulation of osmotic pressure during the apical growth of pollen tubes, and it has been established that variations on cell volume osmotically induced, elicit rapid variations of phospholipid membrane composition and signaling (Zonia & Munnik, 2004). Nevertheless, since pressure probe measurements failed to detect a correlation between osmotic pressure and growth rates during pollen tube elongation (Benkert et al., 1997), one can assume that the movement of anions helps maintain the even osmotic pressure along the tube.

5.4. The GABA effect in the anionic currents from WT hydrated protoplasts

Several studies have focused on ion transport regulation by GABA. Barbosa et al., (2010) demonstrated that GABA promoted NO^{3-} uptake at low $NO^{3-,}$ and NO^{3-} uptake inhibition at high NO^{3-} in *Arabidopsis* seedlings cultivated *in vitro*. Changes in phloem GABA have been positively correlated with nitrate influx during nitrogen deprivation and over the growth cycle of *Brassica napus* (Beuvé et al., 2004). Furthermore, extracellular GABA induces expression of a plasma membrane-located nitrate transporter and stimulates $^{15}NO_3$ influx by the root system (Beuvé et al., 2004; Shelp et al., 2006). The present study implicates Cl^- ions as downstream effectors of GABA signaling in pollen.

The results presented here incite interesting questions regarding the evolution of amino-acid signaling across kingdoms. The malate permeable transporter TaALMT1, present in the plasma membrane of bread wheat (*Triticum aestivum*) root apical cells, was shown to be negatively regulated by GABA. It was suggested that TaALMT1 is a prime candidate for transducing GABA signals in plants (Ramesh et al., 2015). Eight ALMT proteins from 5 plant species (*Arabidopsis*, wheat, barley, rice and grapevine), which included ALMT12 expressed pollen protein, showed that regulation by GABA was a general feature of this family. A model of a human $\alpha_1\beta_2\gamma_2$ $GABA_A$ receptor was constructed that predicts residues important for binding GABA; many of these residues were subsequently validated as part of a neurotransmitter-binding pocket when the crystal structure of a human homopentimeric β_3 subunit $GABA_A$ receptor was resolved (Bergmann et al., 2013; Ramesh et al., 2015). Interestingly, a shared region spanning 12 amino acids was found by comparing the sequences of the mammalian $GABA_A$ receptor and ALMT members using MEME (Motif-based sequence analysis tools) analysis. Site-directed mutagenesis of these amino acids abolished GABA regulation of anion currents. The motif is shared by all ALMT proteins and is required for GABA binding and efficacy. Figure 37 depicts the residues that are also present in the AtALMT12 protein (Ramesh et al., 2015).

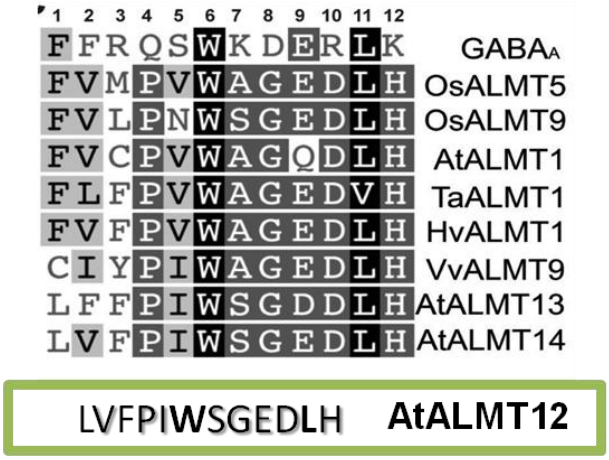

Figure 37. Variation in the residues of the identified motif between ALMT proteins, from different plant species and the human $\alpha_1\beta_2\gamma_2$ $GABA_A$ receptor (figure adapted from Ramesh et al., 2015).

Successful pollen tube growth and orientation involves the interaction of the pollen tube with the pistil. *Arabidopsis* pollen tubes are exposed to different

GABA concentrations that gradually increase along the female tissues, from the stigma (~20 µM) towards the ovule (~500 µM) (Palanivelu et al., 2003). The formation of the GABA gradient in the pistil may depend on pollen tube activity, such as the degradation of GABA within pollen tubes (Palanivelu et al., 2003). In the present study, GABA was first added in the extracellular medium, but no effect on the currents was observed. Nevertheless, when GABA was used in the intracellular or pipette solution, we observed a strong inhibition of the overall anionic currents. The results suggest a regulation of the anionic transporters within the pollen tube. This regulation could also be direct, by binding to specific anionic channels, namely ALMT12, as the presence of both GABA and muscimol produced a very rapid decrease in the initial currents (5 to 10 minutes after entering WC). There are three other compelling pieces of evidence that sustain this hypothesis:

i) the single mutant line *almt12*$^{-/-}$ showed insensitivity to [10 µM]$_{in}$ muscimol;

ii) the biophysical properties after rundown from the previous test group and the test group "*wt* + [10 µM]$_{in}$ muscimol", showed similar values for the fitting parameters V_h and V_s, but different from the control;

iii) the ALMT12 channel has a motif that is shared by all ALMT proteins and is required for GABA binding and efficacy.

Furthermore, the results imply that GABA may also modulate intracellular effectors, e.g. Ca^{2+}, which will in turn regulate the activity of the anionic transporters present in the PM of the tube. Recently, it was demonstrated that exogenous GABA could regulate the level of Ca^{2+} in tobacco pollen tubes through modulation of Ca^{2+}-permeable channels, leading to Ca^{2+} signaling cascades (Yu et al., 2006). The same phenomena might also occur in other plant species, namely *Arabidopsis thaliana*. Interestingly, when 8.5 µM and 0.54 mM [Ca^{2+}] was added to the intracellular pipette solution in Lily pollen protoplasts a high %RD was obtained, in relation to 6.04 nM [Ca^{2+}] control conditions (Tavares et al., 2011a). We here show that *wt* protoplasts treated with 500 µM GABA presented a significantly higher %RD than the measured for the *wt* (control). We then speculate that this difference could be due to the regulation of the channels by Ca^{2+} through GABA modulation.

Renault et al., (2011) used *pop-2* mutant as a model to examine the effects of GABA accumulation on plant development. Specifically, microarray analysis of *pop2-1* seedlings (where no obvious defects were detected in vegetative tissues), were grown in GABA-supplemented medium, revealing that GABA accumulation caused cell elongation defects and a decrease in expression of genes encoding secreted and cell wall-related proteins in *Arabidopsis thaliana*. In particular, the SLAH3 RNA expression level was higher without GABA and significantly higher after 4 days of treatment with 1 mM exogenous GABA, when compared to the wild-type. Thus, GABA accumulation increased *SLAH3* expression levels (Renault et al., 2011). In the present analysis, a transcriptional induction of SLAH3 channels by GABA could only occur several hours after adding GABA to the bath solution. Nevertheless, it is interesting to observe a link between GABA and the SLAH3 channels, and since these channels were shown to be regulated by CPKs, it is tempting to hypothesize that SLAH3 can be modulated by GABA *via* Ca^{2+} regulation. The observed GABA effect on anions currents bestows them an important task in GABA perception during pollen hydration, germination, and probably during tube growth. In the future, it will be interesting to confirm the present results in tube protoplasts. Furthermore, we observed a negative regulation of Cl^- by GABA, and a massive reduction of Cl^- currents with increasing $[GABA]_{in}$.

Interestingly, the ALMT12 channel when expressed in pollen protoplasts shows similar features as the ones observed in guard cells, namely a higher activation in the negative potential range and sensitivity to malate. To the best of our knowledge, the present study shows for the first time, the activity of a plant anionic channel in a mammalian immortalized cell line. Remarkably, the expression of *ALMT12* in COS-7 cells elicits inward currents, confirming the previous statement.

In animals, when GABA binds to the $GABA_A$ receptors, bursts of chloride ion channel activity occur, resulting in membrane hyperpolarization (Twyman & Macdonald, 1991). GABA also exerts its inhibitory effect in the synapses of mature brain neurons by activation of Cl^- currents. In plants, the anion equilibrium potential is normally very positive so that when ALMT proteins are activated there is a depolarization of the PM (Ramesh et al., 2015). Plant action

potentials are largely based on activation of voltage-dependent anion channels. Thus, GABA inhibition of ALMT will tend to hyperpolarize the membrane potential and decrease excitability, similar to the effect of GABA in animal neurons (Ramesh et al., 2015). We show that GABA induces flickering by dramatically altering the activity and the charge passed per time of ALMT12 channels present in the PM of COS-7 cells. In animals, individual $GABA_A$ channels do not open continuously in the presence of GABA but rather flicker open and closed, often in bursts (Snyder, 2002). For example, Fisher & Macdonald, (1997), while studying single-channel properties of $GABA_A$ receptors in mouse L929 cells, observed that in some patches a concentration of 600 µM GABA appeared to cause rapid flickering suggestive of open-channel block. Interestingly, agonist-induced channel block was reported for the nicotinic acetylcholine receptor, which is closely related to the $GABA_A$ receptor (Colquhoun & Ogden, 1988). Similarly, furosemide, a subtype-specific $GABA_A$ antagonist, was shown to block $GABA_A$ receptors by acting as an open-channel blocker, increasing channel flickering and decreasing the deactivation rate, in outside-out patch excised from CA1 pyramidal neuron cells and in the presence of GABA (Banks et al., 1998). In addition, high concentrations (> 1mM) of barbiturates, namely pentobarbitone and phenobarbitone, in the absence or presence of 1 µM GABA, produced a flickering effect along with rapid block of currents, probably due to fast channel block (Rho et al., 1996). The flickering phenomenon might be explained by the binding region spanning 12 amino acids shared between $GABA_A$ animal receptors and the ALMT family plant channels, namely ALMT12. Further elucidation of the observed blocking mechanism requires a more complete analysis.

An interesting fact is that GABA produced a stronger effect when present in the pipette solution, but not outside. GABA may enter the pollen tube cell through a number of transporters that show relatively low (mM range) or high affinities, namely amino acid permease 3 (AAP3), proline transporters 2 (ProT2), and GABA transporters (AtGAT1), a member of the *Arabidopsis* amino acid transporter family, respectively (Grallath et al., 2005; Meyer et al., 2006). The first three also transport glycine, betaine or proline with higher efficiency. AtGAT1 is a proton-driven transporter with high affinity for GABA (µM range),

but it can also transport other related compounds across the plasma membrane (Grallath et al., 2005; Meyer et al., 2006). A mitochondrial membrane localized *Arabidopsis* amino acid//polyamine/organo-cation transporter family (GABA permease or GABP) was found to complement GABA, but not proline transport, in a GABA-transport-deficient yeast mutant (Michaeli et al., 2011; Shelp et al., 2012). A high sequence similarity between the plant glutamate receptor GLR3.7, the animal GLR3.5, and structural homology with a regulatory domain from the mammalian $GABA_{B1}$ receptors was obtained by protein blast, suggesting that GABA might also interact with plant GLRs. Moreover, GABA may be also sensed through unidentified GABA receptors in the extracellular side of the pollen tube (Yu et al., 2014).

5.5. An integrated view of Anion transport and regulation in pollen tubes

Figure 38 is a Physiological Model generated from the data gathered during the course of this work. It depicts a putative feedback regulation system linking pollen tube growth modulation by GABA through anionic transporters. The allocation of these transporters to specific regions of the pollen tube was also taken into account. The Model suggests that GABA, produced by the female tissues, enters the pollen tube cell through a number of GABA-transporters, e.g. AAP3 or ProT2, present in its plasma membrane. Inside the tube cytoplasm GABA regulates the movement of anions across the plasma membrane, by directly binding the activity of ALMT12 channels and indirectly regulating other channels, e.g. SLAH3. The efflux variations caused by the activity of SLAH3 and ALMT12 channels will in turn stimulate the activity of the AtCCC co-transporter and the AtTMEM16 transporters responsible for the anion influx present at the shank of the tube.The anion unbalance generated by GABA is followed by the passive flow of water according to the osmotic gradient, which in turn builds up the hydrostatic pressure needed for cell volume change allowing the tube to grow.

Like all models, this is a minimal representation of the data presented in this thesis, and likely to just represent an anedoctal view of a much more complex regulatory system. Yet, by and large, it does fits in most of the data gathered in

this thesis, and provides a conceptual framework in which various predictions can be experimentally tested, either in the context of the pollen tube Cell Biology, either in term of pollen-pistil communication and reproductive efficiency.

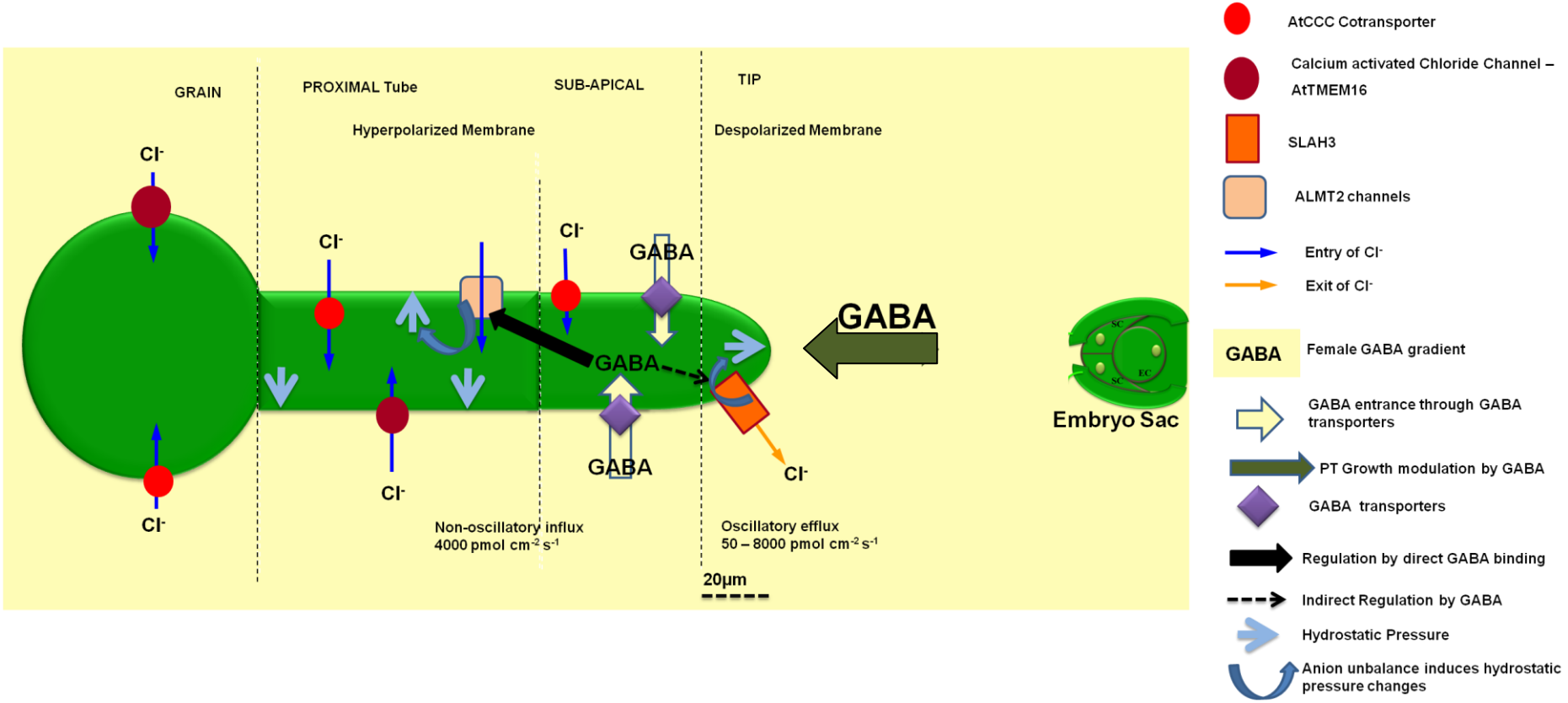

Figure 38. Model Depicting a Putative Feedback-Regulation of Pollen Tube Growth by GABA through Anionic Transporters during Sexual Reproduction in Flowering Plants. Upon landing on a receptive stigma, the pollen grain hydrates and becomes activated. The pollen tube germinates and is immediately exposed to increasing GABA concentrations along the different female tissues, from 20 µM in the stigma, 60 µM in the style, 110 µM in ovary walls, and 160 µM in the septum to 500 µM in integument cells. GABA enters the pollen tube through GABA transporters, and there it directly binds to ALMT12 channels and may regulate other sensitive transporters, e.g. SLAH3. This regulation causes ionic unbalance followed by the passive flow of water according to the osmotic gradient, which in turn supports and signals for growth.

Annex 1. Predicated protein structure of the At1g73020 gene, designated by *AtTMEM16*.

The mammalian CaCC protein was used as template to search an *Arabidopsis* homologous protein by means of the NCBI protein blast program (http://blast.ncbi.nlm.nih.gov/Blast.cgi). The *Arabidopsis* protein sequence identified has not yet been characterized, its function is unknown, and shares a detailed signature domain with the animal counterpart – the Anoctamin family (Interpro: IPR007632; Pfam: PF04547). As the protein function was not established, we used the AtTMEM16 nomenclature. The anoctamin family, which includes anoctamin1-10 (Ano1-10 or TMEM16A-J), is usually divided into two subfamilies, the Ca^{2+}-dependent Cl^- channels (Ano1 and Ano2 or TMEM16A and 16B) and Ca^{2+}-dependent lipid scramblases although with variable lipid preference (Ano3-10 or TMEM16C, 16D, 16F, 16G, and 16J) (Suzuki et al., 2013; Pedemonte & Galietta, 2014). It was initially presumed that all ANOs are Cl^- channels because of the close sequence similarity between ANO family members (ANO1 is 38–45% identical to ANOs −3 to −7, >90% coverage), however a lipid scrambling domain and function was identified in Ano6/TMEM16F (Suzuki et al., 2010; Yu et al., 2015). Moreover, an ANO homolog, Ist2, was also found in yeast (*Saccharomyces cerevisiae*). Here, Ist2p (increased sodium tolerance protein 2) co-localized with proteins of the cortical Endoplasmatic Reticulum (ER) where it binds phosphoinositide lipids at the cytosolic face of the plasma membrane (PM). Ist2p deletion along with other ER-plasma membrane tethering proteins resulted in aberrant phosphatidylinositol 4-phosphate levels and localization. Moreover, the expression of human ANO1 in cells lacking that gene, led to a partial rescue of the KO phenotype. The results suggested two functions, one as an ion channel and another one in the transport of lipids (Wolf et al., 2012). Yu et al., (2015), combining patch clamp recording with measurement of PhosphoLipid Scrambling (PLS), showed that ANO6 elicits robust Ca^{2+}-dependent PLS coinciding with ionic currents that are explained by ionic leak during phospholipid translocation. Curiously, the domain in ANO6 necessary for PLS was sufficient to confer this function on ANO1-ANO6 chimeric protein, which normally does not scramble (Yu et al., 2015). Similarly, a fungal TMEM16

homologue from *Aspergillus fumigates* (afTMEM16) was found to scramble lipids and to form non-selective ion channels with high conductance.

The *Arabidopsis* primary accession number in UniProtKB/Swiss-Prot database is A0MFS9 (the secondary accessions numbers are also be used: Q5XVG1, Q9SSM5). The shared sequence similarity allows several features to be predicted, namely: its subcellular localization, function, and interaction with other proteins. According to this, the Anoctamin-like protein At1g73020 may function as a calcium-activated chloride channel, it's expected to span the PM through 8 transmembrane regions and to interact with several members of the phosphatidylinositol 3-and 4-kinase, cyclin, ubiquitin and plant-specific TFIIB-related family proteins (UniProtKB, $STRING_{10}$). These relations may implicate AtTMEM16 in crucial interesting roles such as, pollen germination and embryogenesis, division control, and regulation of pollen wall formation in *Arabidopsis* (Pina et al., 2005; Huang et al., 2012; Niu et al., 2013).

Furthermore, the AtTMEM16 sequence was submitted to the Phyre2 Protein Fold Recognition Server (Kelley & Sternberg, 2009), and aligned to sequences extracted from PDB. Almost 90%, 581 residues, of the AtTMEM16 sequence was modeled with 100.0% confidence by the single highest scoring template, the tmem16 lipid scramblase in crystal form 2, PDB ID c4witB. The template sequence belongs to a TMEM16 family member from the fungus *Nectria haematococca* (nhTMEM16) that operates as a Ca^{2+}-activated lipid scramblase (Brunner et al., 2014). Recently, the X-ray of this structure was obtained, and each subunit of the homodimeric protein was shown to contain ten transmembrane helices and a hydrophilic membrane-traversing cavity that is exposed to the lipid bilayer as a potential site of catalysis (Brunner et al., 2014). The two sequences shared 23% identity and 37.4% similarly (calculated by the BLSM62 algorithm), and a predicted secondary structure was obtained for AtTMEM16 similar to that of nhTMEM16 protein (Figure 39). As with nhTMEM16, AtTMEM16 contains ten membrane-spanning helices, which differs from the eight transmembrane segments predicted from hydropathy analysis (UniProtKB). Despite the functional breadth, characterized Anoctamin family members appear to share a similar mode of Ca^{2+}-activation (Brunner et al., 2014). The nhTMEM16 hydrophilic cavity contains a highly conserved region

that is embedded within the hydrophobic core of the membrane comprising a Ca^{2+}-binding site, a similar region was obtained for AtTMEM16 protein (Figure A1, Ca^{2+}-binding sites red and purple boxes). The red (identical) and purple (homolog) boxes shown in Figure A1 depicts 5 out of 6 residues shown to be involved in Ca^{2+} modulation (Brunner et al., 2014). Mutations in these residues affected both lipid scrambling in *N. haematococca* TMEM16 and ion conduction in the murine Cl^- channel TMEM16A, namely E452Q and E654Q, respectively (Brunner et al., 2014). The Ca^{2+}-binding site E452Q is conserved in AtTMEM16 protein (Figure A1, query sequence, predicted secondary structure, first red box, position 440). Lipid transporter proteins catalyze the passive movement of lipids between the two leaflets of a bilayer, a process that is essential for membrane biogenesis in the endoplasmic reticulum and the shuffling of lipids in several processes, including blood coagulation, apoptosis, glycosylation and the assembly of the bacterial cell wall (Wolf et al., 2012; Yang et al., 2012; Suzuki et al., 2013; Brunner et al., 2014). Interestingly, Brunner and colleagues were unable to detect ion conductance in nhTMEM16 (Brunner et al., 2014).

Several evidences support the idea that AtTMEM16 protein could be in fact, and solely, a lipid scramblase: i) no ion channel activity was observed by patch-clamp electrophysiology of HEK293T or COS-7 cells expressing the protein, even when co-transfected with CPK17 or CPK20 (similarly to nhTMEM16); ii) it was predicted to interact with phosphatidylinositol kinases, possibly linking AtTMEM16 to the transport of lipids, and iii) the non restricted to the PM localization obtained from the transgenic stable line, Lat52::*AtTMEM16*-GFP, which lead us to hypothesize that AtTMEM16 may co-localize with proteins of the ER, which are being held together by the cytoskeleton, and bind phosphoinositide lipids at the cytosolic face of the PM (similarly to Ist2p). In the future, it will be interesting to verify if AtTMEM16 function as a lipid scramblase by, for example, monitoring the reduction of fluorescently labeled lipids by sodium dithionite on the outer leaflet of liposomes (Brunner et al., 2014). However, the *attmem16* mutant patch clamp results here obtained strongly suggest that AtTMEM16 might (coexist) function as an ion channel, either by a change in the conformational structure induced by Ca^{2+} binding, or by modification of the electrostatics in the close-by subunit cavity, which would regulate the conductive properties of this region (Brunner et al., 2014).

Figure 39. AtTMEM16 predicted secondary structure according to the single highest scoring template PDB ID c4witB. Query sequence refers to AtTMEM16. The sequence is represented according to Phyre2, with residues colored according to the scheme: A, S, T, G, P – small/polar, yellow/orange; M, I, L, V – hydrophobic, green; K, R, E, N, D, H, Q – charged, red; and W, Y, F, C - aromatic + cysteine, blue. Identical residues in the alignment are highlighted with a grey

background. The prediction is 3-state: either α-helix, β-strand or coil. Green helices represent α-helices, blue arrows indicate β-strands and faint lines indicate coil, as depicted in the label. Purple and red boxes depict homolog and identical residues involved in Ca^{2+} binding. Blue box illustrates the positions of residues in α-helix 10 involved in an inter subunit salt bridge at the dimer cavity where lipid interactions are due to occur; no role was attributed to this region. Dark blue long boxes refer to the observed membrane spanning regions of nhTMEM16 (Brunner et al., 2014); the same structure was predicted to AtTMEM16.

6. Bibliography

Allen GJ, Kuchitsu K, Chu SP, Murata Y, Schroeder JI. **1999**. *Arabidopsis* abi1-1 and abi2-1 phosphatase mutations reduce abscisic acid-induced cytoplasmic calcium rises in guard cells. *The Plant cell* **11**: 1785–98.

Amien S, Kliwer I, Márton ML, Debener T, Geiger D, Becker D, Dresselhaus T. **2010**. Defensin-like ZmES4 mediates pollen tube burst in maize via opening of the potassium channel KZM1. *PLoS biology* **8**: e1000388.

De Angeli A, Monachello D, Ephritikhine G, Frachisse J-M, Thomine S, Gambale F, Barbier-Brygoo H. **2006**. The nitrate/proton antiporter AtCLCa mediates nitrate accumulation in plant vacuoles. *Nature* **442**: 939–42.

De Angeli A, Thomine S, Frachisse J-M, Ephritikhine G, Gambale F, Barbier-Brygoo H. **2007**. Anion channels and transporters in plant cell membranes. *FEBS letters* **581**: 2367–74.

Ashley RH. **1996**. *Ion Channels: A Practical Approach*. Oxford University Press.

Ayadi A, David P, Arrighi J-F, Chiarenza S, Thibaud M-C, Nussaume L, Marin E. **2015**. Reducing the Genetic Redundancy of *Arabidopsis* PHOSPHATE TRANSPORTER1 Transporters to Study Phosphate Uptake and Signaling. *Plant physiology* **167**: 1511–26.

Bader CR, Bertrand D, Schwartz EA. **1982**. Voltage-activated and calcium-activated currents studied in solitary rod inner segments from the salamander retina. *The Journal of physiology* **331**: 253–84.

Banks MI, Li TB, Pearce RA. **1998**. The synaptic basis of GABAA,slow. *The Journal of neuroscience* **18**: 1305–1317.

Barbier-Brygoo H, De Angeli A, Filleur S, Frachisse J-M, Gambale F, Thomine S, Wege S. **2011**. Anion Channels/Transporters in Plants: From Molecular Bases to Regulatory Networks. *Annual review of plant biology*: 25–51.

Barbier-Brygoo H, Vinauger M, Colcombet J, Ephritikhine G, Frachisse J-M, Maurel C. **2000**. Anion channels in higher plants: functional characterization, molecular structure and physiological role. *Biochimica et biophysica acta* **1465**: 199–218.

Barbosa JM, Singh NK, Cherry JH, Locy RD. **2010**. Nitrate uptake and utilization is modulated by exogenous gamma-aminobutyric acid in *Arabidopsis* thaliana seedlings. *Plant physiology and biochemistry* **48**: 443–50.

Barish ME. **1983**. A transient calcium-dependent chloride current in the immature Xenopus oocyte. *The Journal of physiology* **342**: 309–25.

Becker JD, Boavida LC, Carneiro J, Haury M, Feijó JA. **2003**. Transcriptional Profiling of *Arabidopsis* Tissues Reveals the Unique Characteristics of the Pollen Transcriptome. *Plant Physiology* **133**: 713–725.

Becker JD, Feijó JA. **2007**. How many genes are needed to make a pollen tube? Lessons from transcriptomics. *Annals of botany* **100**: 1117–23.

Becker D, Geiger D, Dunkel M, Roller A, Bertl A, Latz A, Carpaneto A, Dietrich P, Roelfsema MRG, Voelker C, et al. 2004. AtTPK4, and *Arabidopsis* tandem-pore K+ channel, poised to control the pollen membrane voltage in a pH- and Ca2+-dependent manner. *Sciences-New York* **101**: 15621–15626.

Becq F. **1996**. Ionic channel rundown in excised membrane patches. *Biochimica et biophysica acta* **1286**: 53–63.

Benkert R, Obermeyer G, Bentrup F-W. **1997**. The turgor pressure of growing lily pollen tubes. *Protoplasma* **198**: 1–8.

Berendse F, Scheffer M. **2009**. The angiosperm radiation revisited, an ecological explanation for Darwin's "abominable mystery." *Ecology Letters* **12**: 865–872.

Berger F, Hamamura Y, Ingouff M, Higashiyama T. **2008**. Double fertilization – caught in the act. *Trends in Plant Science* **13**: 437–443.

Bergmann R, Kongsbak K, Sørensen PL, Sander T, Balle T. **2013**. A Unified Model of the GABAA Receptor Comprising Agonist and Benzodiazepine Binding Sites. *PLoS ONE* **8**: e52323.

Berkefeld H, Fakler B, Schulte U. **2010**. Ca2+-Activated K+ Channels: From Protein Complexes to Function. *Physiological Reviews*: 1437–1459.

Beuvé N, Rispail N, Laine P, Cliquet J, Ourry A, Le Deunff E. **2004**. Putative role of γ-aminobutyric acid as a long-distance signal in up-regulation of nitrate uptake in Brassica napus L. *Plant Cell and Environment* **27**: 1035–1046.

Binder K, Wegner LH, Heidecker M, Zimmermann U. **2003**. Gating of Cl- currents in protoplasts from the marine alga Valonia utricularis depends on the transmembrane Cl- gradient and is affected by enzymatic cell wall degradation. *The Journal of membrane biology* **191**: 165–78.

Boavida LC, McCormick S. **2007**. Temperature as a determinant factor for increased and reproducible in vitro pollen germination in *Arabidopsis* thaliana. *The Plant Journal* **52**: 570–582.

Boavida LC, Vieira AM, Becker JD, Feijó JA. **2005**. Gametophyte interaction and sexual reproduction: how plants make a zygote. *The International journal of developmental biology* **49**: 615–32.

Bock KW, Honys D, Ward JM, Padmanaban S, Nawrocki EP, Hirschi KD, Twell D, Sze H. **2006**. Integrating Membrane Transport with Male Gametophyte Development and Function through Transcriptomics1[W]. *Plant Physiology* **140**: 1151–1168.

Bown AW, Shelp BJ. **1997**. The metabolism and functions of g-aminobutyric acid. *Plant Physiology* **115**: 1–5.

Brearley J, Venis MA, Blatt MR. **1997**. The effect of elevated CO2 concentrations on K+ and anion channels of Vicia faba L. guard cells. *Planta* **203**: 145–154.

Breygina MA, Matveeva NP, Ermakov IP. **2009a**. The role of Cl− in pollen germination and tube growth. *Russian Journal of Developmental Biology* **39**: 157–164.

Breygina MA, Smirnova A V, Maslennikov M V, Matveeva NP, Yermakov IP. **2010**. Effects of anion channel blockers NPPB and DIDS on tobacco pollen tube growth and its mitochondria state. *Cell and Tissue Biology* **4**: 289–296.

Breygina MA, Smirnova A V, Matveeva NP, Yermakov IP, Yermako. **2009b**. Membrane potential changes during pollen germination and tube growth. *Tsitologyia* **51**: 815–823.

Brunner JD, Lim NK, Schenck S, Duerst A, Dutzler R. **2014**. X-ray structure of a calcium-activated TMEM16 lipid scramblase. *Nature* **516**: 207–212.

Caputo A, Caci E, Ferrera L, Pedemonte N, Barsanti C, Sondo E, Pfeffer U, Ravazzolo R, Zegarra-Moran O, Galietta LJ V. **2008**. TMEM16A, a membrane protein associated with calcium-dependent chloride channel activity. *Science (New York, N.Y.)* **322**: 590–4.

Carew M a, Yang X, Schultz C, Shears SB. **2000**. Myo-Inositol 3,4,5,6-Tetrakisphosphate Inhibits an Apical Calcium-Activated Chloride Conductance in Polarized Monolayers of a Cystic Fibrosis Cell Line. *The Journal of biological chemistry* **275**: 26906–13.

Cellier F, Conéjéro G, Ricaud L, Luu DT, Lepetit M, Gosti F, Casse F. **2004**. Characterization of AtCHX17, a member of the cation/H+ exchangers, CHX family, from *Arabidopsis* thaliana suggests a role in K+ homeostasis. *The Plant journal : for cell and molecular biology* **39**: 834–46.

Cenis JL. **1992**. Rapid extraction of fungal DNA for PCR amplification. *Nucleic acids research* **20**: 2380.

Certal AC, Almeida RB, Carvalho LM, Wong E, Moreno N, Michard E, Carneiro J, Rodriguéz-Léon J, Wu H-M, Cheung AY, et al. 2008. Exclusion of a proton ATPase from the apical membrane is associated with cell polarity and tip growth in Nicotiana tabacum pollen tubes. *The Plant Cell* **20**: 614–634.

Chen Z-H, Hills A, Lim CK, Blatt MR. **2010**. Dynamic regulation of guard cell anion channels by cytosolic free Ca2+ concentration and protein phosphorylation. *The Plant journal : for cell and molecular biology* **61**: 816–25.

Chen J, Li L, Liu Z, Yuan Y, Guo L, Mao D, Tian L, Chen L, Luan S, Li D. **2009**. Magnesium transporter AtMGT9 is essential for pollen development in *Arabidopsis*. *Cell research* **19**: 887–98.

Cheng J, Wang Z, Yao F, Gao L, Ma S, Sui X, Zhang Z. **2015**. Down-Regulating CsHT1, a Cucumber Pollen-Specific Hexose Transporter, Inhibits Pollen Germination, Tube Growth, and Seed Development. *Plant Physiology* **168**: 635–647.

Cheung AY. **1996**. The pollen tupe growth pathway: its molecular and biochemical contributions and responses to pollination. *Sexual Plant Reproduction* **9**: 330–336.

Cheung AY, Wu H-M. **2007**. Structural and functional compartmentalization in pollen tubes. *Journal of experimental botany* **58**: 75–82.

Cheung AY, Wu H-M. **2008**. Structural and signaling networks for the polar cell growth machinery in pollen tubes. *Annual review of plant biology* **59**: 547–72.

Clough SJ, Bent AF. **1998**. Floral dip: A simplified method for Agrobacterium-mediated transformation of *Arabidopsis* thaliana. *Plant Journal* **16**: 735–743.

Colcombet J, Lelièvre F, Thomine S, Barbier-Brygoo H, Frachisse J-M. **2005**. Distinct pH regulation of slow and rapid anion channels at the plasma membrane of *Arabidopsis* thaliana hypocotyl cells. *Journal of experimental botany* **56**: 1897–903.

Colcombet J, Thomine S, Guern J, Frachisse J-M, Barbier-Brygoo H. **2001**. Nucleotides provide a voltage-sensitive gate for the rapid anion channel of *Arabidopsis* hypocotyl cells. *The Journal of biological chemistry* **276**: 36139–45.

Colmenero-Flores JM, Martínez G, Gamba G, Vázquez N, Iglesias DJ, Brumós J, Talón M. **2007**. Identification and functional characterization of cation-chloride cotransporters in plants. *The Plant journal : for cell and molecular biology* **50**: 278–92.

Colquhoun D, Ogden DC. **1988**. Activation of ion channels in the frog end-plate by high concentrations of acetylcholine. *Journal of Physiology* **395**: 131–159.

Dietrich P, Hedrich R. **1994**. Interconversion of Fast and Slow Gating Modes of Gcac1, a Guard-Cell Anion Channel. *Planta* **195**: 301–304.

Dreinhöfer J, Gögelein H, Greger R. **1988**. Blocking kinetics of Cl− channels in colonic carcinoma cells (HT29) as revealed by 5-nitro-2-(3-

phenylpropylamino)benzoic acid (NPPB). *Biochimica et Biophysica Acta (BBA) - Biomembranes* **946**: 135–142.

Dutta R, Robinson KR. **2004**. Identification and Characterization of Stretch-Activated Ion Channels in Pollen Protoplasts. *Plant Physiology* **135**: 1398–1406.

Edwards KC, Johnstone C, Thompsom C. **1991**. A simple and rapid method for the preparation of plant genomic DNA for PCR analysis. *Nucleic Acids Res.* **19**: 1349.

Ehrhardt DW, Frommer WB. **2012**. New Technologies for 21st Century Plant Science. *The Plant cell* **24**: 374–394.

Fan L-M, Wang YF, Wang H, Wu WH. **2001**. In vitro *Arabidopsis* pollen germination and characterization of the inward potassium currents in *Arabidopsis* pollen grain protoplasts. *Journal of experimental botany* **52**: 1603–14.

Fan L-M, Wang YF, Wu WH. **2003**. Outward K+ channels in Brassica chinensis pollen protoplasts are regulated by external and internal pH. *Protoplasma* **220**: 143–52.

Fan L-M, Wu W-H, Yang H-Y. **1999**. Identification and Characterization of the Inward K+ Channel in the Plasma Membrane of Brassica Pollen Protoplasts. *Plant Cell Physiol.* **40**: 859–865.

Von der Fecht-Bartenbach JJ, Bogner M, Dynowski M, Ludewig U. **2010**. CLC-b mediated NOFormula/H+ exchange across the tonoplast of *Arabidopsis* vacuoles. *Plant & cell physiology* **51**: 960–968.

Von der Fecht-Bartenbach J, Bogner M, Krebs M, Stierhof Y-D, Schumacher K, Ludewig U. **2007**. Function of the anion transporter AtCLC-d in the trans-Golgi network. *The Plant journal : for cell and molecular biology* **50**: 466–74.

Feijó JA, Costa SS, Prado AM, Becker JD, Certal AC. **2004**. Signalling by tips. *Current opinion in plant biology* **7**: 589–98.

Feijó JA, Malhó R, Obermeyer G. **1995**. Ion dynamics and its possible role during in vitro pollen germination and tube growth. *Protoplasma* **187**: 155–167.

Feijó JA, Sainhas J, Hackett GR, Kunkel JG, Hepler PK. **1999**. Growing pollen tubes possess a constitutive alkaline band in the clear zone and a growth-dependent acidic tip. *The Journal of cell biology* **144**: 483–96.

Feijó JA, Sainhas J, Holdaway-Clarke TL, Cordeiro S, Kunkel JG, Hepler PK. **2001**. Cellular oscillations and the regulation of growth: the pollen tube paradigm. *BioEssays : news and reviews in molecular, cellular and developmental biology* **23**: 86–94.

Fisher JL, Macdonald RL. **1997**. Single channel properties of recombinant GABAA receptors containing gamma 2 or delta subtypes expressed with alpha 1 and beta 3 subtypes in mouse L929 cells. *The Journal of physiology* **505 (Pt 2**: 283–97.

Frachisse JM, Colcombet J, Guern J, Barbier-Brygoo H. **2000**. Characterization of a nitrate-permeable channel able to mediate sustained anion efflux in hypocotyl cells from *Arabidopsis* thaliana. *The Plant journal : for cell and molecular biology* **21**: 361–71.

Frelet-Barrand A, Kolukisaoglu HU, Plaza S, Ruffer M, Azevedo L, Hortensteiner S, Marinova K, Weder B, Schulz B, Klein M. **2008**. Comparative Mutant Analysis of *Arabidopsis* ABCC-Type ABC Transporters: AtMRP2 Contributes to Detoxification, Vacuolar Organic Anion Transport and Chlorophyll Degradation. *Plant and Cell Physiology* **49**: 557–569.

Frietsch S, Wang Y-F, Sladek C, Poulsen LR, Romanowsky SM, Schroeder JI, Harper JF. **2007**. A cyclic nucleotide-gated channel is essential for polarized tip growth of pollen. *Proceedings of the National Academy of Sciences of the United States of America* **104**: 14531–6.

Geiger D, Maierhofer T, Al-Rasheid K a S, Scherzer S, Mumm P, Liese A, Ache P, Wellmann C, Marten I, Grill E, et al. 2011. Stomatal closure by fast abscisic acid signaling is mediated by the guard cell anion channel SLAH3 and the receptor RCAR1. *Science* **4**.

Gogelein H. **1988**. Chloride channels in epithelia. *Biochim et Biophys Acta* **947**: 521–547.

Grallath S, Weimar T, Meyer A, Gumy C, Suter-Grotemeyer M, Neuhaus J-M, Rentsch D. **2005**. The AtProT Family. Compatible Solute Transporters with Similar Substrate Specificity But Differential Expression Patterns. *Plant Physiology* **137**: 117–126.

Greger R. **1996**. *Comprehensive Human Physiology*. Springer.

Griessner M, Obermeyer G. **2003**. Characterization of whole-cell K+ currents across the plasma membrane of pollen grain and tube protoplasts of Lilium longiflorum. *The Journal of membrane biology* **193**: 99–108.

Gu Y, Fu Y, Dowd P, Li S, Vernoud V, Gilroy S, Yang Z. **2005**. A Rho family GTPase controls actin dynamics and tip growth via two counteracting downstream pathways in pollen tubes. *Journal of Cell Biology* **169**: 127–138.

Gutermuth T, Lassig R, Portes M-T, Maierhofer T, Romeis T, Borst J-W, Hedrich R, Feijó J a, Konrad KR. **2013**. Pollen tube growth regulation by free anions depends on the interaction between the anion channel SLAH3 and calcium-dependent protein kinases CPK2 and CPK20. *The Plant cell* **25**: 4525–43.

Halliwell J V, Whitaker M, Ogden D. **1987**. Using microelectrodes.1–15.

Hamamura Y, Saito C, Awai C, Kurihara D, Miyawaki A, Nakagawa T, Kanaoka MM, Sasaki N, Nakano A, Berger F. **2011**. Live-Cell Imaging Reveals the Dynamics of Two Sperm Cells during Double Fertilization in *Arabidopsis* thaliana. *Current Biology*.

Hamill OP, Marty A, Neher E, Sakmann B, Sigworth FJ. **1981**. Improved Patch-Clamp Techniques for High-Resolution Current Recording from Cells and Cell-Free Membrane Patches. *Pflügers Archiv* **391**: 85–100.

Harada H, Kuromori T, Hirayama T, Shinozaki K, Leigh R a. **2004**. Quantitative trait loci analysis of nitrate storage in *Arabidopsis* leading to an investigation of the contribution of the anion channel gene, AtCLC-c, to variation in nitrate levels. *Journal of experimental botany* **55**: 2005–14.

Hartzell C, Putzier I, Arreola J. **2005**. Calcium-activated chloride channels. *Annual review of physiology* **67**: 719–758.

Hartzell HC, Yu K, Xiao Q, Chien L-T, Qu Z. **2009**. Anoctamin/TMEM16 family members are Ca2+-activated Cl- channels. *The Journal of physiology* **587**: 2127–39.

Hechenberger M, Schwappach B, Fischer WN, Frommer WB, Jentsch TJ, Steinmeyer K. **1996**. A family of putative chloride channels from *Arabidopsis* and functional complementation of a yeast strain with a CLC gene disruption. *The Journal of biological chemistry* **271**: 33632–8.

Hedrich R, Busch H, Raschke K. **1990**. Ca2+ and nucleotide dependent regulation of voltage dependent anion channels in the plasma membrane of guard cells. *The EMBO journal* **9**: 3889–92.

Helling D, Possart A, Cottier S, Klahre U, Kost B. **2006**. Pollen tube tip growth depends on plasma membrane polarization mediated by tobacco PLC3 activity and endocytic membrane recycling. *The Plant cell* **18**: 3519–3534.

Henderson SW, Wege S, Qiu J, Blackmore DH, Walker AR, Tyerman SD, Walker RR, Gilliham M. **2015**. Grapevine and *Arabidopsis* Cation-Chloride Cotransporters Localize to the Golgi and Trans-Golgi Network and Indirectly In fl uence Long-Distance Ion Transport and Plant Salt Tolerance 1 [OPEN]. *Plant physiology* **169**: 2215–2229.

Hepler PK, Lovy-Wheeler Al, Mckenna ST, Kunkel JG. **2006**. Ions and Pollen Tube Growth. *Plant Cell Monographs* **3**: 47–69.

Hepler PK, Vidali L, Cheung AY. **2001**. Polarized cell growth in higher plants. *Annual review of cell and developmental biology* **17**: 159–187.

Hiscock SJ. **2011**. Sexual plant reproduction. *Annals of Botany* **108**: 585–587.

Hodgkin AL, Huxley AF. **1952**. A quantitative description of membrane current and its application to conduction and excitation in nerve. *Journal of Physiology* **117**: 500–544.

Hoekenga O a, Maron LG, Piñeros M a, Cançado GM a, Shaff J, Kobayashi Y, Ryan PR, Dong B, Delhaize E, Sasaki T, et al. 2006. AtALMT1, which encodes a malate transporter, is identified as one of several genes critical for aluminum tolerance in *Arabidopsis*. *Proceedings of the National Academy of Sciences of the United States of America* **103**: 9738–43.

Holdaway-Clarke TL, Feijó JA, Hackett GR, Kunkel JG, Hepler PK. **1997**. Pollen Tube Growth and the Intracellular Cytosolic Calcium Gradient Oscillate in Phase while Extracellular Calcium Influx Is Delayed. *The Plant cell* **9**: 1999–2010.

Holdaway-Clarke TL, Hepler PK. **2003**. Control of pollen tube growth: role of ion gradients and fluxes. *New Phytologist* **159**: 539–563.

Holsinger KE. **2000**. Reproductive systems and evolution in vascular plants. *Proceedings of the National Academy of Sciences, USA* **97**: 7037–42.

Honys D, Twell D. **2003**. Comparative analysis of the *Arabidopsis* pollen transcriptome. *Plant physiology* **132**: 640–52.

Honys D, Twell D. **2004**. Transcriptome analysis of haploid male gametophyte development in *Arabidopsis*. *Genome biology* **5**: R85.

Huang F, Wong X, Jan LY. **2012**. Calcium-activated chloride channels. *Pharmacological Reviews* **64**: 1–15.

Hwang J, Gu Y, Lee Y-JJ, Yang Z. **2005**. Oscillatory ROP GTPase Activation Leads the Oscillatory Polarized Growth of Pollen Tubes (C Waterman-Storer, Ed.). *Molecular Biology of the Cell* **16**: 5385–5399.

Jackson M. **1997**. Whole-Cell Voltage Clamp Recording. *Current Protocols in Neuroscience*: 1–29.

Jentsch TJ. **2009**. CLC chloride channels and transporters: from genes to protein structure, pathology and physiology. *Critical reviews in biochemistry and molecular biology* **44**: 64.

Johannes E, Crofts a, Sanders D. **1998**. Control of Cl- efflux in chara corallina by cytosolic pH, free ca2+, and phosphorylation indicates a role of plasma membrane anion channels in cytosolic pH regulation. *Plant physiology* **118**: 173–81.

Jossier M, Kroniewicz L, Dalmas F, Le Thiec D, Ephritikhine G, Thomine S, Barbier-Brygoo H, Vavasseur A, Filleur S, Leonhardt N. **2010**. The *Arabidopsis* vacuolar anion transporter, AtCLCc, is involved in the regulation of

stomatal movements and contributes to salt tolerance. *The Plant Journal* **64**: 563–576.

Keller B, Hedrich R, Raschke K. **1989**. Voltage-dependent anion channels in the plasma membrane of guard cells. *Nature* **341**: 450–453.

Kelley L a, Sternberg MJE. **2009**. Protein structure prediction on the Web: a case study using the Phyre server. *Nature Protocols* **4**: 363–371.

Koester J. **1991**. *Principles of Neural Science* (ER Kandel, JH Schwartz, and TM Jessell, Eds.). New York: Elsevier Science.

Kollmeier M, Dietrich P, Bauer CS, Horst WJ, Hedrich R. **2001**. Aluminum Activates a Citrate-Permeable Anion Channel in the Aluminum-Sensitive Zone of the Maize Root Apex. A Comparison Between an Aluminum- Sensitive and an Aluminum-Resistant Cultivar. *Plant physiology* **126**: 397–410.

Kong X-Q, Gao X-H, Sun W, An J, Zhao Y-X, Zhang H. **2011**. Cloning and functional characterization of a cation-chloride cotransporter gene OsCCC1. *Plant molecular biology* **75**: 567–78.

Kovermann P, Meyer S, Hörtensteiner S, Picco C, Scholz-Starke J, Ravera S, Lee Y, Martinoia E. **2007**. The *Arabidopsis* vacuolar malate channel is a member of the ALMT family. *The Plant journal : for cell and molecular biology* **52**: 1169–80.

Kroeger J, Geitmann A. **2012**. The pollen tube paradigm revisited. *Current Opinion in Plant Biology* **15**: 618–624.

Krogsgaard-Larsen P, Johnston GA. **1978**. Structure-activity studies on the inhibition of GABA binding to rat brain membranes by muscimol and related compounds. *Journal of neurochemistry* **30**: 1377–82.

Kühtreiber W, Jaffe LF. **1990**. Detection of Extracellular Calcium Gradients with a Calcium-specific Vibrating Electrode. *The Journal of Cell Biology* **110**: 1565–1573.

Kuromori T, Sugimoto E, Shinozaki K. **2011**. *Arabidopsis* mutants of AtABCG22, an ABC transporter gene, increase water transpiration and drought susceptibility. *The Plant Journal* **67**: 885–894.

Lancien M, Roberts MR. **2006**. Regulation of *Arabidopsis* 14-3-3 gene expression by GABA. *Plant, Cell and Environment* **29**: 1430–1436.

Li LG, Sokolov LN, Yang YH, Li DP, Ting J, Pandy GK, Luan S. **2008**. A mitochondrial magnesium transporter functions in *Arabidopsis* pollen development. *Molecular Plant* **1**: 675–685.

Liem KF, Tremml G, Roelink H, Jessell TM. **1995**. Dorsal differentiation of neural plate cells induced by BMP-mediated signals from epidermal ectoderm. *Cell* **82**: 969–979.

Loraine AE, Mccormick S, Estrada A, Patel K, Qin P. **2013**. RNA-Seq of *Arabidopsis* Pollen Uncovers Novel Transcription and Alternative Splicing. *Plant Physiology* **162**: 1092–1109.

Lu Y, Chanroj S, Zulkifli L, Johnson M a., Uozumi N, Cheung AY, Sze H. **2011**. Pollen Tubes Lacking a Pair of K+ Transporters Fail to Target Ovules in *Arabidopsis*. *the Plant Cell Online* **23**: 81–93.

Lv Q, Tang R, Liu H, Gao X, Li Y, Zheng H, Zhang H. **2009**. Cloning and molecular analyses of the *Arabidopsis* thaliana chloride channel gene family. *Plant Science* **176**: 650–661.

Malhó R, Liu Q, Monteiro D, Rato C, Camacho L, Dinis a. **2006**. Signalling pathways in pollen germination and tube growth. *Protoplasma* **228**: 21–30.

Malhó R, Read ND, Trewavas a. J, Pais MS. **1995**. Calcium Channel Activity during Pollen Tube Growth and Reorientation. *The Plant cell* **7**: 1173–1184.

Marmagne A, Vinauger-Douard M, Monachello D, de Longevialle AF, Charon C, Allot M, Rappaport F, Wollman F-A, Barbier-Brygoo H, Ephritikhine G. **2007**. Two members of the *Arabidopsis* CLC (chloride channel) family, AtCLCe and AtCLCf, are associated with thylakoid and Golgi membranes, respectively. *Journal of experimental botany* **58**: 3385–93.

Marten H, Hyun T, Gomi K, Seo S, Hedrich R, Roelfsema MRG. **2008**. Silencing of NtMPK4 impairs CO-induced stomatal closure, activation of anion channels and cytosolic Casignals in Nicotiana tabacum guard cells. *The Plant journal : for cell and molecular biology* **55**: 698–708.

Marten H, Konrad KR, Dietrich P, Roelfsema MRG, Hedrich R. **2007**. Ca2+-dependent and -independent abscisic acid activation of plasma membrane anion channels in guard cells of Nicotiana tabacum. *Plant physiology* **143**: 28–37.

Marty A, Neher E. **1995**. Tight-Seal Whole-Cell Recording. In: Sakmann B, Neher E, eds. Single-Channel Recording. New York: Springer US, 31–52.

Mascarenhas JP. **1993**. Molecular Mechanisms of Pollen Tube Growth and Differentiation. *The Plant cell* **5**: 1303–1314.

Matveyeva NP, Andreyuk DS, Yermakov IP. **2003**. Transport of Cl – across the Plasma Membrane during Pollen Grain Germination in Tobacco. *Biochemistry (Moscow)* **68**: 1247–1251.

McCormick S. **2007**. PLANT SCIENCE: Reproductive Dialog. *Science* **317**: 606–607.

Messerli MA, Créton R, Jaffe LF, Robinson KR. **2000**. Periodic Increases in Elongation Rate Precede Increases in Cytosolic Ca2+ during Pollen Tube Growth. *Developmental Biology* **222**: 84–98.

Messerli MA, Danuser G, Robinson KR. **1999**. Pulsatile influxes of H+, K+ and Ca2+ lag growth pulses of Lilium longiflorum pollen tubes. *Journal of cell science* **112 (Pt 1**: 1497–509.

Messerli MA, Robinson KR. **1997**. Tip localized Ca2+ pulses are coincident with peak pulsatile growth rates in pollen tubes of Lilium longiflorum. *Journal of cell science* **110 (Pt 1**: 1269–78.

Messerli MA, Smith PJS, Lewis RC, Robinson KR. **2004**. Chloride fluxes in lily pollen tubes: a critical reevaluation. *The Plant journal : for cell and molecular biology* **40**: 799–812.

Meyer A, Eskandari S, Grallath S, Rentsch D. **2006**. AtGAT1, a high affinity transporter for gamma-aminobutyric acid in *Arabidopsis* thaliana. *The Journal of biological chemistry* **281**: 7197–204.

Meyer S, Mumm P, Imes D, Endler A, Weder B, Al-Rasheid K a S, Geiger D, Marten I, Martinoia E, Hedrich R. **2010**. AtALMT12 represents an R-type anion channel required for stomatal movement in *Arabidopsis* guard cells. *The Plant journal : for cell and molecular biology*: 1054–1062.

Michaeli S, Fait A, Lagor K, Nunes-Nesi A, Grillich N, Yellin A, Bar D, Khan M, Fernie AR, Turano FJ, et al. 2011. A mitochondrial GABA permease connects the GABA shunt and the TCA cycle, and is essential for normal carbon metabolism. *Plant Journal* **67**: 485–498.

Michard E, Alves F, Feijó JA. **2009**. The role of ion fluxes in polarized cell growth and morphogenesis: the pollen tube as an experimental paradigm. *The International journal of developmental biology* **53**: 1609–22.

Michard E, Dias PN, Feijó JA. **2008**. Tobacco pollen tubes as cellular models for ion dynamics: improved spatial and temporal resolution of extracellular flux and free cytosolic concentration of calcium and protons using pHluorin and YC3.1 CaMeleon. *Sexual Plant Reproduction* **21**: 169–181.

Michard E, Lima PT, Borges FS, Silva AC, Portes MT, Carvalho JE, Gilliham M, Liu L-HL-H, Obermeyer G, Feijó JA. **2011**. Glutamate receptor-like genes form Ca2+ channels in pollen tubes and are regulated by pistil D-serine. *Science* **332**: 434–7.

Miledi R, Molenaar PC, Polak RL. **1982**. Free and bound acetylcholine in frog muscle. *J Physiol* **333**: 189–199.

Mindell JA, Maduke M, Miller C, Grigorieff N. **2001**. Projection structure of a ClC-type chloride channel at 6.5 A resolution. *Nature* **409**: 219–23.

Mouline K, Véry A-A, Gaymard F, Boucherez J, Pilot G, Devic M, Bouchez D, Thibaud J-B, Sentenac H. **2002**. Pollen tube development and competitive ability are impaired by disruption of a Shaker K+ channel in *Arabidopsis*. *Genes & Development* **16**: 339–350.

Nakamura S, Miki-Hirosige H. **1982**. Coated vesicles and cell plate formation in the microspore mother cell. *Journal of Ultrastructure Research* **80**: 302–311.

Negi J, Matsuda O, Nagasawa T, Oba Y, Takahashi H, Kawai-Yamada M, Uchimiya H, Hashimoto M, Iba K. **2008**. CO2 regulator SLAC1 and its homologues are essential for anion homeostasis in plant cells. *Nature* **452**: 483–486.

Neher E, Sakmann B. **1976**. Single-channel currents recorded from membrane of denervated frog muscle fibres. *Nature* **260**: 799–802.

Neher E, Sakmann B. **1992**. The patch clamp technique. *Scientific American* **266**: 44–51.

Nicholson SH, Suckling CJ, Iversen LL. **1979**. GABA analogues: conformational analysis of effects on [3H]GABA binding to postsynaptic receptors in human cerebellum. *Journal of Neurochemistry* **32**: 249–252.

Numberger M, Draguhn A. **1996**. *Patch-Clamp Technique*. Germany: Spektrum Akademischer Verlag.

Obermeyer G, Kolb HA. **1993**. K+ channels in the plasma membrane of Lily pollen protoplasts. *Botanica Acta* **106**: 26.31.

Obermeyer G, Weisenseel MH. **1991**. Calcium channel blocker and calmodulin antagonists affect the gradient of free calcium ions in lily pollen tubes. *European journal of cell biology* **56**: 319–27.

Ogden D, Stanfield P. **1988**. Patch clamp techniques for single channel and whole-cell recording.53–78.

Oh JE, Kwon Y, Kim JH, Noh H, Hong SW, Lee H. **2011**. A dual role for MYB60 in stomatal regulation and root growth of *Arabidopsis* thaliana under drought stress. *Plant Molecular Biology* **77**: 91–103.

Ohshiro J, Yamamura H, Suzuki Y, Imaizumi Y. **2014**. Modulation of TMEM16A-channel activity as Ca^{2+} activated Cl^{-} conductance via the interaction with actin cytoskeleton in murine portal vein. *Journal of pharmacological sciences* **125**: 107–11.

Palanivelu R, Brass L, Edlund AF, Preuss D. **2003**. Pollen tube growth and guidance is regulated by POP2, an *Arabidopsis* gene that controls GABA levels. *Cell* **114**: 47–59.

Pandey S, Zhang W, Assmann SM. **2007**. Roles of ion channels and transporters in guard cell signal transduction. *FEBS letters* **581**: 2325–36.

Parton RM, Fischer-Parton S, Trewavas AJ, Watahiki MK. **2003**. Pollen tubes exhibit regular periodic membrane trafficking events in the absence of apical extension. *Journal of cell science* **116**: 2707–2719.

Pedemonte N, Galietta LJ V. **2014**. Structure and function of TMEM16 proteins (anoctamins). *Physiological reviews* **94**: 419–59.

Pei Z-M, Kuchitsu K, Ward JM, Schwarz M, Schroeder JI. **1997**. Differential Abscisic Acid Regulation of Guard Cell Slow Anion Channels in *Arabidopsis* Wild-Type and abi1 and abi2 Mutants. *The Plant Cell* **9**: 409.

Pei ZM, Ward JM, Harper JF, Schroeder JI. **1996**. A novel chloride channel in Vicia faba guard cell vacuoles activated by the serine/threonine kinase, CDPK. *The EMBO journal* **15**: 6564–74.

Penner R. **1995**. *A Practical Guide to Patch Clamping*. Springer US.

Pierson ES, Miller DD, Callaham DA, Shipley AM, Rivers BA, Cresti M, Hepler PK. **1994**. Pollen tube growth is coupled to the extracellular calcium ion flux and the intracellular calcium gradient: effect of BAPTA-type buffers and hypertonic media. *The Plant cell* **6**: 1815–28.

Pina C, Pinto F, Feijó JA, Becker JD. **2005**. Gene Family Analysis of the *Arabidopsis* Pollen Transcriptome Reveals Biological Implications for Cell Growth , Division Control , and Gene Expression Regulation. *Plant Physiology* **138**: 744–756.

Piñeros MA, Kochian L V. **2001**. A patch-clamp study on the physiology of aluminum toxicity and aluminum tolerance in maize. Identification and characterization of Al(3+)-induced anion channels. *Plant physiology* **125**: 292–305.

Qu H-Y, Shang Z-L, Zhang S-L, Liu L-M, Wu J-Y. **2007**. Identification of hyperpolarization-activated calcium channels in apical pollen tubes of Pyrus pyrifolia. *New phytologist* **174**: 524–36.

Raghavan V. **2006**. *Double Fertilization*. Berlin Heidelberg: Springer-Verlag.

Raichaudhuri A, Peng M, Naponelli V, Chen S, Sánchez-Fernández R, Gu H, Gregory JF, Hanson AD, Rea P a. **2009**. Plant Vacuolar ATP-binding Cassette Transporters That Translocate Folates and Antifolates in Vitro and Contribute to Antifolate Tolerance in Vivo. *The Journal of biological chemistry* **284**: 8449–60.

Ramesh SA, Tyerman SD, Xu B, Bose J, Kaur S, Conn V, Domingos P, Ullah S, Wege S, Shabala S, et al. 2015. GABA signalling modulates plant

growth by directly regulating the activity of plant-specific anion transporters. *Nature Communications* **6**: 7879.

Rathore KS, Cork JR, Robinson KR. **1991**. A cytoplasmic gradient of Ca2+ is correlated with the growth of lily pollen tubes. *Developmental biology* **148**: 612–619.

Rato C, Monteiro D, Hepler PK, Malhó R. **2004**. Calmodulin activity and cAMP signalling modulate growth and apical secretion in pollen tubes. *Plant Journal* **38**: 887–897.

Reiss HD, Herth W. **1985**. Nifedipine-sensitive calcium channels are involved in polar growth of lily pollen tubes. *Journal of cell science* **76**: 247–54.

Renault H, El Amrani A, Palanivelu R, Updegraff EP, Yu A, Renou JP, Preuss D, Bouchereau A, Deleu C. **2011**. GABA accumulation causes cell elongation defects and a decrease in expression of genes encoding secreted and cell wall-related proteins in *Arabidopsis* thaliana. *Plant and Cell Physiology* **52**: 894–908.

Rho JM, Donevan SD, Rogawski MA. **1996**. Direct activation of GABAA receptors by barbiturates in cultured rat hippocampal neurons. *The Journal of physiology* **497 (Pt 2**: 509–22.

Roberts SK. **2006**. Plasma membrane anion channels in higher plants and their putative functions in roots. *New Phytologist* **169**: 647–666.

Robertson WR, Clark K, Young JC, Sussman MR. **2004**. An *Arabidopsis* thaliana plasma membrane proton pump is essential for pollen development. *Genetics* **168**: 1677–87.

Robinson KR, Messerli M a. **2002**. Pulsating ion fluxes and growth at the pollen tube tip. *Science's STKE : signal transduction knowledge environment* **2002**: pe51.

Roelfsema MRG, Hanstein S, Felle HH, Hedrich R. **2002**. CO2 provides an intermediate link in the red light response of guard cells. *The Plant journal : for cell and molecular biology* **32**: 65–75.

Roelfsema MRG, Hedrich R. **2005**. In the light of stomatal opening: new insights into "the Watergate". *The New phytologist* **167**: 665–91.

Roelfsema MRG, Levchenko V, Hedrich R. **2004**. ABA depolarizes guard cells in intact plants, through a transient activation of R- and S-type anion channels. *The Plant Journal* **37**: 578–588.

Roy S, Holdaway-Clarke T, Hackett G, Kunkel J, Lord E, Hepler P. **1999**. Uncoupling secretion and tip growth in lily pollen tubes: evidence for the role of calcium in exocytosis. *The Plant journal : for cell and molecular biology* **19**: 379–86.

Sasaki T, Mori IC, Furuichi T, Munemasa S, Toyooka K, Matsuoka K, Murata Y, Yamamoto Y. **2010**. Closing plant stomata requires a homolog of an aluminum-activated malate transporter. *Plant & cell physiology* **51**: 354–65.

Schiøtt M, Romanowsky SM, Baekgaard L, Jakobsen MK, Palmgren MG, Harper JF. **2004**. A plant plasma membrane Ca2+ pump is required for normal pollen tube growth and fertilization. *Proceedings of the National Academy of Sciences of the United States of America* **101**: 9502–7.

Schmid A, Blum R, Krause E. **1998**. Characterization of cell volume-sensitive chloride currents in freshly prepared and cultured pancreatic acinar cells from early postnatal rats. *The Journal of Physiology* **513**: 453–65.

Schmidt C, Schelle I, Liao YJ, Schroeder JI. **1995**. Strong regulation of slow anion channels and abscisic acid signaling in guard cells by phosphorylation and dephosphorylation events. *Proceedings of the National Academy of Sciences of the United States of America* **92**: 9535–9.

Schmidt C, Schroeder JI. **1994**. Anion Selectivity of Slow Anion Channels in the Plasma Membrane of Guard Cells (Large Nitrate Permeability). *Plant physiology* **106**: 383–391.

Schroeder BC, Cheng T, Jan YN, Jan LY. **2008**. Expression cloning of TMEM16A as a calcium-activated chloride channel subunit. *Cell* **134**: 1019–29.

Schroeder J, Hagiwara S. **1989**. Cytosolic calcium regulates ion channels in the plasma membrane of Vicia faba guard cells. *nature* **338**: 427–430.

Schroeder JI, Keller BU. **1992**. Two types of anion channel currents in guard cells with distinct voltage regulation. *Proceedings of the National Academy of Sciences of the United States of America* **89**: 5025–9.

Schroeder JI, Schmidt C, Sheaffer J. **1993**. Identification of High-Affinity Slow Anion Channel Blockers and Evidence for Stomatal Regulation by Slow Anion Channels in Guard Cells. *The Plant cell* **5**: 1831–1841.

SchulzLessdorf B, Lohse G, Hedrich R. **1996**. GCAC1 recognizes the pH gradient across the plasma membrane A pH-sensitive and ATP-dependent anion channel links guard cell membrane potential to acid and energy metabolism.pdf. *The Plant Journal* **10**: 993–1004.

Schwiebert LM, Estell K, Propst SM. **1999**. Chemokine expression in CF epithelia: implications for the role of CFTR in RANTES expression. *Am.J.Physiol.* **276**.

Selinski J, Scheibe R. **2014**. Pollen tube growth: where does the energy come from? *Plant Signaling & Behavior* **9**: e977200.

Shang Z, Ma L, Zhang H, He R, Wang X, Cui S, Sun D. **2005**. Ca2+ influx into lily pollen grains through a hyperpolarization-activated Ca2+-permeable channel

which can be regulated by extracellular CaM. *Plant & cell physiology* **46**: 598–608.

Shelp BJ, Bown AW, Faure D. **2006**. Extracellular gamma-aminobutyrate mediates communication between plants and other organisms. *Plant physiology* **142**: 1350–1352.

Shelp BJ, Bozzo GG, Zarei A, Simpson JP, Trobacher CP, Allan WL. **2012**. Strategies and tools for studying the metabolism and function of γ-aminobutyrate in plants. II. Integrated analysis. *Botany* **90**: 781–793.

Shipley AM, Feijó JA. **1999**. The use of the vibrating technique to study steady extracellular currents during pollen germination and tube growth. In: Cresti M, Moscatelli A, eds. Fertilisation in Higher Plants: molecular and cytological aspects. Berlin, Heidelberg: Springer-Verlag, 235–250.

Simillion C, Vandepoele K, Van Montagu MCE, Zabeau M, Van de Peer Y. **2002**. The hidden duplication past of *Arabidopsis* thaliana. *Proceedings of the National Academy of Sciences* **99**: 13627–13632.

Sivitz AB, Reinders A, Ward JM. **2008**. *Arabidopsis* sucrose transporter AtSUC1 is important for pollen germination and sucrose-induced anthocyanin accumulation. *Plant physiology* **147**: 92–100.

Snyder SH. **2002**. *Neuropsychiatry and Behavioral Neurosciences* (SC Yudofsky and RE Hales, Eds.). American Psychiatric Publishing.

Song L-F, Zou J, Zhang W, Wu W-H, Wang Y. **2009**. Ion transporters involved in pollen germination and pollen tube tip-growth. *Plant signaling & behavior* **4**: 1193–5.

Straub SCK, Fishbein M, Livshultz T, Foster Z, Parks M, Weitemier K, Cronn RC, Liston A. **2011**. Building a model: developing genomic resources for common milkweed (Asclepias syriaca) with low coverage genome sequencing. *BMC genomics* **12**: 211.

Su H, Zhu J, Cai C, Pei W, Wang J, Dong H, Ren H. **2012**. FIMBRIN1 Is Involved in Lily Pollen Tube Growth by Stabilizing the Actin Fringe. *The Plant cell* **5**.

Suzuki J, Fujii T, Imao T, Ishihara K, Kuba H, Nagata S. **2013**. Calcium-dependent Phospholipid Scramblase Activity of TMEM16 Protein Family Members. *Journal of Biological Chemistry* **288**: 13305–13316.

Suzuki J, Umeda M, Sims PJ, Nagata S. **2010**. Suzuki & Nagata; Ca2+-dependent phospholipid scrambling by TMEM16F. *Nature* **468**: 834–838.

Sze H, Li X, Palmgren M. **1999**. Energization of plant cell membranes by H+-pumping ATPases. Regulation and biosynthesis. *The Plant cell* **11**: 677–90.

Sze H, Padmanaban S, Cellier F, Honys D, Cheng N-H, Bock KW, Conéjéro G, Li X, Twell D, Ward JM, et al. 2004. Expression Patterns of a Novel AtCHX Gene Family Highlight Potential Roles in Osmotic Adjustment and K+ Homeostasis in Pollen Development. *Plant Physiology* **136**: 2532–2547.

Tanaka I, Kitazume C, Ito M. **1987**. The isolation and culture of Lily pollen protoplasts. *Plant Science* **50**: 205–211.

Tavares B. **2011**. Anionic Currents in Pollen Grain Protoplasts from *Arabidopsis* thaliana and Lilium longiflorum. *Repositório da Universidade de Lisboa - Teses de Doutoramento*: 1–142.

Tavares B, Dias PN, Domingos P, Moura TF, Feijó JA, Bicho A. **2011a**. Calcium-regulated anion channels in the plasma membrane of Lilium longiflorum pollen protoplasts. *New phytologist* **192**: 45–60.

Tavares B, Domingos P, Dias PN, Feijó JA, Bicho A. **2011b**. The essential role of anionic transport in plant cells: the pollen tube as a case study. *Journal of experimental botany* **62**: 2273–98.

Twell D, Wing R, Yamaguchi J, McCormick S. **1989**. Isolation and expression of an anther-specific gene from tomato. *Molecular & general genetics* **217**: 240–5.

Twyman RE, Macdonald RL. **1991**. Kinetic properties of the glycine receptor main- and sub-conductance states of mouse spinal cord neurones in culture. *The Journal of physiology* **435**: 303–31.

Vahisalu T, Kollist H, Wang Y-F, Nishimura N, Chan W-Y, Valerio G, Lamminmäki A, Brosché M, Moldau H, Desikan R, et al. 2008. SLAC1 is required for plant guard cell S-type anion channel function in stomatal signalling. *Nature* **452**: 487–91.

Wang Y-F, Fan L-M, Zhang W-Z, Zhang W, Wu W-H. **2004**. Ca2+-Permeable Channels in the Plasma Membrane of *Arabidopsis* Pollen Are Regulated by Actin Microfilaments. *Plant Physiology* **136**: 3892–3904.

Wang Y, Zhang W-Z, Song L-F, Zou J-J, Su Z, Wu W-H. **2008**. Transcriptome analyses show changes in gene expression to accompany pollen germination and tube growth in *Arabidopsis*. *Plant physiology* **148**: 1201–11.

Ward JM, Mäser P, Schroeder JI. **2009**. Plant ion channels: gene families, physiology, and functional genomics analyses. *Annual review of physiology* **71**: 59–82.

Wege S, Jossier M, Filleur S, Thomine S, Barbier-Brygoo H, Gambale F, De Angeli A. **2010**. The proline 160 in the selectivity filter of the *Arabidopsis* NO3-/H+ exchanger AtCLCa is essential for nitrate accumulation in planta. *The Plant journal : for cell and molecular biology*.

Von Weikersthal SF, Barrand M a, Hladky SB. **1999**. Functional and molecular characterization of a volume-sensitive chloride current in rat brain endothelial cells. *The Journal of physiology* **516 (Pt 1**: 75–84.

Weisenseel MH, Jaffe LF. **1976**. The Major Growth Current Through Lily Pollen Tubes Enters as K+ and Leaves as H+. *Planta* **133**: 1–7.

White M, Miller C. **1979**. A voltage-gated anion channel from the electric organ of Torpedo californica. *Journal of Biological Chemistry*.

Wolf W, Kilic A, Schrul B, Lorenz H, Schwappach B, Seedorf M. **2012**. Yeast Ist2 recruits the endoplasmic reticulum to the plasma membrane and creates a ribosome-free membrane microcompartment. *PloS one* **7**: e39703.

Wu J-Y, Qu H-Y, Shang Z-L, Tao S-T, Xu G-H, Wu J, Wu H-Q, Zhang S-L. **2011**. Reciprocal regulation of Ca^{2}+-activated outward K+ channels of Pyrus pyrifolia pollen by heme and carbon monoxide. *The New phytologist* **189**: 1060–8.

Wu Y, Xu X, Li S, Liu T, Ma L, Shang Z. **2007**. Heterotrimeric G-protein participation in *Arabidopsis* pollen germination through modulation of a plasmamembrane hyperpolarization-activated Ca2+-permeable channel. *New phytologist* **176**: 550–9.

Yadav V, Molina I, Ranathunge K, Castillo IQ, Rothstein SJ, Reed JW. **2014**. ABCG transporters are required for suberin and pollen wall extracellular barriers in *Arabidopsis*. *The Plant cell* **26**: 3569–88.

Yang YD, Cho H, Koo JY, Tak MH, Cho Y, Shim W-S, Park SP, Lee J, Lee B, Kim B-M, et al. 2008. TMEM16A confers receptor-activated calcium-dependent chloride conductance. *Nature* **455**: 1210–1215.

Yang H, Kim A, David T, Palmer D, Jin T, Tien J, Huang F, Cheng T, Coughlin SR, Jan YN, et al. 2012. TMEM16F forms a Ca2+-activated cation channel required for lipid scrambling in platelets during blood coagulation. *Cell* **151**: 111–22.

Yoon GM, Dowd PE, Gilroy S, McCubbin AG. **2006**. Calcium-dependent protein kinase isoforms in Petunia have distinct functions in pollen tube growth, including regulating polarity. *The Plant cell* **18**: 867–878.

Yu FH, Mantegazza M, Westenbroek RE, Robbins C a, Kalume F, Burton K a, Spain WJ, McKnight GS, Scheuer T, Catterall W a. **2006**. Reduced sodium current in GABAergic interneurons in a mouse model of severe myoclonic epilepsy in infancy. *Nature neuroscience* **9**: 1142–1149.

Yu K, Whitlock JM, Lee K, Ortlund E a, Yuan Cui Y, Hartzell HC. **2015**. Identification of a lipid scrambling domain in ANO6/TMEM16F. *eLife* **4**: 1–23.

Yu GH, Zou J, Feng J, Peng XB, Wu JY, Wu YL, Palanivelu R, Sun MX. **2014**. Exogenous γ-aminobutyric acid (GABA) affects pollen tube growth via modulating putative Ca2+-permeable membranechannels and is coupled to negative regulation on glutamate decarboxylase. *Journal of Experimental Botany* **65**: 3235–3248.

Zifarelli G, Pusch M. **2007**. CLC chloride channels and transporters: a biophysical and physiological perspective. *Biochemical Pharmacology*.

Zonia L, Cordeiro S, Feijó JA. **2001**. Ion dynamics and hydrodynamics in the regulation of pollen tube growth. *Sexual Plant Reproduction* **14**: 111–116.

Zonia L, Cordeiro S, Tupý J, Feijó JA. **2002**. Oscillatory Chloride Efflux at the Pollen Tube Apex Has a Role in Growth and Cell Volume Regulation and Is Targeted by Inositol 3,4,5,6-Tetrakisphosphate. *The Plant Cell* **14**: 2233–2249.

Zonia L, Munnik T. **2004**. Osmotically Induced Cell Swelling versus Cell Shrinking Elicits Specific Changes in Phospholipid Signals in Tobacco Pollen Tubes. *Plant Physiology* **134**: 813–823.